

NIST-GCR-98-753

**Determination of Properties and the Prediction of the
Energy Release Rate of Materials in the ISO 9705
Room-Corner Test**

S. E. Dillon, W. H. Kim and J. G. Quintiere
Department of Fire Protection Engineering
University of Maryland
College Park, MD 20742

NIST

**United States Department of Commerce
Technology Administration
National Institute of Standards and Technology**

NIST-GCR-98-753

**Determination of Properties and the Prediction of the
Energy Release Rate of Materials in the ISO 9705
Room-Corner Test**

Prepared for

U.S. Department of Commerce
National Institute of Standards and Technology
Gaithersburg, MD 20899

By

S. E. Dillon, W. H. Kim and J. G. Quintiere
Department of Fire Protection Engineering
University of Maryland
College Park, MD 20742

June 1998
Issued July 1998



Notice

This report was prepared for the Building and Fire Research Laboratory of the National Institute of Standards and Technology under grant number 60NANB2D1266. The statement and conclusions contained in this report are those of the authors and do not necessarily reflect the views of the National Institute of Standards and Technology or the Building and Fire Research Laboratory.

**DETERMINATION OF PROPERTIES AND THE
PREDICTION OF THE ENERGY RELEASE RATE
OF MATERIALS IN THE ISO 9705 ROOM-CORNER TEST.**

S. E. Dillon, W. H. Kim and J. G. Quintiere
Department of Fire Protection Engineering
University of Maryland
College Park, MD 20742

INTERIM REPORT

June, 1998

Prepared for:

U.S. Department of Commerce
National Institute of Standards and Technology
Laboratory of Building and Fire Research
Washington, D.C. 20234

Determination of Properties and the Prediction of the Energy Release Rate of Materials in the ISO 9705 Room/Corner Test

S. E. Dillon, W. H. Kim and J. G. Quintiere

ABSTRACT

A simulation model is implemented in order to predict the performance of materials in the ISO 9705 Room-Corner Test. These materials were tested by the L S Fire Laboratories of Italy, and the data they provided is analyzed in this report. A method was established to define material properties including the heat of combustion, heat of gasification, thermal inertia, ignition temperature and the total energy per unit area. These methods were developed from refinements in the theoretical model of ignition and in resolving time dependent effects in the Cone Calorimeter. The materials examined consist of some of the worst behaving since they melt, drip, expand and de-laminate from the wall and ceiling configuration of the room-corner test. Corrections have been included in the simulation modeling to account for these effects. the correction involves reducing the total energy per unit area content of the material to accordingly reduce its contribution as a wall-ceiling oriented element. An empirical correlation based on a linearized upward flame spread model is shown to provide very good correlation to the flashover time in the full-scale ISO test.

Keywords: simulation, fire growth, room-corner test, material fire properties.

TABLE OF CONTENTS

LIST OF TABLES	viii
LIST OF FIGURES	ix
NOMENCLATURE.....	xi
1. INTRODUCTION.....	1
1.1 Room-Corner Tests	1
1.2 Current Model	2
1.3 Project Objective and Goals.....	4
<i>Technical Improvements</i>	4
<i>Code Improvements</i>	4
<i>Simulation Evaluation</i>	4
2. DESCRIPTION OF MATERIALS	6
3. MATERIAL PROPERTIES	11
3.1 Ignition Properties	12
3.2 Flame Spread Properties	17
3.4 Heat of Combustion (ΔH_C)	19
<i>Definition</i>	19
<i>Determining ΔH_C</i>	20
1. Peak Rate of Energy Release ($\Delta H_{C, peak}$).....	22
2. Average Rate of Energy Release ($\Delta H_{C, peak avg.}$)	23
3. Overall Energy Release ($\Delta H_{C, overall avg.}$).....	24
3.5 Heat of Gasification (L).....	39
<i>Definition</i>	39
<i>Cone Calorimeter Heat Flux</i>	41
<i>Energy Release Rate Methods</i>	44
1. Peak Energy Release Rate (L_{peak})	45
2. Average Energy Release Rate Around the Peak ($L_{peak avg.}$).....	45
3. Average Overall Test Results ($L_{overall avg.}$).....	46
<i>Specimen Mass Loss Methods</i>	61

4. Peak Energy Release Rate (L_{peak}) by Mass Loss	62
5. Average Energy Release Rate Around the Peak ($L_{peak\ avg.}$) by Mass Loss.....	63
6. Average Overall Test Results ($L_{overall\ avg.}$) by Mass Loss.....	63
<i>Heat of Gasification Value Analysis</i>	77
3.6 Total Energy Per Unit Area (Q'').....	82
3.7 Material Property Conclusion	97
4. FIRE GROWTH PREDICTIONS	99
4.1 Fire Growth Model.....	99
4.2 Material Properties Used	99
<i>Adjusted Properties for Melting/Dripping Materials</i>	100
4.3 Results.....	102
<i>R 4.01, Fire Retarded Chipboard</i>	104
<i>R 4.02 Paper Faced Gypsum Board</i>	105
<i>R 4.03 Polyurethane Foam Panel with Aluminum Facing</i>	106
<i>R 4.05, Fire Retarded Extruded Polystyrene Board</i>	106
<i>R 4.06, Clear Acrylic Glazing</i>	108
<i>R 4.07, Fire Retarded PVC</i>	110
<i>R 4.08, 3-Layered, Fire Retarded Polycarbonate Panel</i>	111
<i>R 4.09, Varnished Massive Timber</i>	111
<i>R 4.10, Fire Retarded Plywood</i>	113
<i>R 4.11, Normal Plywood</i>	114
<i>R 4.20, Fire Retarded Expanded Polystyrene Board (40 mm)</i>	115
<i>R 4.21, Fire Retarded Expanded Polystyrene Board (80 mm)</i>	116
<i>Time to Reach Flashover</i>	117
4.5 Lateral Flame Spread.....	118
5. UPWARD FLAME SPREAD ACCELERATION FACTOR.....	119
6. CONCLUSIONS.....	126
ACKNOWLEDGEMENTS.....	127
REFERENCES	128

APPENDICES	130
Appendix A – LSF Cone Calorimeter Data	131
<i>A.1 – Nomenclature</i>	132
<i>A.2 – Cone Calorimeter Data</i>	133
<i>A.3 – Ignition Data</i>	352
<i>A.4 – Heat of Combustion Data</i>	389
<i>A.5 – Heat of Gasification Data</i>	416
<i>A.6 – Total Energy Per Unit Area Data</i>	443
Appendix B – Su, Chen-Hsiang, “Downward and Lateral Flame Spread in Roland Apparatus Phase 5”, M. S. Degree Scholarly Paper, Department of Fire Protection Engineering, University of Maryland, college Park, Maryland. ...	457
Appendix C – Thureson, Per, “Fire Tests of Linings According to Room/Corner Test, ISO 9705”, Swedish National Testing and Research Institute, Fire Technology, Report 95R22049, January, 1996.	508
Appendix D – Quintiere’s Fire Growth Model.....	594
<i>D.1 – Quintiere J G., “A Simulation Model for Fire Growth on Materials Subject to a Room/Corner Test”, Fire Safety Journal, Volume 18, 1992.</i>	595
<i>D.2—Fire Growth Model Source Code</i>	620

LIST OF TABLES

Table 3. 1: Material Modeling Properties.....	11
Table 3. 2: Estimated Critical Flux for Ignition.....	15
Table 3. 3: Ignition and Flame Spread Properties of the LSF Materials.....	19
Table 3. 4: Average, effective heat of combustion (ΔH_c) values calculated by three methods.....	25
Table 3. 5: Effective Heat of Gasification (L) Values Calculated by Six Methods.....	77
Table 3. 6: Energy Release per Unit Area of Material.....	83
Table 4. 1: Ignition, Flame Spread and Energy Release Properties of the LSF Materials used for Modeling.	103
Table 4. 2: Comparison of the Time to Reach Flashover (1,000 kW) for the Full-Scale Room/Corner Tests and the Model Predictions.	118
Table 5. 1: Flame Spread Acceleration Factor for Swedish, EUREFIC and LSF Materials.	125

LIST OF FIGURES

Figure 1. 1: Simulation Model Features.....	3
Figure 3. 1: Typical Interpretive Plot of Ignition Data in Order to Derive Properties.....	16
Figure 3. 2: A Typical Burning Process in the Roland Apparatus.....	18
Figure 3. 3: Example of Time-Varying Heat of Combustion Measured in the Cone Calorimeter: R 4.08, 3-Layer Polycarbonate Panel at 50 kW/m ²	21
Figure 3. 4: Example of Peak, Peak Average and Overall Average Energy Release Rates per Unit Area Measured in the Cone Calorimeter: R 4.08 at 50 kW/m ²	21
Figure 3. 5: Method of Determining the Peak, Peak Average and Overall Average Heat of Combustion Values: R 4.08, 3-Layer Polycarbonate Panel at 50 kW/m ²	23
Figure 3. 6: Example of an Average Heat of Combustion ($\overline{\Delta H_c}$) Determination: R 4.08 at 50 kW/m ²	24
Figure 3. 7: Example of Burning Rate per Unit Area (\dot{m}'') Prediction: R 4.08, 3-Layer Polycarbonate Panel at 50 kW/m ²	40
Figure 3. 8: Example of Energy Release Rate per Unit Area (\dot{Q}'') Prediction: R 4.08 at 50 kW/m ²	41
Figure 3. 9: Example of Heat of Gasification (L) Determination Using Energy Release Rates per Unit Area with Respect to the External Heat Flux in the Cone Calorimeter: R 4.05, Fire Retarded Extruded Polystyrene.....	45
Figure 3. 10: Example of Steady Burning Rate (\dot{m}) Determination: R 4.08, 3-Layer Polycarbonate Panel.	47
Figure 3. 11: Example of Heat of Gasification (L) Determination Using Specimen Mass Loss Rates per Unit Area with Respect to the External Heat Flux in the Cone Calorimeter: R 4.05, Fire Retarded Extruded Polystyrene.....	62
Figure 3. 12: Typical Energy Release Rate per Unit Area and Specimen Mass for Gypsum Board, R 4.02, in the Cone Calorimeter.	78
Figure 3. 13: Typical Energy Release Rate and Specimen Mass for Polyurethane Foam Board with Paper Facing, R 4.04, in the Cone Calorimeter.	79
Figure 3. 14: Average Heat of Combustion Values for Fire Retarded PVC, R 4.07.....	80
Figure 3. 15: Various Energy Release Rates for Fire Retarded PVC, R 4.07, in the Cone Calorimeter	80

Figure 3. 16: Peak Energy Release and Mass Loss Rates for Varnished Massive Timber, R 4.09, at Different External Heat Flux Levels in the Cone Calorimeter.....	81
Figure 3. 17: Typical Total Energy per Unit Area (Q'') Determination: R 4.05, Extruded Polystyrene Board.	83
Figure 3. 18: Comparison of Methods for Predicting the Energy Release Rate of a Thermoplastic Material in the Cone Calorimeter: R 4.08.	97
Figure 3. 19: Comparison of Methods for Predicting the Energy Release Rate of a Charring Material in the Cone Calorimeter: R 4.11, Normal Plywood.	98
Figure 4. 1: Idealized Heat Flux Distributions.	101
Figure 4. 2: Full-Scale Energy Release Rate for Fire Retarded Chipboard, R 4.01.	104
Figure 4. 3: Full-Scale Energy Release Rate for Paper Faced Gypsum Board, R 4.02.	105
Figure 4. 4: Full-Scale Energy Release Rate for Polyurethane Foam Panel with Aluminum Facing, R 4.03, Using Material Properties for Polyurethane Panel with Paper Facing, R 4.04.	107
Figure 4. 5: Full-Scale Energy Release Rate for Extruded Polystyrene Board, R 4.05.	108
Figure 4. 6: Full-Scale Energy Release Rate for Acrylic Glazing, R 4.06.	109
Figure 4. 7: Full-Scale Energy Release Rate for R 4.07 Fire Retarded PVC.	110
Figure 4. 8: Full-Scale Energy Release Rate for 3-Layered, Fire Retarded Polycarbonate Panel, R 4.08.	112
Figure 4. 9: Full-Scale Energy Release Rate for Varnished Massive Timber, R 4.09.	113
Figure 4. 10: Full-Scale Energy Release Rate for Fire Retarded Plywood, R 4.10.	114
Figure 4. 11: Full-Scale Energy Release Rate for Normal Plywood, R 4.11.	115
Figure 4. 12: Full-Scale Energy Release Rate for Fire Retarded Expanded Polystyrene Board (40 mm), R 4.20.	116
Figure 4. 13: Full-Scale Energy Release Rate for Fire Retarded Expanded Polystyrene Board (80 mm), R 4.21.	117
Figure 5. 1: Time to Flashover as a Function of the Flame Spread Acceleration Factor.	121
Figure 5. 2: Dimensionless Time as a Function of the Flame Spread Acceleration Factor.	121
Figure 5. 3: $\tau_{fo} - l - \tau_b$ versus b	123
Figure 5. 4: $\tau_{fo} - l$ versus a	124

NOMENCLATURE

A	-	area
b	-	upward flame spread acceleration factor
c	-	specific heat
D	-	specimen width
H	-	flame height
ΔH_c	-	effective heat of combustion
k	-	thermal conductivity
k _{pc}	-	thermal inertia
k _f	-	flame length coefficient (0.01 m ² /kW)
l _m	-	mean beam length
L	-	effective heat of gasification
m	-	mass
q	-	heat transfer
Q	-	energy
t	-	time
T	-	temperature
V	-	flame spread velocity
α	-	absorptivity
ϵ	-	emissivity
κ	-	absorption coefficient
ρ	-	density
σ	-	Stefan-Boltzmann constant (5.670 x 10 ⁻¹¹ kW/m ² ·K ⁴)
Φ	-	lateral flame spread coefficient

Subscripts

b	-	burnout
c	-	convective
eff	-	effective
ext	-	external
f	-	flame
fo	-	flashover
ig	-	ignition
min	-	minimum
net	-	net amount
r	-	radiation
rr	-	re-radiation
s	-	surface
v	-	vaporization
peak	-	at the peak energy release rate
peak avg.	-	averaged over 80% above of the peak energy release rate
overall avg.	-	average of the overall properties during steady, sustained burning

Superscripts

- (X'') - per unit area
- (\dot{X}) - per unit time
- (\bar{X}) - average value

Determination of Properties and the Prediction of the Energy Release Rate of Materials in the ISO 9705 Room-Corner Test

S. E. Dillon, W. H. Kim and J. G. Quintiere

1.0 INTRODUCTION

Room-corner tests have originated because of the lack of confidence in traditionally used standard flammability tests to determine the fire hazard of interior finish materials for walls and ceilings. Traditional standard tests give an index rating that is related to hazard. The measure of performance in the full-scale room test is usually the time to flashover or the rate of energy release produced during the fire growth on the material. Other factors include the extent of spread and the temperature and heat flux in the room. Various acceptance criteria have been proposed for this test protocol.

1.1 Room-Corner Tests

Several formal test protocols are in use, and they shall be summarized here. They include tests listed by American Society of Testing and Materials (ASTM), Uniform Building Code (UBC) and International Standards Organization (ISO).

1. ASTM Proposed Method for Room Fire Test of Wall and Ceiling Materials and Assemblies

Room: 2.44 x 3.66 x 2.44 m high

Door on short wall: 2.06 x 0.76 m wide

Burner: 0.30 x 0.30 m square sand burner with face 0.30 m above floor, propane fuel

Location: Corner, in contact with both walls ("edge of the diffusion surface shall be 2.5 cm from the wall", however it is not clear if this practice is followed, and we shall regard the burner as flush with the walls).

Ignition: 40 kW for 5 min. followed by 160 kW for 10 min.

2. Uniform Building Code Standard No. 42-2 Standard Test Method for Evaluating Room Fire Growth Contribution of Textile Wall Covering

Room: 2.44 x 3.66 x 2.44 m high

Door on short wall: 2.06 x 0.76 m wide

Burner: 0.30 x 0.30 m square sand burner with face 0.30 m above floor, propane fuel

Location: Corner, with the diffusion surface 5 cm from each wall (the diffusion surface is 0.6 cm from the burner edge due to the steel wall thickness, however we shall regard it as displaced 5 cm).

Ignition: 40 kW for 5 min. followed by 150 kW for 10 min.

3. ISO 9750, Fire Tests - Reaction to Fire - Full-scale Room Fire Tests for Surface Products, International Standards Organization

Room: 2.40 x 3.60 x 2.40 m high

Door on short wall: 2.00 x 0.80 m wide

Burner: 0.17 x 0.17 m square sand burner with face 0.15 m above floor, propane fuel

Location: Corner, in contact with both walls.

Ignition: 100 kW for 10 min. followed by 300 kW for 10 min.

In the ASTM and UBC tests, the material is mounted on 13 mm thick ordinary gypsum board along three walls opposite the doorway. Also, 2 ft. Strips can be used in the UBC test instead of covering the full wall. In the ISO and ASTM tests, the material can also be mounted on the ceiling.

As can be seen from these three test procedures, a primary difference in the test is the burner ignition source. Results show that the energy release rate of the burner and its heat flux to the wall along with the duration of the exposure make a difference in the performance of the material. This is particularly true for thin materials, such as wall coverings, which can burn-out during the application of the burner ignition pulse. Although the energy release rate of the corner burner can be the same or similar, as in the ASTM and UBC tests, the burner positions from the wall are different. This results in different burner heat fluxes which influence ignition and energy release rate.

Research has been conducted since 1991 on developing and examining a fire growth simulation model to predict the material performance in such room corner tests [1-7]. These applications include the ISO and the UBC tests.

For analyses of the Boras and Eurific program results [], it was found that plausible variations within the range of uncertainties in the material property data could sometimes make a significant difference in the time to reach 1 MW or flashover. The biggest differences occurred for the thin materials in which burnout was a factor. In the textile tests, burnout was always a factor, and the predictions are not as accurate as for thick materials. Moreover, the ignitor was found to be a more critical variable, in that a high heat flux ignitor could lead to early burnout, and then no subsequent propagation. But a lower heat flux ignitor would have the opposite effect. The duration of the ignitor is also felt to be important [16]. In both the UBC and ISO protocols, the ignitor procedure is fixed. The risk in these tests is that the ignitor scenario of the test does not tell the entire story of the potential fire hazard. A predictive model, even without high accuracy, can give a much broader perspective on the nature of the hazard.

When the model was first developed, the philosophy was to include the most obvious significant features of the fire growth process. As we became aware of more significant effects, then the need for a more elaborate or appropriate model became apparent. Unfortunately, most of the full scale results have not included information on the dynamic flame spread processes in their presentation of results. The burn patterns recorded in the UBC tests were valuable in this regard, and suggest the need for improvement on the lateral and downward spread effects.

The model has proven to yield good, but not perfect, overall results. It is also clear that for some materials, relatively small changes in their properties can lead to very dramatic differences in the full scale test predictions. This is particularly true for the thin or small burn time materials. This is likely not a mathematical artifact, but a real indication that some materials are on the threshold of a critical condition, namely the brink of flashover. This threshold is not only dependent on the material, but on the test protocol. Most importantly, a key variable is also the ignitor burner prescription. We have seen that small changes in the burner heat flux has also led to a case of from no propagation to one of flashover for a textile wall material. The effect was also observed in actual tests.

1.4 Project Objective and Goals

Objective: The proposed research seeks to develop and assess a simulation model to predict the fire growth on commercial materials used in construction and finish applications.

In order to advance the accuracy and confidence in the simulation model, we have proposed to do work in three categories:

1. Technical improvements
2. Code improvements
3. Simulation performance against new databases.

1.4.1 Technical Improvements

Several aspects of the simulation model can be improved. These are based on experience with our tests against data, and are based on advances in our understanding of ignition sources.

Several studies have examined the heat flux from controlled fires to vertical walls [11-13]. These provide correlations for the heat flux in terms of the energy release rate and arrangement of the fire. This heat flux information has been found to be very important for the performance of materials in the room-corner scenario, and more generally for wall fire spread. More experimental results are needed in this area, and are viewed as crucial for these problems. We believe that the prediction of such heat fluxes is beyond the state of the art, and only experimental correlations are practical solutions in the near future. We have examined the available correlations and will eventually develop an improved algorithm for the simulation model. We have also embarked on an experimental study with L S Fire Laboratories to map out the wall heat flux in the ISO Room-Corner Test Method over a range of burner power outputs and diameters. We hope to report on this work in several months.

The second major goal was improvement of the the lateral and downward flame spread model based on the local radiative heat flux distribution. We have skirted this issue since test runs of the model have demonstrated little effect of the lateral and downward spread contributions in the ISO protocol.

1.4.2. Code Improvements

Over time, the code has become more cluttered as more scenarios have been considered. This involves the location, duration, and energy release rate of the burner; and the distribution of the materials on the walls and ceiling of the room. In addition, the input and output of the code has not lent itself to ease of use or analysis. Based on the performance of the code, it appears that it is now time to invest in a structured computer code with graphical output suggestive of

presentation in Figure 1.1 along with other graphs of significance. We propose that this be done with suitable student support having expertise in the computer sciences and programming areas. We think we can secure this resource effectively and economically at the university. Such a streamlined code will become more valuable, and presumably of benefit to the NIST/BFRL program as we procede. We are planning this effort for the third year (98/99) of the study.

1.4.3. Simulation Evaluation

The previous database has included over 30 tests of materials in the ISO or UBC test protocols. We have become aware of several more recent databases that would be available to us in this study. These include full-scale results and bench-scale data to establish the needed material property data. The databases include the following:

1. LSF laboratories, Italy: 12 construction materials, ISO test protocol
2. BRI (Hasemi), Japan: 19 “ “ “
3. NIST/BFRL (Ohlemiller) 1 composite (vinyl ester glass) at nominally 30, 60 and 150 kW, corner test [14]
4. NIST/BFRL (Madrzykowski) 3 exterior siding materials, corner test.

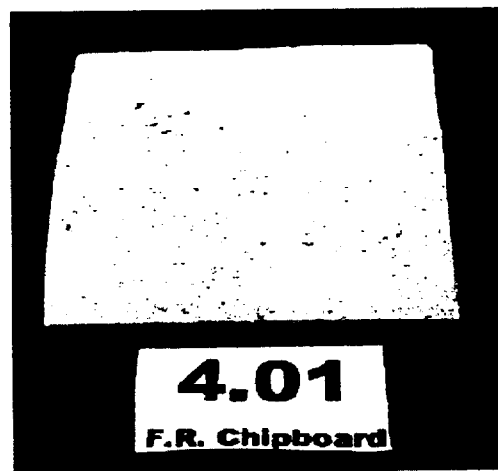
We would also attempt to use other data as available, such as the large 4.9 m high corner tests of the EUREFIC series involving 5 more materials [15]. These databases would bring the entire available set of corner configuration tests to over 70. This interim report will present the results of the LSF database. It should be noted that the materials in that database were selected to challenge the process. Many melt and drip, one is a three-layered hollow structure, and many do not maintain their integrity with the wall and ceiling surfaces. We have also processed most of the BRI data and will report on those results in the near future.

2. DESCRIPTION OF MATERIALS

Thirteen materials were provided to the University of Maryland, for prediction of their performance in full-scale tests using a fire growth model. These materials are the same as the ones tested in the Cone Calorimeter and Roland apparatus at the L. S. Fire Laboratories (LSF), Moutano, Italy. Each material was tested five times at four different external heat flux levels—25, 35, 40 and 50 kW/m²—for a total of twenty tests. The energy release rate, heat of combustion and specimen mass with respect to time data from the Cone tests are provided in Appendix A.1. These same materials were also tested using the ISO 9705 room/corner test protocol at the Swedish National Testing and Research Institute, Boras, Sweden [28]. These materials are listed below—the number preceding each material refers to the LSF designation for each material and will be used interchangeably with the full name throughout this report. A brief description of the material properties and the manner in which the samples were mounted for the full-scale room/corner test are provided. All of the materials were conditioned at 20 ± 5 °C prior to the full-scale tests. Photographs of the samples are also provided.

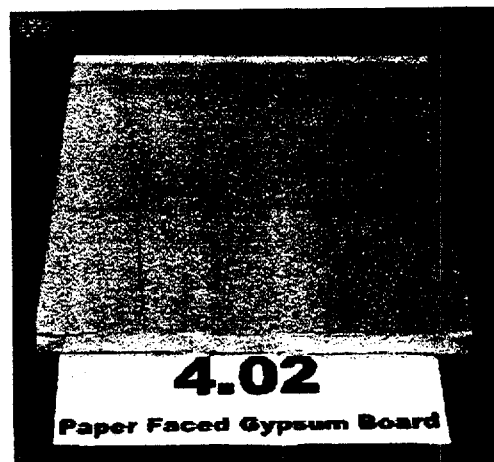
R 4.01 Fire Retarded Chipboard

- Thickness: 12 mm
- Density: 805 kg/m³
- Moisture content: 6.8 %
- Mounting: Nailed to the light weight concrete walls and ceiling.



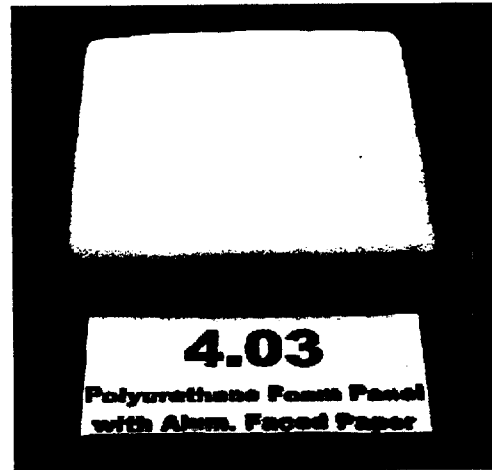
R 4.02 Paper Faced Gypsum Wallboard

- Thickness: 12.5 mm
- Density: 720 kg/m³
- Mounting: Nailed to the light weight concrete walls and ceiling.



R 4.03 Polyurethane Foam Panel with Aluminum Paper Facing

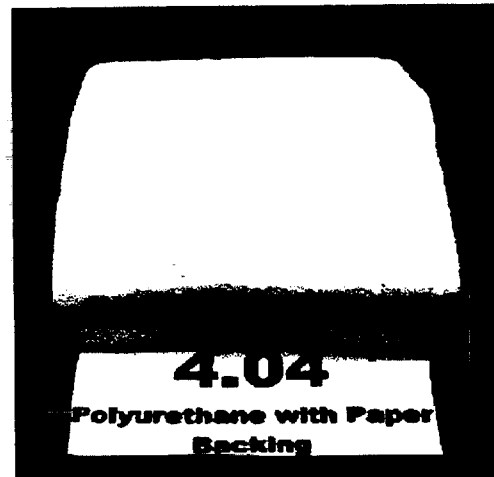
- Thickness: 41 mm
- Density: 38 kg/m³
- Area weight: 2.03 kg/m²
- Mounting: Glued to a non-combustible board called "Promatek H", density 870 kg/m³, with a water based contact adhesive called "Casco 3880". The non-combustible boards were nailed to the light weight concrete walls and ceiling before the polyurethane foam panels were glued.



R 4.04 Polyurethane Foam Panel with Paper Facing

- Thickness: 40 mm
- Density: 38 kg/m³

The properties for this material were used to predict the performance of the polyurethane foam panel with aluminum facing, R 4.03, due to the problems encountered in extrapolating adequate material properties (see Section 3).



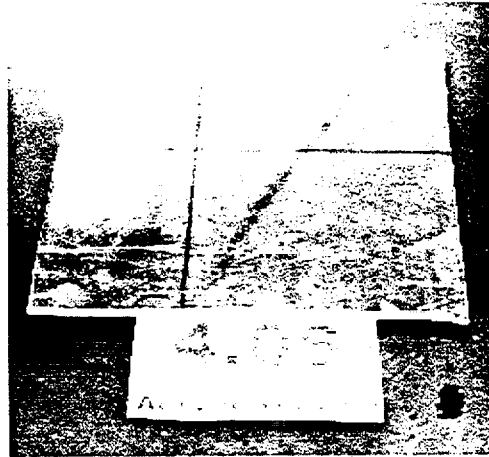
R 4.05 Fire Retarded, Extruded Polystyrene Board (40 mm)

- Thickness: 40 mm
- Density: 33 kg/m³
- Mounting: Glued to a non-combustible board called "Promatek H", density 870 kg/m³, with a water based contact adhesive called "Casco 3880". The non-combustible boards were nailed to the light weight concrete walls and ceiling before the polystyrene boards were glued.



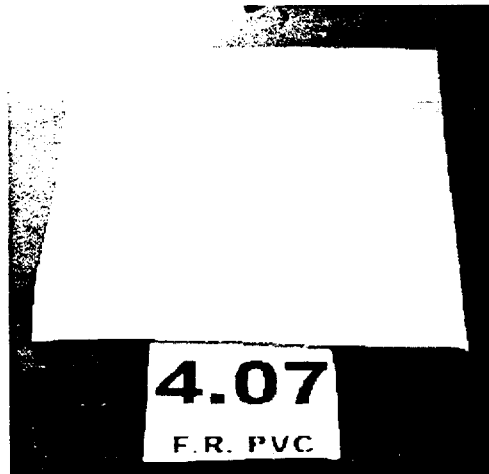
R 4.06 Clear Acrylic Glazing

- Thickness: 3 mm
- Density: 1150 kg/m³
- Mounting: Screwed to a frame of light steel profiles spaced 40 mm from the light weight concrete walls and ceiling.



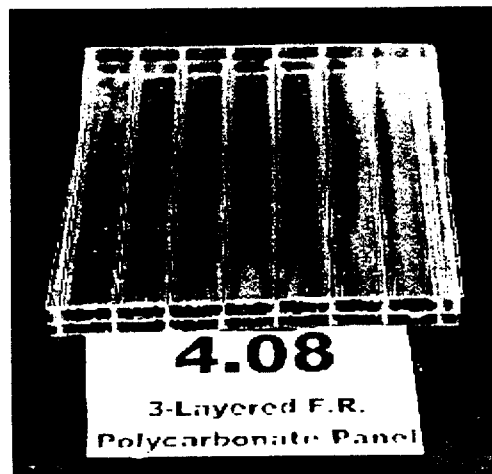
R 4.07 Fire Retarded PVC

- Thickness: 3 mm
- Density: 1505 kg/m³
- Mounting: Screwed to a frame of light steel profiles spaced 40 mm from the light weight concrete walls and ceiling.



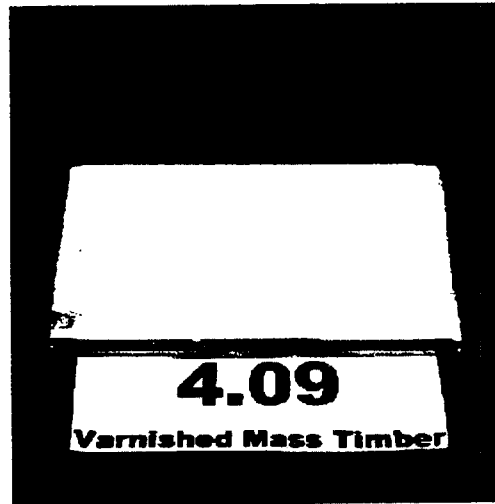
R 4.08 3-Layered Clear, Fire Retarded Polycarbonate Panel

- Thickness: 16 mm
- Density: 1200 kg/m³
- Area weight: 2.9 kg/m²
- Mounting: Screwed to a frame of light steel profiles spaced 40 mm from the light weight concrete walls and ceiling.



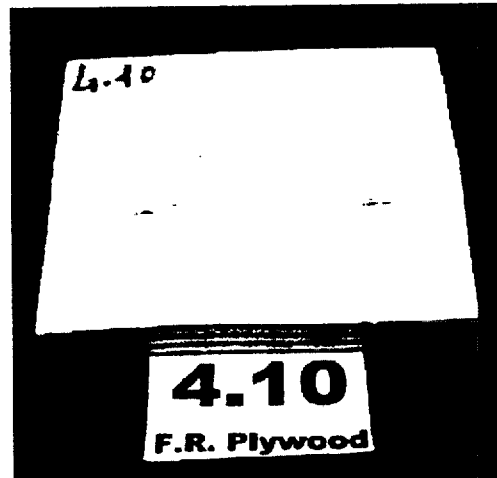
R 4.09 Varnished Massive Timber Paneling

- Thickness: 9 mm
- Area weight: 3.4 kg/m²
- Moisture content: 9.6 %
- Mounting: Nailed to the light weight concrete walls and ceiling.



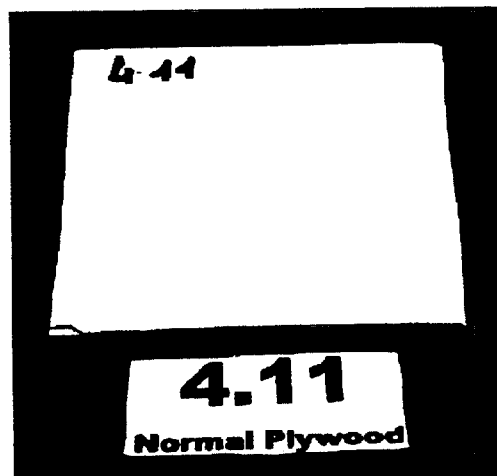
R 4.10 Fire Retarded Plywood

- Thickness: 15 mm
- Density: 460 kg/m³
- Moisture content: 9.8 %
- Mounting: Nailed to the light weight concrete walls and ceiling.



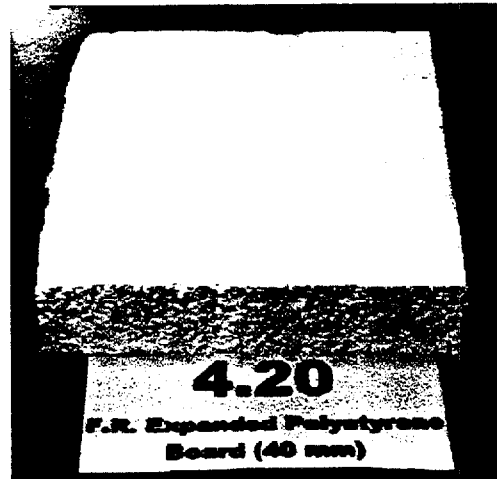
R 4.11 Normal Plywood

- Thickness: 15 mm .
- 440 kg/m³ measured density
- Moisture Content: 11.3 %
- Mounting: Plywood was nailed to the light weight concrete walls and ceiling.



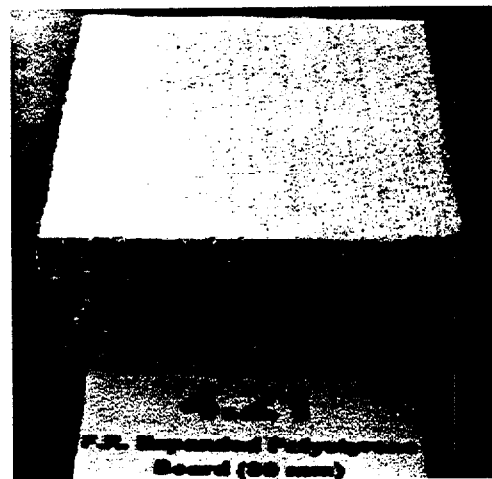
R 4.20 Fire Retarded, Expanded Polystyrene Board (40 mm)

- Thickness: 40 mm
- Density: 30 kg/m³
- Mounting: Glued to a non-combustible board called "Promatek H", density 870 kg/m³, with a water based contact adhesive called "Casco 3880". The non-combustible boards were nailed to the light weight concrete walls and ceiling before the polystyrene boards were glued.



R 4.21 Fire Retarded, Expanded Polystyrene Board (80 mm)

- Thickness: 80 mm
- Density: 17 kg/m³
- Mounting: Glued to a non combustibile board called "Promatek H", density 870 kg/m³, with a water based contact adhesive called "Casco 3880". The non combustibile boards were nailed to the light weight concrete walls and ceiling before the polystyrene boards were glued.



3. MATERIAL PROPERTIES

The material properties required to run the fire growth model are typically derived from data provided by the Cone Calorimeter (ASTM E-1354, ISO 5660) and the Lateral Ignition and Flame Spread Test (LIFT, ASTM E-1321, ISO 5658). However, for this analysis the flame spread data was provided by the Roland apparatus instead of the LIFT [26]. These modeling properties are listed in Table 3.1.

Table 3. 1: Material Modeling Properties.

Material Property	Symbol	Test Method
1. Ignition Temperature	T_{ig}	Cone, LIFT or Roland
2. Minimum Temperature for Lateral Flame Spread	$T_{s, min}$	LIFT or Roland
3. Thermal Inertia	$k\rho c$	Cone or LIFT
4. Lateral Flame Spread Parameter	Φ	LIFT or Roland
5. Effective Heat of Combustion	ΔH_C	Cone
6. Effective Heat of Gasification	L	Cone
7. Total Energy per Unit Area	Q''	Cone

Previous analyses of the performance of materials have used inconsistent methods for determining the material properties. Therefore a more systematic method for accurately determining these properties will be developed. This systematic method will then be applied to all of the materials and used to predict the performance in the full-scale room/corner test.

3.1 Ignition Properties

From ignition data we seek to determine the properties: (1) $k\rho c$, thermal inertia; and (2) T_{ig} , ignition temperature. The LSF Cone Calorimeter data consists of five repeat tests at irradiance levels of 25, 35, 40 and 50 kW/m². No effort was made to determine the critical irradiance for ignition (\dot{q}_α'') by experimental trial and error. Consequently, this value was found by extrapolation.

A modification of the ASTM E-1321 (LIFT) procedure was used to find $k\rho c$ and T_{ig} . However, since \dot{q}_α'' was not explicitly part of the data set, a variation of the procedure was used. Background information needed to support this variation is presented below in terms of some new theoretical results.

The radiative heating of a semi-infinite solid undergoing Newtonian cooling, $h(T_{ig} - T_\infty)$, results in a surface temperature:

$$T_s - T_\infty = \frac{\dot{q}_i''}{h} \left(1 - \exp(\tau) \operatorname{erfc} \sqrt{\tau} \right) \quad (3.1)$$

where

$$\tau = h^2 t / (k\rho c),$$

and

\dot{q}_i'' is the incident heat radiative heat flux,

h is the cooling coefficient for linearized heat losses to the environment at temperature, T_∞ .

For \dot{q}_i'' very large, or τ small

$$1 - \exp(\tau) \operatorname{erfc} \sqrt{\tau} \approx (\pi \tau / 4)^{1/2}. \quad (3.2)$$

Consequently for this limit condition, the ignition time (t_{ig}) is found when T_s attains T_{ig} :

$$t_{ig} = \frac{\pi}{4} k\rho c \frac{(T_{ig} - T_\infty)^2}{\dot{q}_i''}. \quad (3.3)$$

In general, the net heat flux at the surface can be expressed as

$$\dot{q}'' = \dot{q}_i'' - h_c (T_s - T_\infty) - \sigma (T_s^4 - T_\infty^4) \quad (3.4)$$

where the surface emissivity and absorptivity have been taken as unity. The radiation from the environment appears if the surface can fully view the surroundings at the environment temperature. For the Cone Calorimeter, we ignore this term because the heater element covers most of the space above the sample. Janssens [8] includes this term in his analysis. From the integral analysis of Quintiere and Iqbal [15] it is shown for T_∞ as the initial and environment temperature that

$$\frac{d}{dt} \int_0^\delta (T - T_\infty) dx = \dot{q}'' \quad (3.5)$$

where δ is a thermal penetration depth. Selecting an approximate temperature profile as

$$T - T_\infty = \frac{\dot{q}'' \delta}{2k} \left(1 - \frac{x}{\delta}\right)^2 \quad (3.6)$$

gives upon substitution

$$\frac{d}{dt} (\dot{q}'' \delta^2) = 6 \frac{k}{\rho c} \dot{q}'' \quad (3.7)$$

Originally this equation was solved by ignoring the time dependence on \dot{q}'' , here an improved solution can be obtained by approximating

$$\int_0^t \dot{q}'' dt \approx \left[\frac{\dot{q}''(t) + \dot{q}''(0)}{2} \right] t \quad (3.8)$$

From Eq. (3.4), $\dot{q}''(0) = \dot{q}_i''$. Therefore, integrating Eq. (3.7) gives

$$\delta^2 = 3\alpha \left[\frac{2 - \beta(T_s)}{1 - \beta(T_s)} \right] t \quad (3.9a)$$

where

$$\beta(T_s) = \frac{[\sigma(T_s^4 - T_\infty^4) + h_c(T_s - T_\infty)]}{\dot{q}_i''} \quad (3.9b)$$

Letting $T_s = T_{ig}$ and $x = 0$, Eqns. (3.6) and (3.9) give a solution for the ignition time as

$$t_{ig} = \frac{4}{3} k\rho c \left(\frac{1 - \beta}{2 - \beta} \right) \left(\frac{T_{ig} - T_\infty}{\dot{q}''(T_{ig})} \right)^2 \quad (3.10a)$$

where

$$\dot{q}''(T_{ig}) = \dot{q}_i'' - \sigma(T_{ig}^4 - T_\infty^4) - h_c(T_{ig} - T_\infty) \quad (3.10b)$$

and

$$\beta = \frac{\sigma(T_{ig}^4 - T_\infty^4) + h_c(T_{ig} - T_\infty)}{\dot{q}_i''} = \frac{\dot{q}_\alpha''}{\dot{q}_i''} \quad (3.10c)$$

As $\beta \rightarrow 0$ for \dot{q}_{ig}'' large, the coefficient in Eq. (3.10a) is 2/3 compared to $\pi/4$ in the more exact result of Eq. (3). Atreya [2] found by a similar integral analysis that this coefficient depends on

kW/m², respectively.

According to the above theory, the critical flux for ignition occurs where $t_{ig} \rightarrow \infty$ and therefore, $\beta = 1$ and

$$\dot{q}_{\alpha}^{\cdot} = \sigma (T_{ig}^4 - T_{\infty}^4) + h_c (T_{ig} - T_{\infty}) \equiv h (T_{ig} - T_{\infty}) . \quad (3.11)$$

In general, Eq. (3.10a) can be written as

$$t_{ig} = C \text{ kpc} \frac{(T_{ig} - T_{\infty})^2}{(\dot{q}_i^{\cdot} - \dot{q}_{\alpha}^{\cdot})^2} \quad (3.12)$$

where C, depends on \dot{q}_i^{\cdot} or β , approaching $\pi/4$ for large \dot{q}_i^{\cdot} .

A plot of ignition data as $t_{ig}^{-1/2}$ versus \dot{q}_i^{\cdot} can yield information to obtain kpc and T_{ig} . The intercept at $t_{ig}^{-1/2} = 0$ gives $\dot{q}_i^{\cdot} = \dot{q}_{\alpha}^{\cdot}$. From Eq. (3.11) and with an experimental value determined for the critical heat flux, then T_{ig} can be found. The slope of the data, $[(C \text{ kpc})^{1/2} T_{ig} - T_{\infty}]^{-1}$, gives kpc. Here we have used $C = \pi/4$ for the case of large \dot{q}_i^{\cdot} . Figure 3.1 illustrates this for ignition data of fiberboard taken in the LIFT apparatus with $h_c = 15 \text{ W/m}^2\text{-K}$. The critical flux of 16 kW/m^2 gives T_{ig} of $394 \text{ }^{\circ}\text{C}$ and $\text{kpc} = 1.1 (\text{kW/m}^2\text{-K})^2\text{-s}$. Alternatively, kpc can be determined as in the ASTM E-1321 procedure from the slope of data on a plot of $\dot{q}_{\alpha}^{\cdot} / \dot{q}_i^{\cdot}$ versus $t_{ig}^{1/2}$. In implementing the procedure illustrated in Figure 3.1 for Cone data, we estimated the intercept on the horizontal axis by extrapolating the low flux data, and develop kpc from the slope of the high flux data. For the Cone, we selected $h_c = 10 \text{ W/m}^2\text{-K}$ [5].

Janssens [8] recommended an empirical alternative to Eq. (12) which is

$$\frac{\dot{q}_i^{\cdot}}{\dot{q}_{\alpha}^{\cdot}} = 1 + 0.73 \tau_{ig}^{-0.547} \quad (3.13)$$

where τ_{ig} is given in Eq. (3.1) with h defined in Eq. (3.11). A plot of $t_{ig}^{-.547}$ versus incident heat flux will give the critical flux as the zero intercept on the horizontal axis.

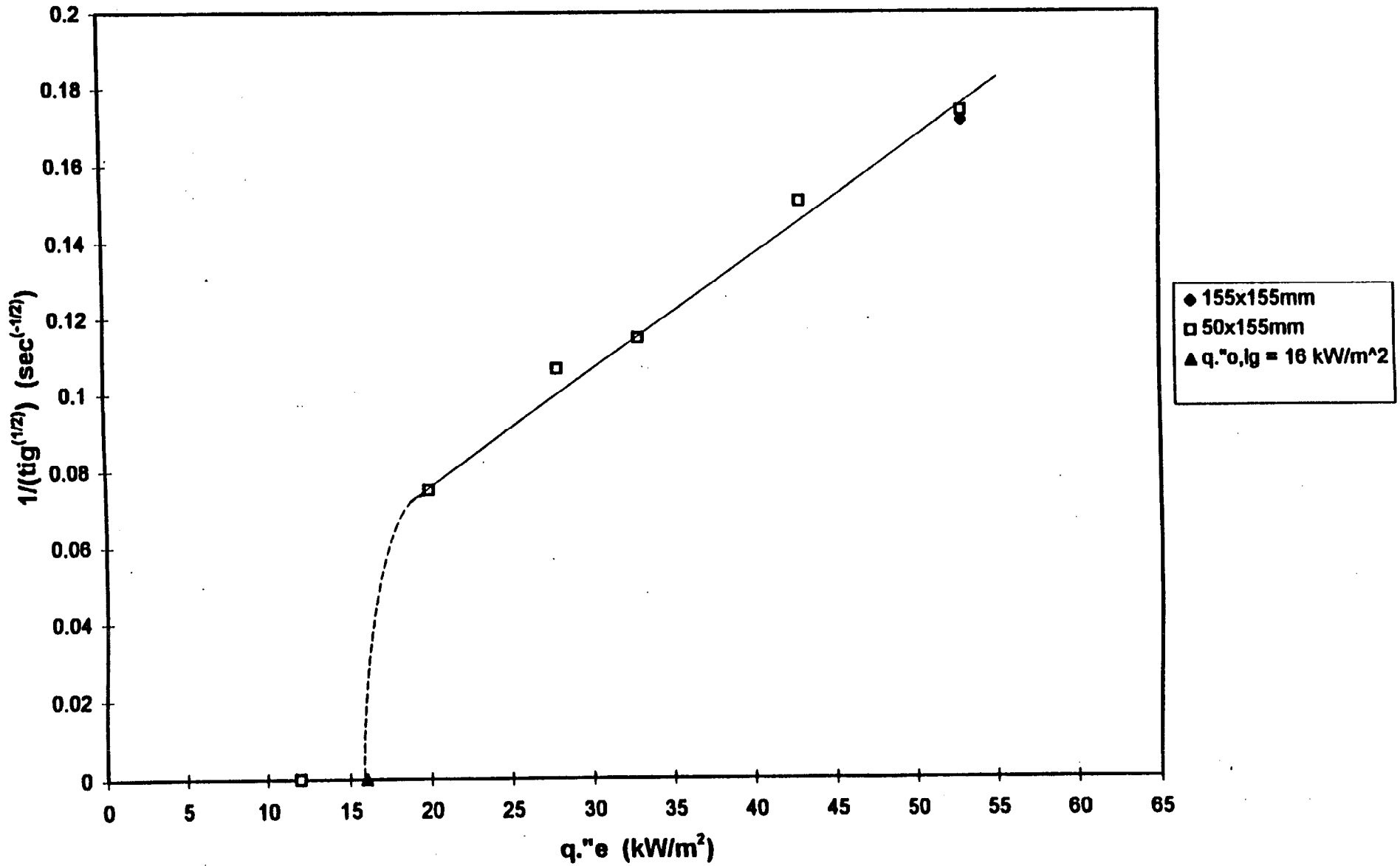
Table 3.1 gives a comparison of the values for the critical flux by Eqns. (3.12) and (3.13). We adopted the results using Eq. (3.12), but as can be seen the two estimates in Table 3.1 are very similar. The figures showing the data and selected curve fits are shown in Appendix A.3: Ignition Data.

Table 3.2
Estimated Critical Flux for Ignition

<u>Material</u>	<u>Eq. (12)</u> (kW/m ²)	<u>Eq. (13)</u> (kW/m ²)
R401 FR CHIP	25	25
R402 GYPSUM	26	24
R403 PUR+AL	--	--
R404 PUR+PAPER	6	8
R405 XPS40	7	7
R406 ACRYLIC GL	4	3.5
R407 FR PVC	16	15
R407 FR PVC	16	15
R408 FR POLYCARB	24	23
R409 MASS TIMBER	10	11
R410 FR PLY	22	21
R411 PLY	8	7
R420 EPS40	8	7
R421 EPS80	23	23

1/(sqrt t_{ig}) vs. External Heat Flux
7-Q1 medium density Fiberboard

16



3.2 Flame Spread Properties

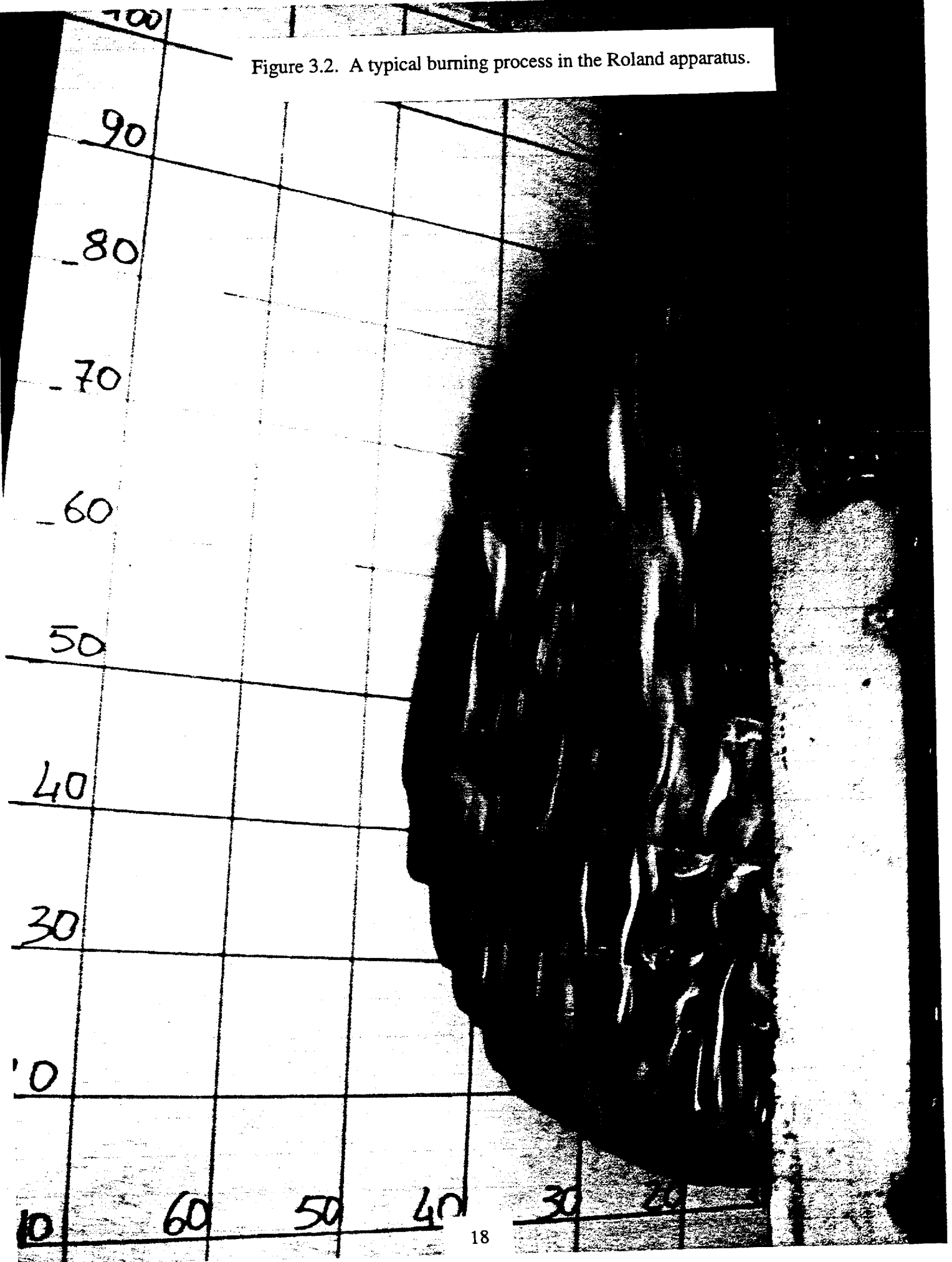
Property data on lateral and downward flame spread were not obtained using the procedure of ASTM E 1321 (LIFT), but the apparatus of LSF designated as the Roland Intermediate Fire Test. This device consists of a small (ASTM E 162) radiant panel inclined at 35 degrees and 100 mm from 1 m x 1.5 m high specimen. The incident heat flux varies from about 40 kW/m² near the heater and decreases to about 1 kW/m² laterally and about 10 kW/m² downward. Flame spread rates are measured in the lateral and downward directions at positions of known heat flux much like in ASTM E 1321. Figure 3.2 displays a typical flame spread process in the Roland apparatus. The governing equation for the flame spread velocity, V , is given by

$$V = \frac{\Phi}{k\rho c (T_{ig} - T_s)^2} \quad (3.14)$$

where Φ is the flame heating parameter, and T_s is the local temperature caused by the incident heat flux. T_{ig} and $k\rho c$ are determined from the ignition data of the Cone Calorimeter (Section 3.1). For materials which melt and drip, the downward flame spread can be considerably influenced by these effects. For non-melting materials, the lateral and downward properties are expected to be comparable. However, the range on spread data recordable for downward spread is small and insufficient to give accurate results for Φ . In addition, melting materials could influence lateral spread as well since a trough at the bottom of the specimen could collect the flaming melt and drips. In particular, the polystyrene materials exhibited such behavior to the extent that nearly two modes of lateral spread could be perceived: one due to surface flame spread, the other more rapid spread due to the propagation over the melted material in the bottom drip tray. Although this bi-modal spread is an artifact of the apparatus, the same behavior is exhibited in the room-corner test for the wall material. Needless to say, the melting, dripping, swelling and delaminating effects of the materials can have a profound effect on flame spread both in the apparatus and in the end-use condition. In our room-corner fire simulation model, we will only use the properties associated with lateral spread in the Roland apparatus.

The details of the analysis of the Roland data were done by Su [18] and can be found in Appendix B. Downward and Lateral Flame Spread in Roland Apparatus Phase 5. A summary of the flame spread and ignition property data are shown in Table 3.2.

Figure 3.2. A typical burning process in the Roland apparatus.



The ignition and flame spread properties were derived by the methods above and are presented in Table 3.3.

Table 3. 3: Ignition and Flame Spread Properties of the LSF Materials.

Material	T_{ig} (°C)	$T_{s,min}$ (°C)	$k\rho c$ [(kW/m ² K) ² s]	ϕ (kW ² /m ³)
R 4.01, FR. Chipboard	505	507	4.024	0.0
R 4.02, Gypsum	515	517	0.549	0.0
R 4.03, PU/Alum.*	---	---	---	0.0
R 4.04, PU/Paper	250	77	0.199	8.7
R 4.05, Ext. PS40	275	77	1.983	1.2
R 4.06, Acrylic	195	195	2.957	---
R 4.07, FR. PVC	415	352	1.306	0.2
R 4.08, 3-Layer PC	495	167	1.472	0.0
R 4.09, Mass Timber	330	77	0.530	6.9
R 4.10, FR. Plywood	480	197	0.105	0.7
R 4.11, Plywood	290	147	0.633	2.2
R 4.20, Exp. PS40	295	77	1.594	4.2
R 4.21, Exp. PS80	490	77	0.557	7.1

* Material properties could not be extrapolated from the test data

3.4 Heat of Combustion (ΔH_C)

Definition

The enthalpy of combustion or heat of combustion (ΔH_C) is a constant material property, representing the total amount of energy released by a unit mass of fuel (kJ/g) when it is completely oxidized through the combustion process. Heat of combustion values can be determined using an oxygen bomb calorimeter which forces all of the material to combust in a pure oxygen atmosphere while the vessel temperature and specimen mass loss are carefully monitored. Heat losses from the system are minimized so that the heat release can be accurately determined by the temperature rise. The gross heat of combustion, $\Delta H_{C, gross}$, can then be calculated by dividing the total heat release by the total specimen mass loss. Gross heat of combustion values for many materials are presented by Tewarson [27]. However, complex materials like wood and composites like gypsum wallboard burning in more realistic conditions will not exhibit the gross heat of combustion values obtained in the oxygen bomb. Char formation, moisture evaporation and other complex effects will cause a reduced $\Delta H_{C, gross}$ to be observed. Therefore an effective heat of combustion, $\Delta H_{C, eff}$, which better represents the material burning in actual conditions needs to be determined. This effective value (simply referred to as ΔH_C

for convenience) can be used to determine the energy release rate per unit area from a material based on the mass loss rate by:

$$\dot{Q}'' = \Delta H_c \cdot \dot{m}'' \quad (3.14)$$

where \dot{Q}'' is the energy release rate per unit area (kW/m²) and \dot{m}'' is the mass loss rate per unit area (g/s·m²). In this definition of the effective heat of combustion, \dot{m}'' of a burning material may not represent the mass of the fuel alone and can represent a loss of moisture or other products. This can result in complications in the determination of suitable values for predicting performance.

Determining ΔH_c

The time-varying and average effective heat of combustion were measured by LSF using the Cone Calorimeter. Each material was tested a total of twenty times at 25, 35, 40 and 50 kW/m². The Cone Calorimeter standard [1] specifies the time-varying heat of combustion value to be calculated by

$$\Delta H_c(t) = \frac{\dot{Q}''(t)}{\dot{m}''(t)}$$

where $\dot{Q}''(t)$ and $\dot{m}''(t)$ are the energy release rate and mass loss rate per unit area at time t . Similarly, the average heat of combustion is calculated by

$$\Delta H_c = \frac{Q}{\Delta m} \quad (3.15)$$

where Q is the total energy released during the test and Δm is the total specimen mass loss.

Because ΔH_c is typically considered to be a constant material property, it should not vary with temperature, burning rate or incident heat flux. Nevertheless, the Cone data indicates that the measured heat of combustion values were not constant with respect to time, and in some cases varied significantly throughout the test (see Figure 3.3). These fluctuations are most likely due to complex burning effects and inaccuracies in the oxygen consumption calorimetry method used to determine the values. Therefore three different methods will be utilized for determining constant effective heat of combustion values from the Cone Calorimeter data: based on (1) the peak energy release rate, (2) an average energy release rate around the peak and (3) the overall energy released during the test. Example of these three energy release rates are presented in Figure 3.4.

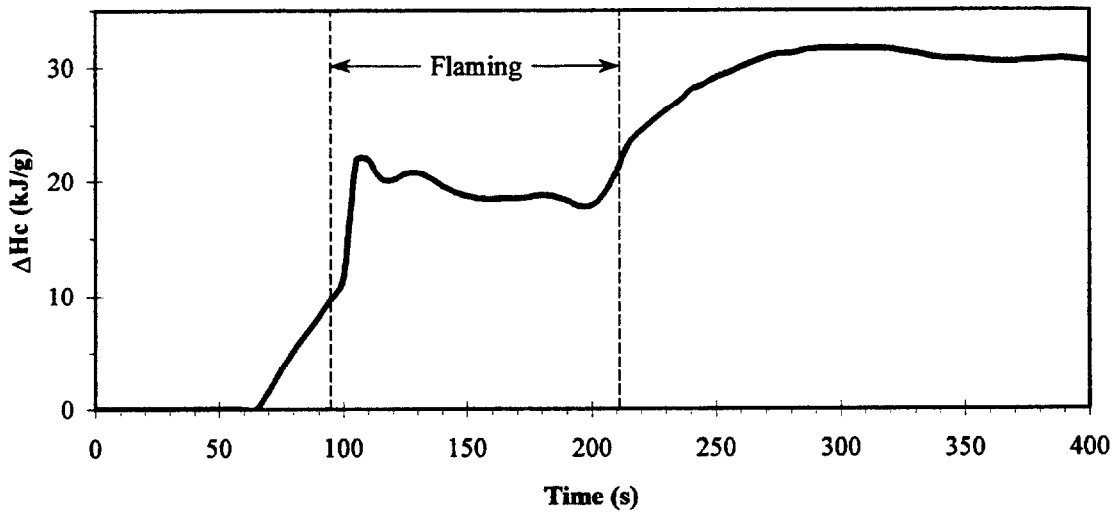


Figure 3. 3: Example of Time-Varying Heat of Combustion Measured in the Cone Calorimeter: R 4.08, 3-Layer Polycarbonate Panel at 50 kW/m^2 .

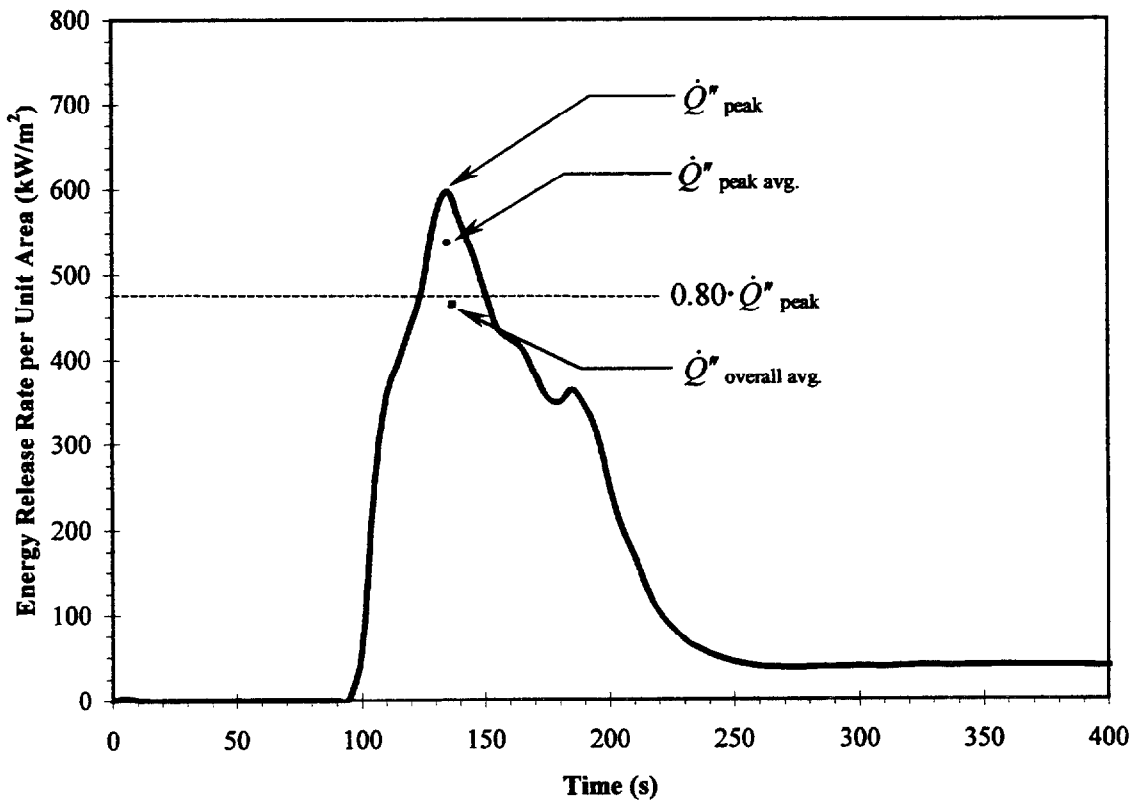


Figure 3. 4: Example of Peak, Peak Average and Overall Average Energy Release Rates per Unit Area Measured in the Cone Calorimeter: R 4.08 at 50 kW/m^2

Due to the fact that not all of the samples ignited or exhibited continuous flaming, only the test data associated with ignition and sustained burning were used to determine the effective ΔH_C values. In a few tests the LSF data reports ignition of a sample, but inspection of the energy release rate versus time graphs clearly indicated that actual sustained flaming did not occur. Data from these types of tests will be omitted from the determination of the heat of combustion values.

Examples of $\Delta H_{C, peak}$, $\Delta H_{C, peak avg.}$ and $\Delta H_{C, overall avg.}$ values are shown graphically in Figure 3.5 and the three effective ΔH_C values for each material are presented in Table 3.4. Theoretically all three of these values should be identical, and as the table indicates there is reasonably good agreement between the values. The three methods for determining ΔH_C are explained below.

1. Peak Rate of Energy Release ($\Delta H_{C, peak}$)

For each Cone test in which the material ignited, a peak or maximum rate of energy release (\dot{Q}''_{peak}) occurs (see Figure 3.4). A heat of combustion value can be determined which directly coincides with the time at which the peak energy release rate occurs (see Figure 3.5). This "peak" value does not represent the maximum heat of combustion that was measured, but in fact represents the heat of combustion value associated with the peak energy releases rate.

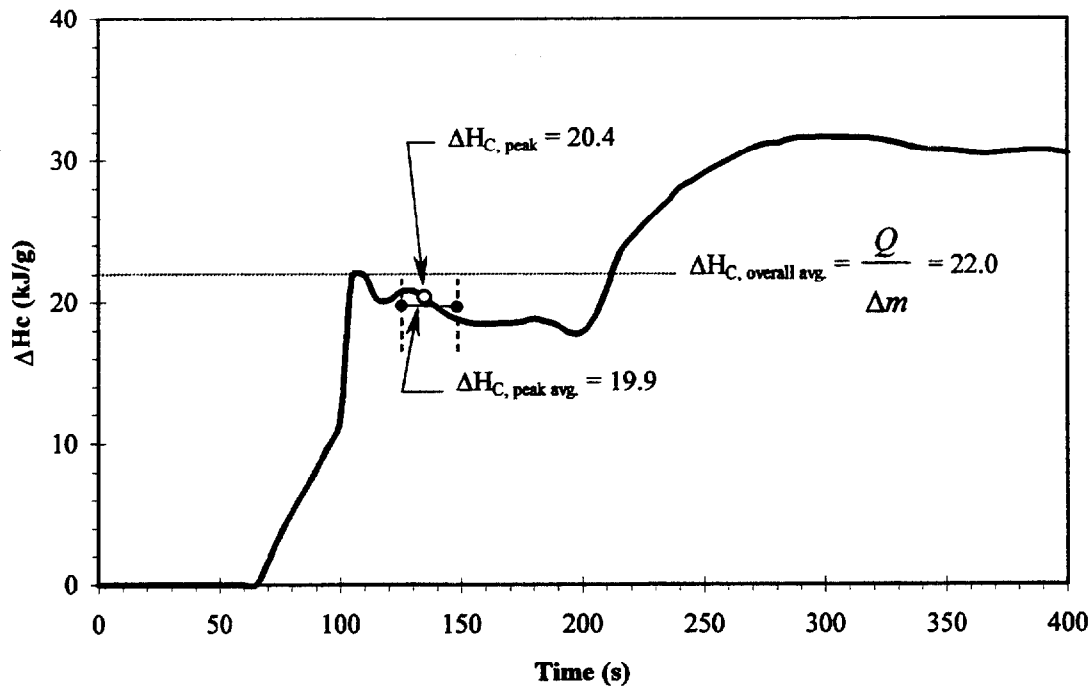


Figure 3.5: Method of Determining the Peak, Peak Average and Overall Average Heat of Combustion Values: R 4.08, 3-Layer Polycarbonate Panel at 50 kW/m².

All of the “peak” heat of combustion values measured for a particular material can then be averaged to determine an average, $\overline{\Delta H_{C, peak}}$, value. When plotted with respect to the external heat flux, the average value represents a horizontal “best-fit” line through the peak value data (see Figure 3.6). These average heat of combustion values are listed in table 3.4. This average peak heat of combustion value can be used in Equation 3.14 to determine the typical peak energy release rate associated with a material.

2. Average Rate of Energy Release ($\Delta H_{C, peak avg.}$)

Another method of using the peak energy release rate as a basis for determining the effective heat of combustion is to take an average energy release rate per unit area around the peak value. For this analysis, it is estimated that an average peak energy release rate occurs approximately 20% below the peak value. Therefore, the $\dot{Q}''_{peak avg}$ shown in Figure 3.4 is an integrated average of the measured energy release rates above 80% of the peak value. The “peak average” value is intended to represent an energy release rate that is more consistent with steady burning as opposed to an instantaneous maximum value. This averaging method reduces the effects of a sudden, possibly uncharacteristic spike in the energy release rate and smoothes the data while still taking into account the most intense burning of the material.

The peak average heat of combustion, $\Delta H_{C, peak avg.}$, is taken to be a numerical average of the measured heat of combustion values over the same time interval that the energy release rate is averaged. The time period over which the heat of combustion values are averaged is illustrated in Figure 3.5. An average value, $\overline{\Delta H_{C, peak avg.}}$, is calculated to be a numerical average of the individual peak average values from each test.

3. Overall Energy Release ($\Delta H_{C, overall avg.}$)

The overall heat of combustion values, $\Delta H_{C, overall avg.}$, were calculated by LSF by dividing the total heat evolved from each sample by the total specimen mass loss, as in Equation 3.15. This is the typical method of determining an effective heat of combustion value by the Cone Calorimeter test standard [1]. This “overall” value represents an average of the burning characteristics over the entire test duration.

As with the previous two methods, the average overall value, $\overline{\Delta H_{C, overall avg.}}$, for a particular material is determined by taking the numerical average of the values calculated from each Cone test.

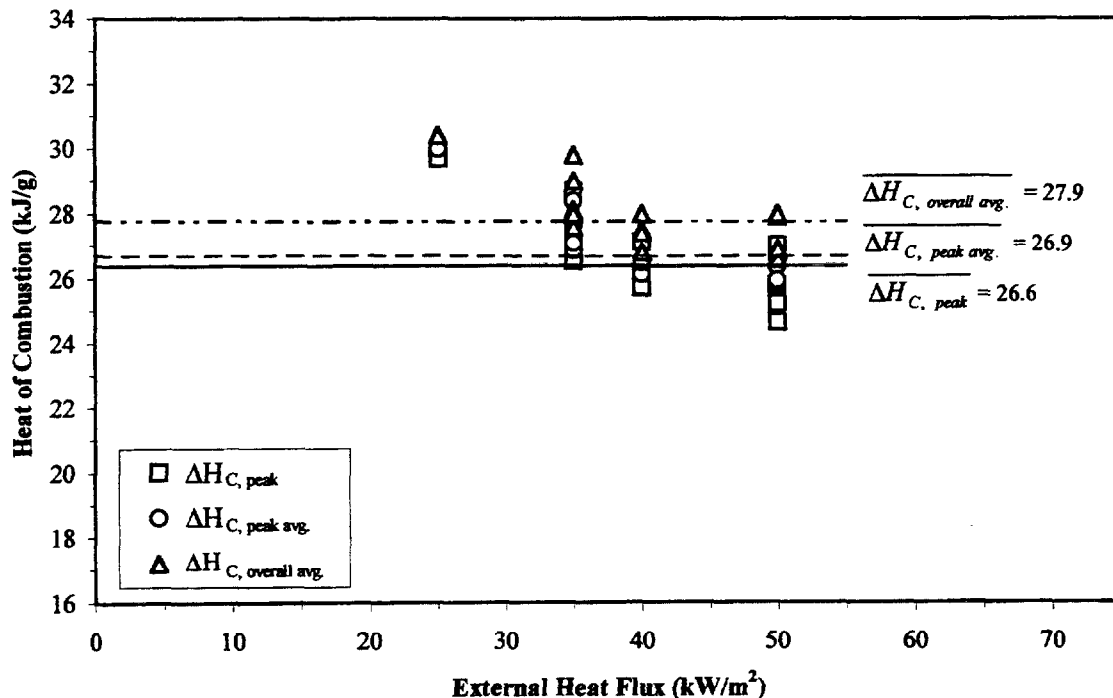


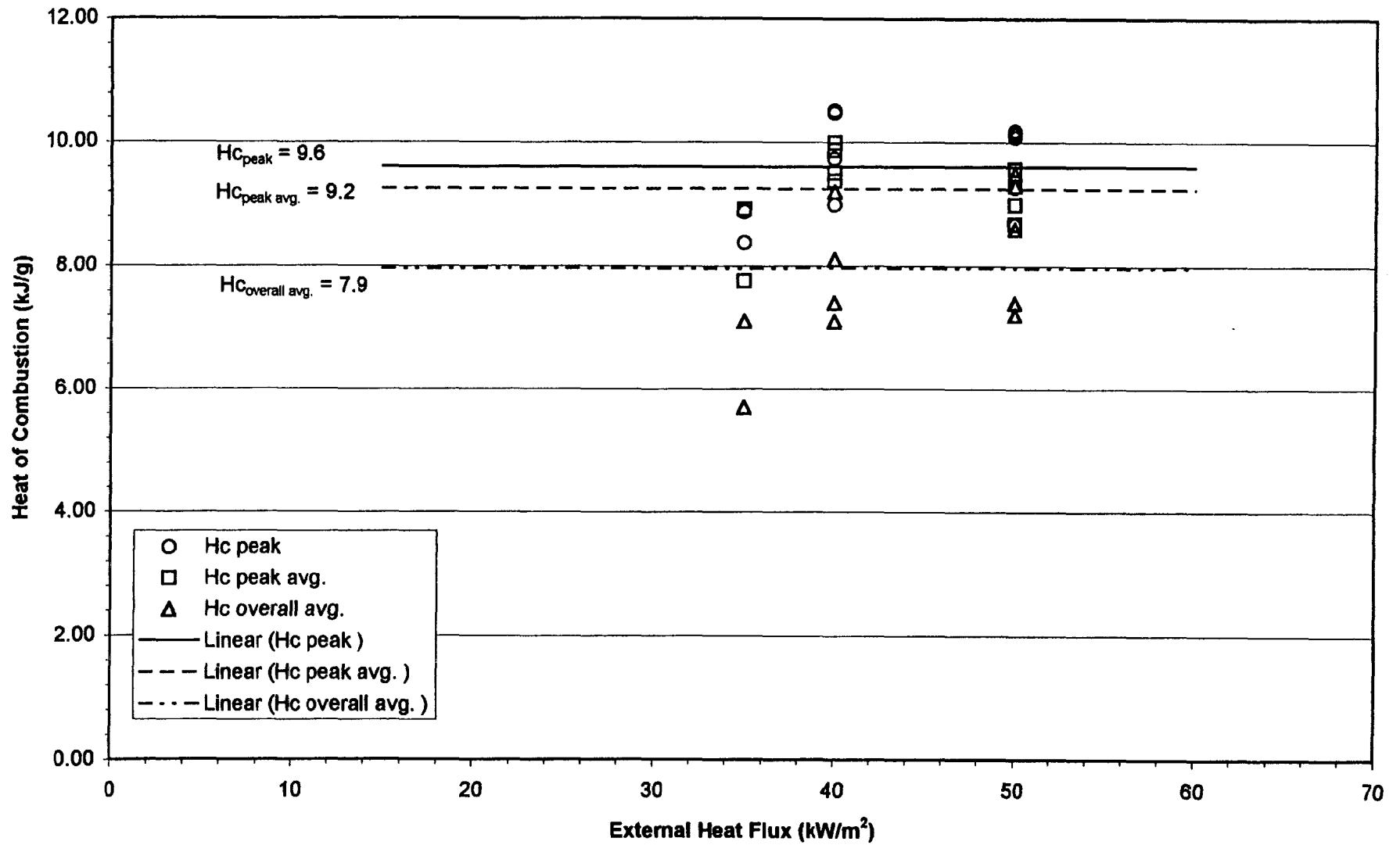
Figure 3. 6: Example of an Average Heat of Combustion ($\overline{\Delta H_C}$) Determination: R 4.08 at 50 kW/m².

Table 3. 4: Average, effective heat of combustion (ΔH_c) values calculated by three methods.

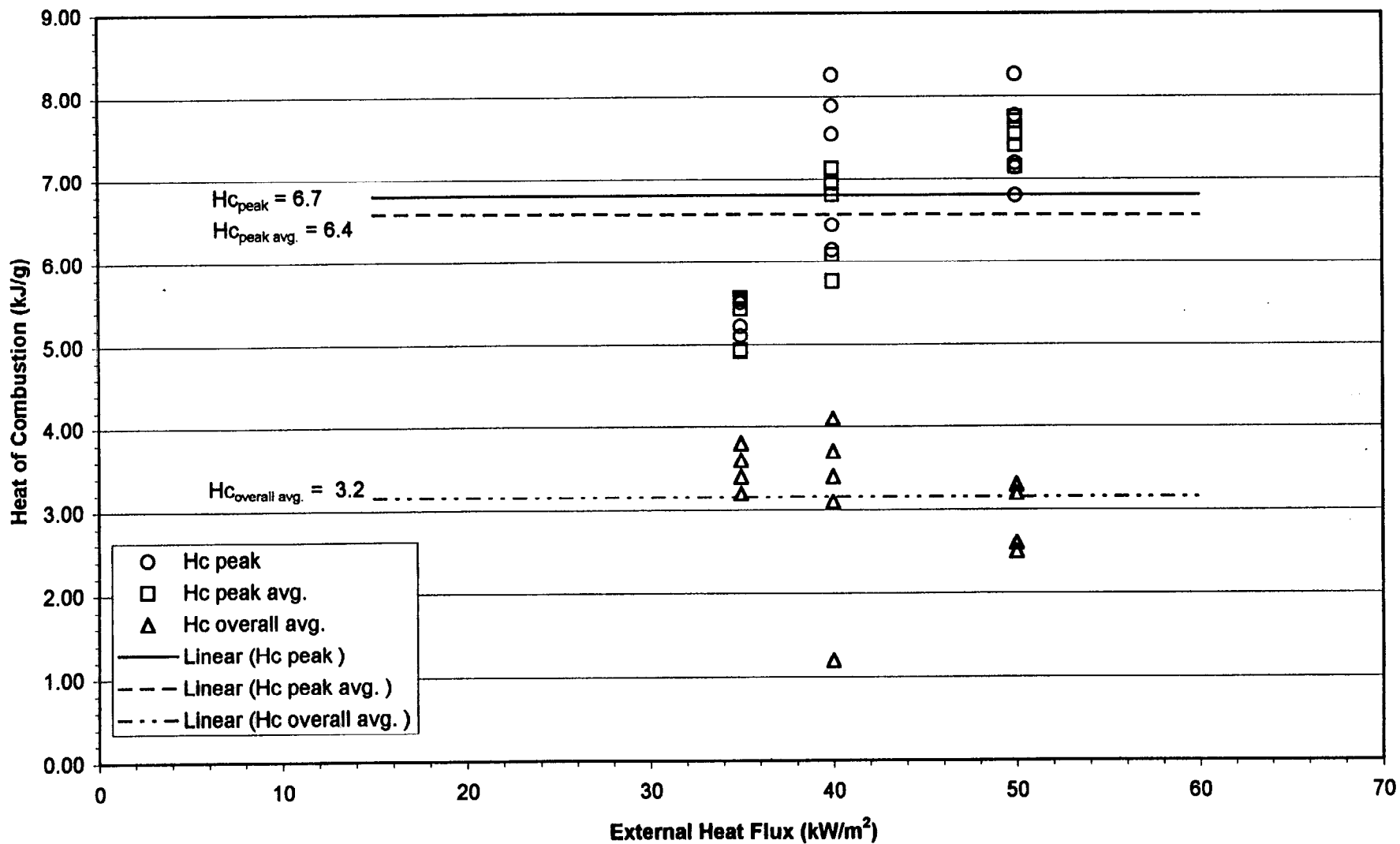
Material	$\overline{\Delta H}_{C, peak}$ (kJ/g)	$\overline{\Delta H}_{C, peak avg.}$ (kJ/g)	$\overline{\Delta H}_{C, overall avg.}$ (kJ/g)
R 4.01, FR. Chipboard	9.6	9.2	7.9
R 4.02, Gypsum	6.7	6.4	3.2
R 4.03, PU/Alum.	16.3	16.3	18.2
R 4.04, PU/Paper	19.3	18.9	18.0
R 4.05, Ext. PS40	28.5	27.8	28.2
R 4.06, Acrylic	24.2	24.1	24.0
R 4.07, FR. PVC	10.2	9.9	6.8
R 4.08, 3-Layer PC	19.5	19.5	21.5
R 4.09, Mass Timber	17.3	16.3	15.7
R 4.10, FR. Plywood	11.6	11.2	10.3
R 4.11, Plywood	12.1	11.9	10.8
R 4.20, Exp. PS40	27.4	27.5	27.8
R 4.21, Exp. PS80	26.6	26.9	27.9

The graphs for determining the average heat of combustion values form Appendix A.4 are presented here.

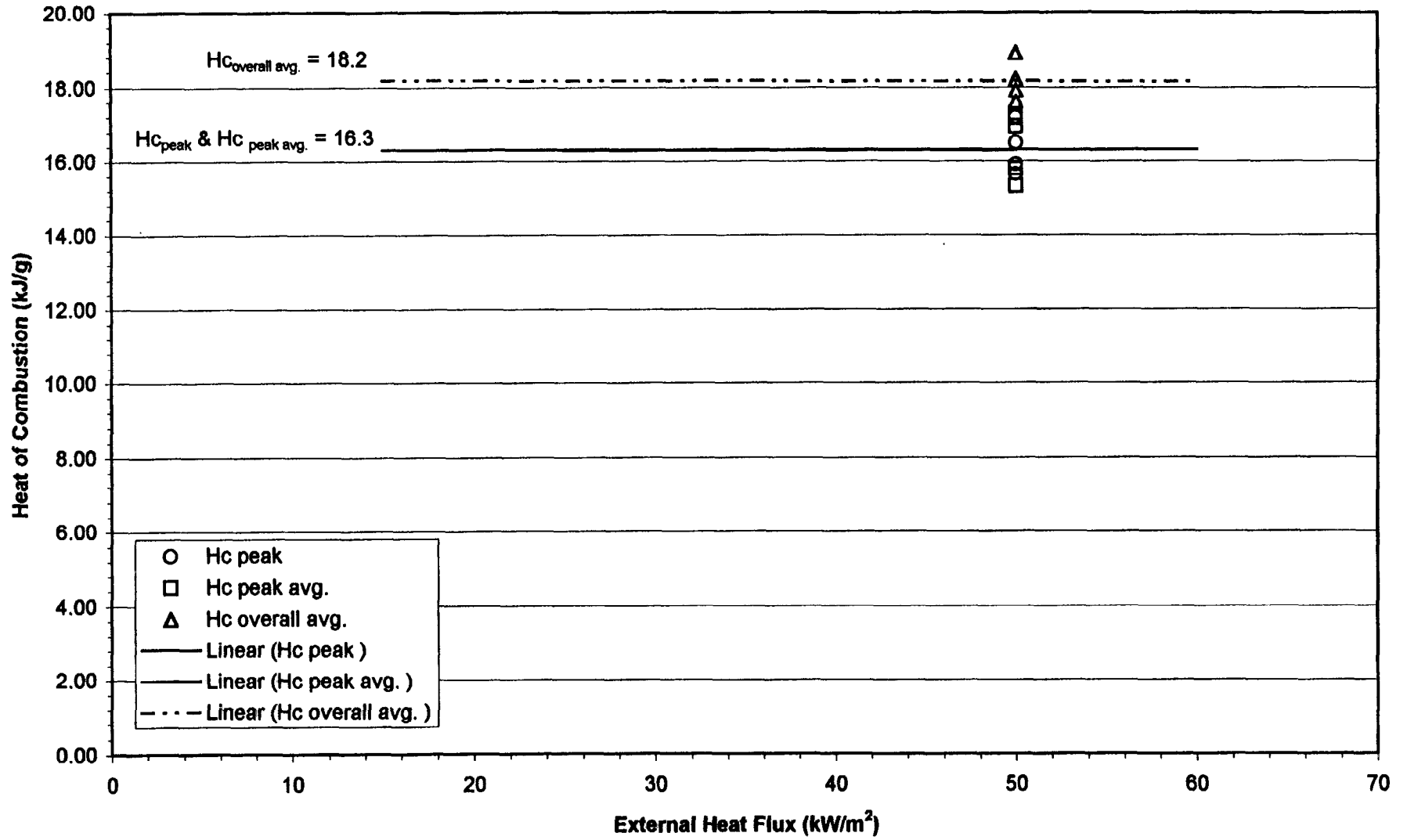
4.01 F.R. Chipboard: Heat of Combustion vs. External Heat Flux



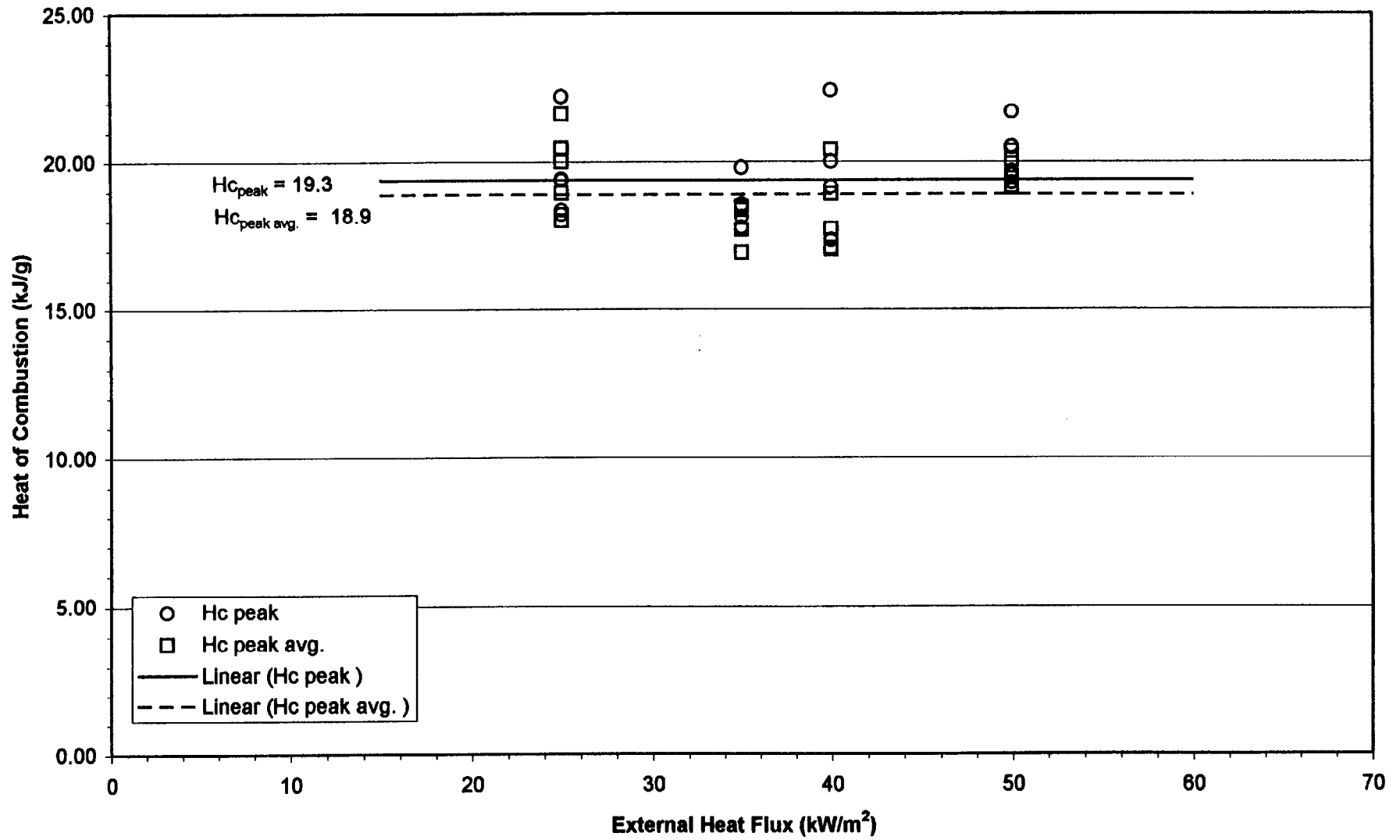
4.02 Paper Faced Gypsum Board: Heat of Combustion vs. External Heat Flux



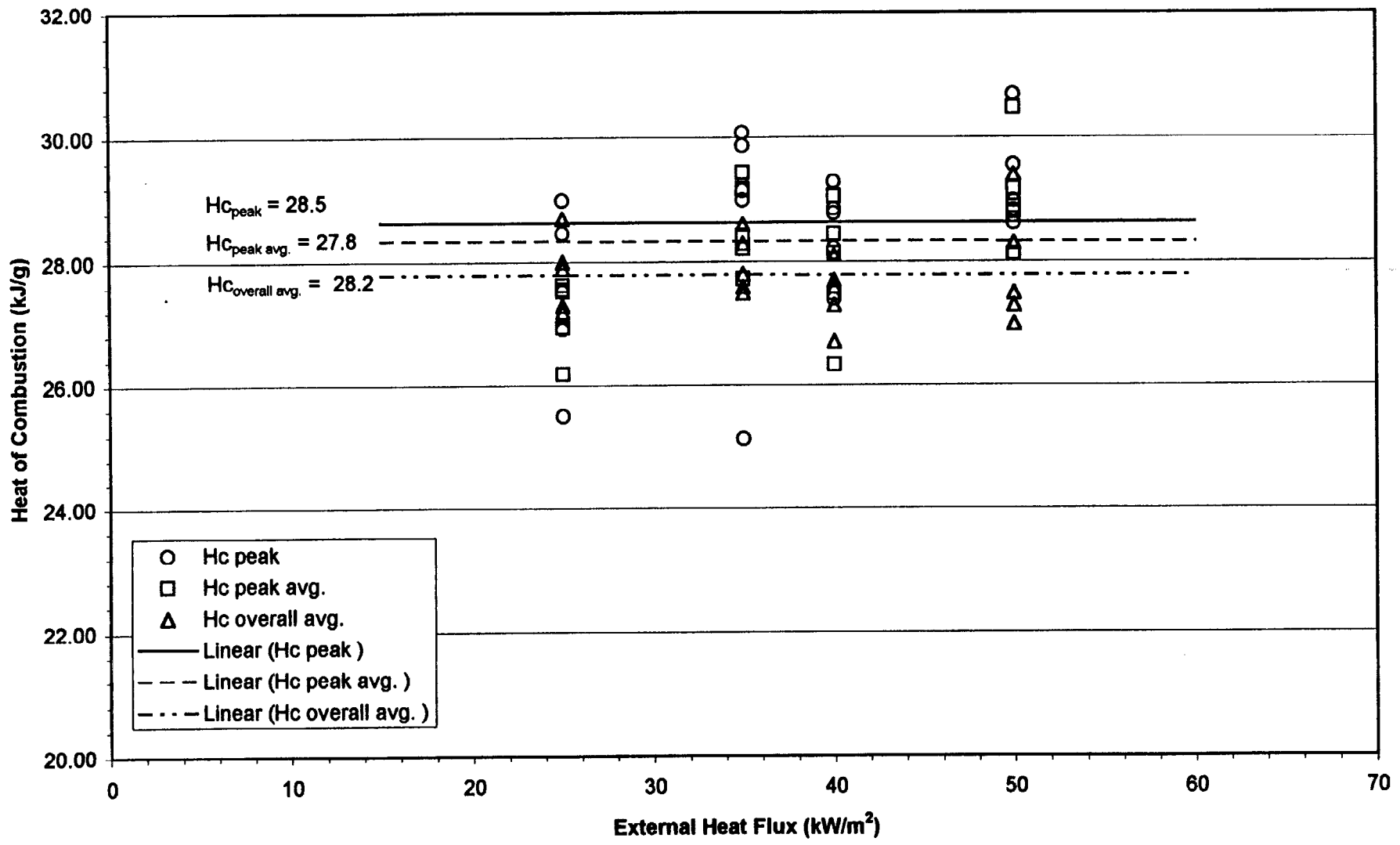
R 4.03 Heat of Combustion vs. External Heat Flux



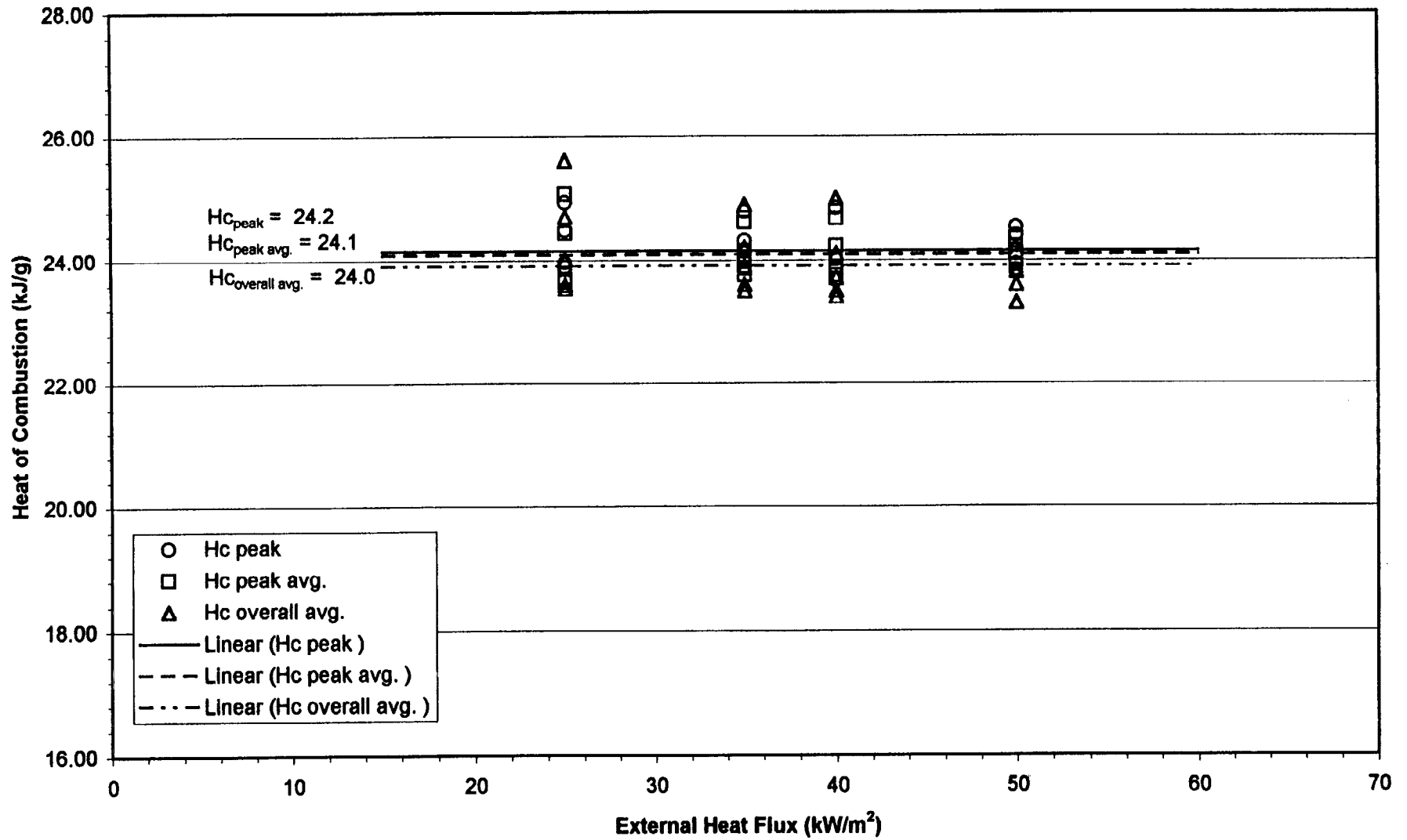
4.04 Polyurethane with Paper Backing: Heat of Combustion vs. External Heat Flux



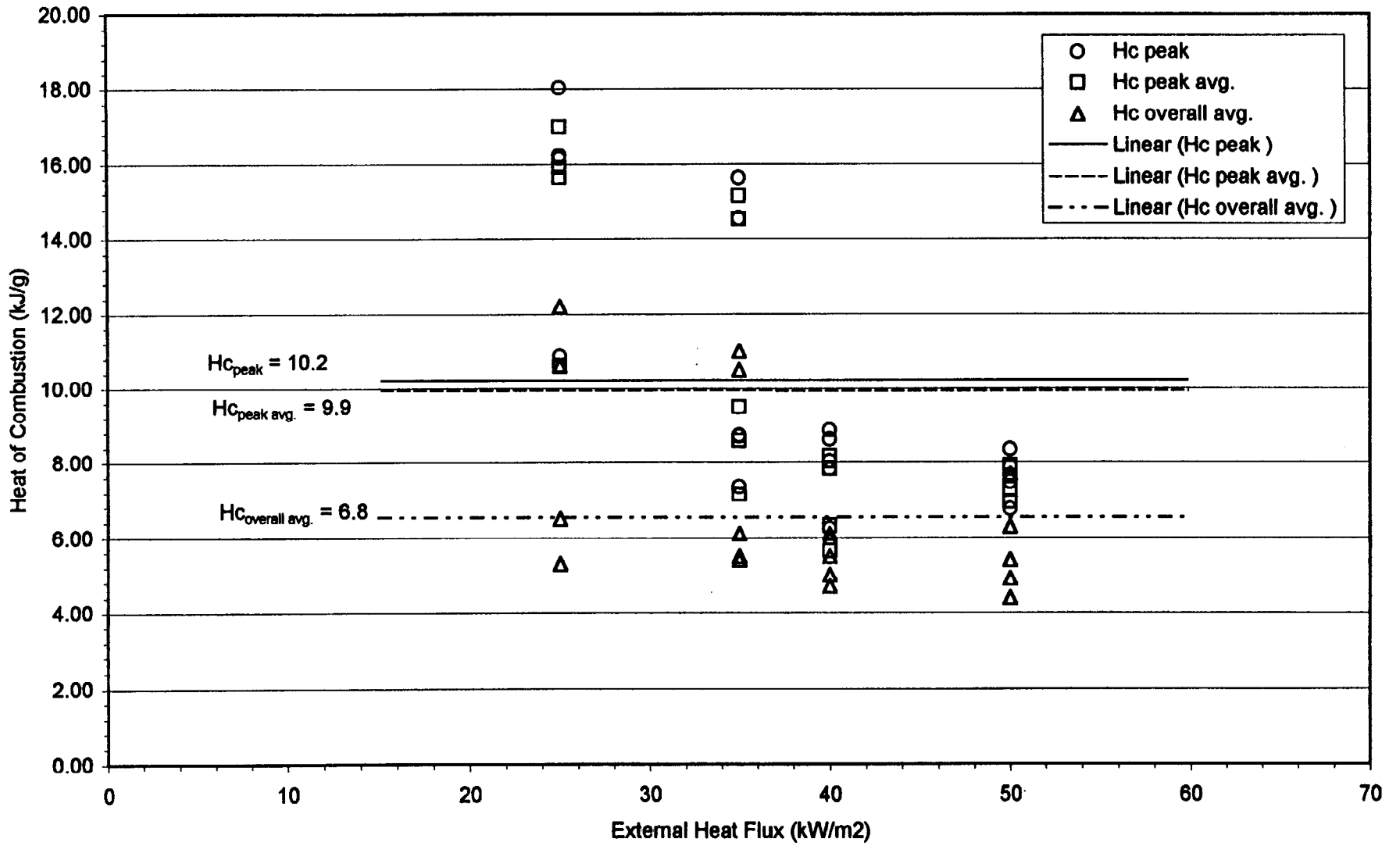
4.05 F.R. Extruded Polystyrene Board (40 mm): Heat of Combustion vs. External Heat Flux



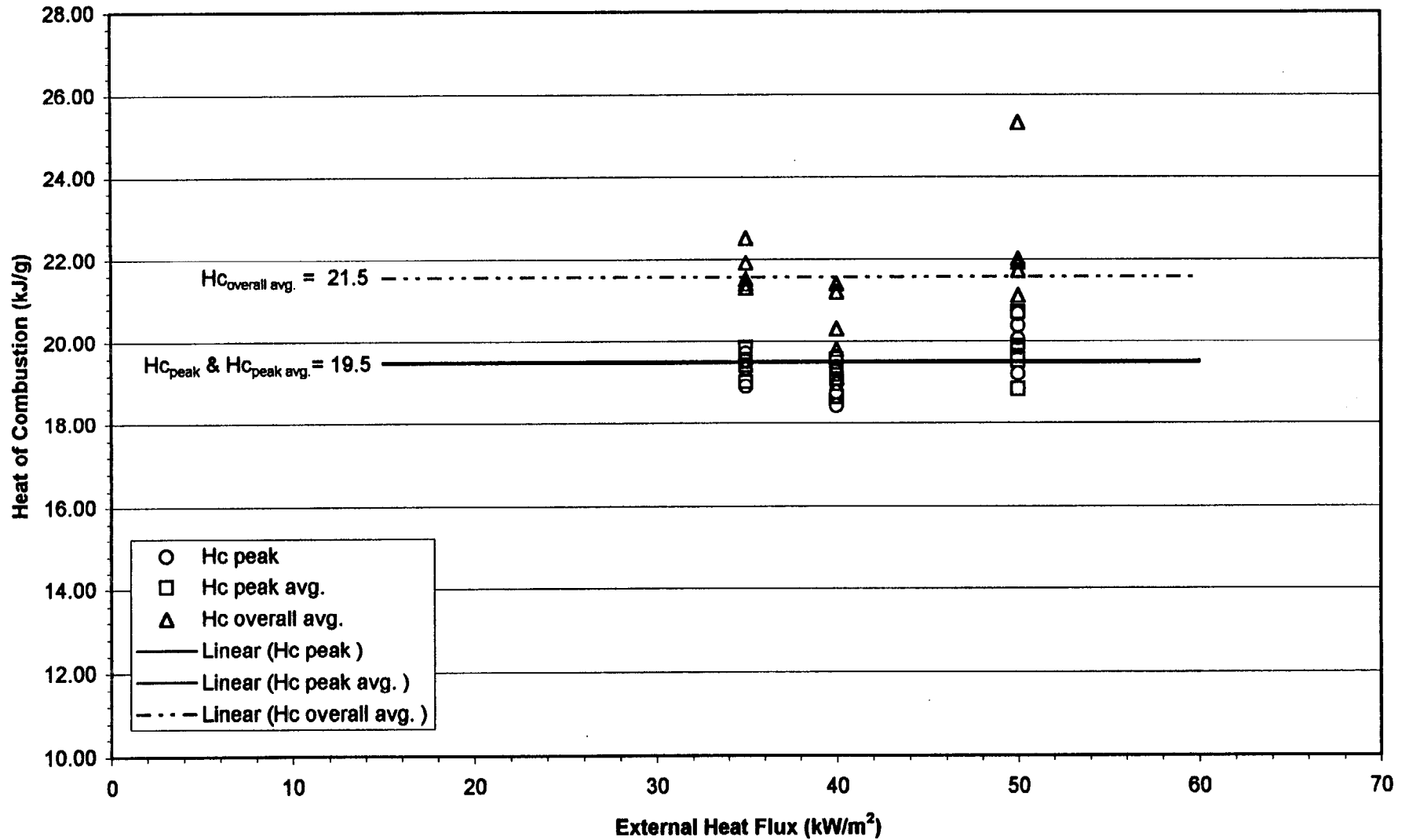
4.06 Acrylic Glazing: Heat of Combustion vs. External Heat Flux



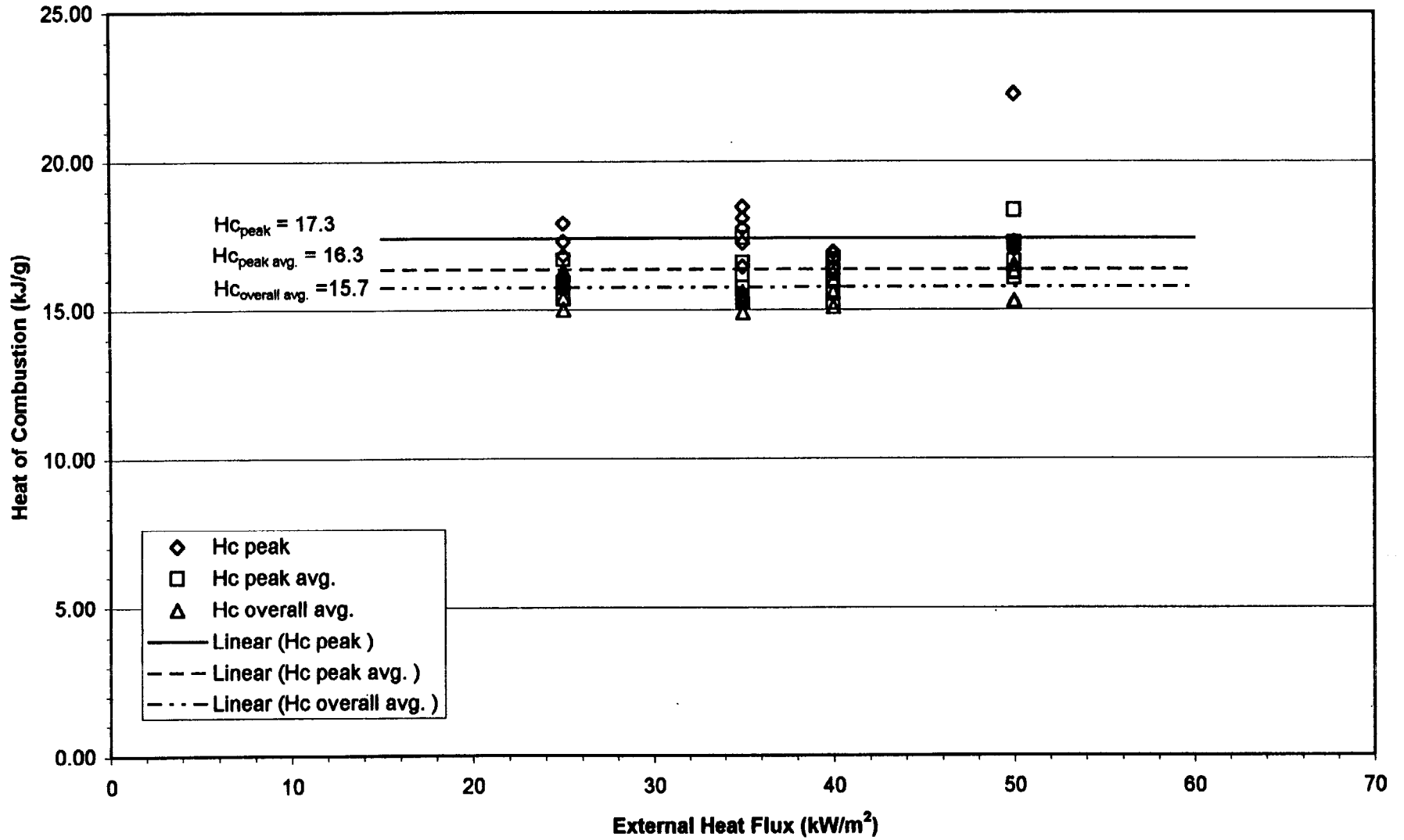
4.07 F.R. PVC: Heat of Combustion vs. External Heat Flux



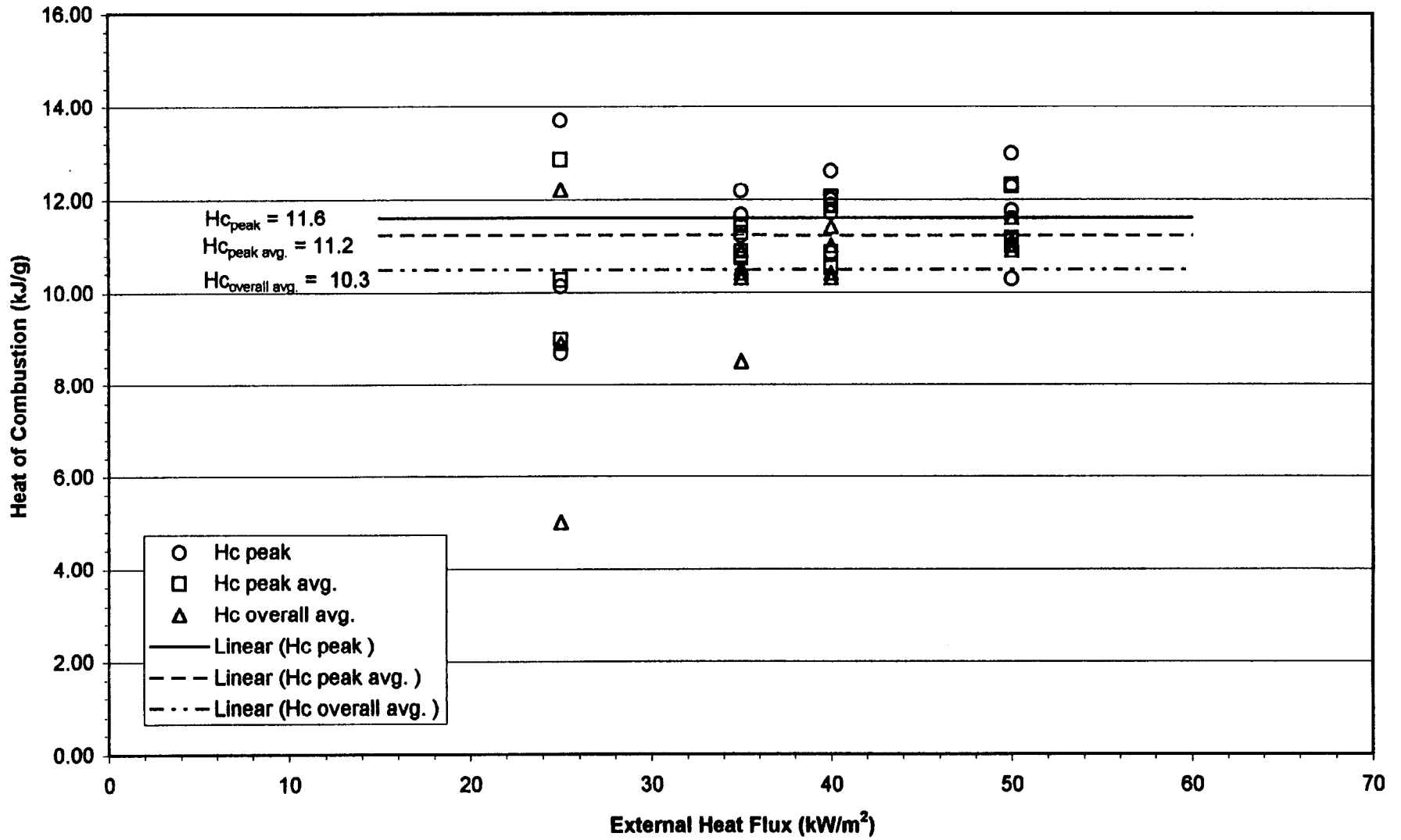
4.08 3-Layered F.R. Polycarbonate Panel: Heat of Combustion vs. External Heat Flux



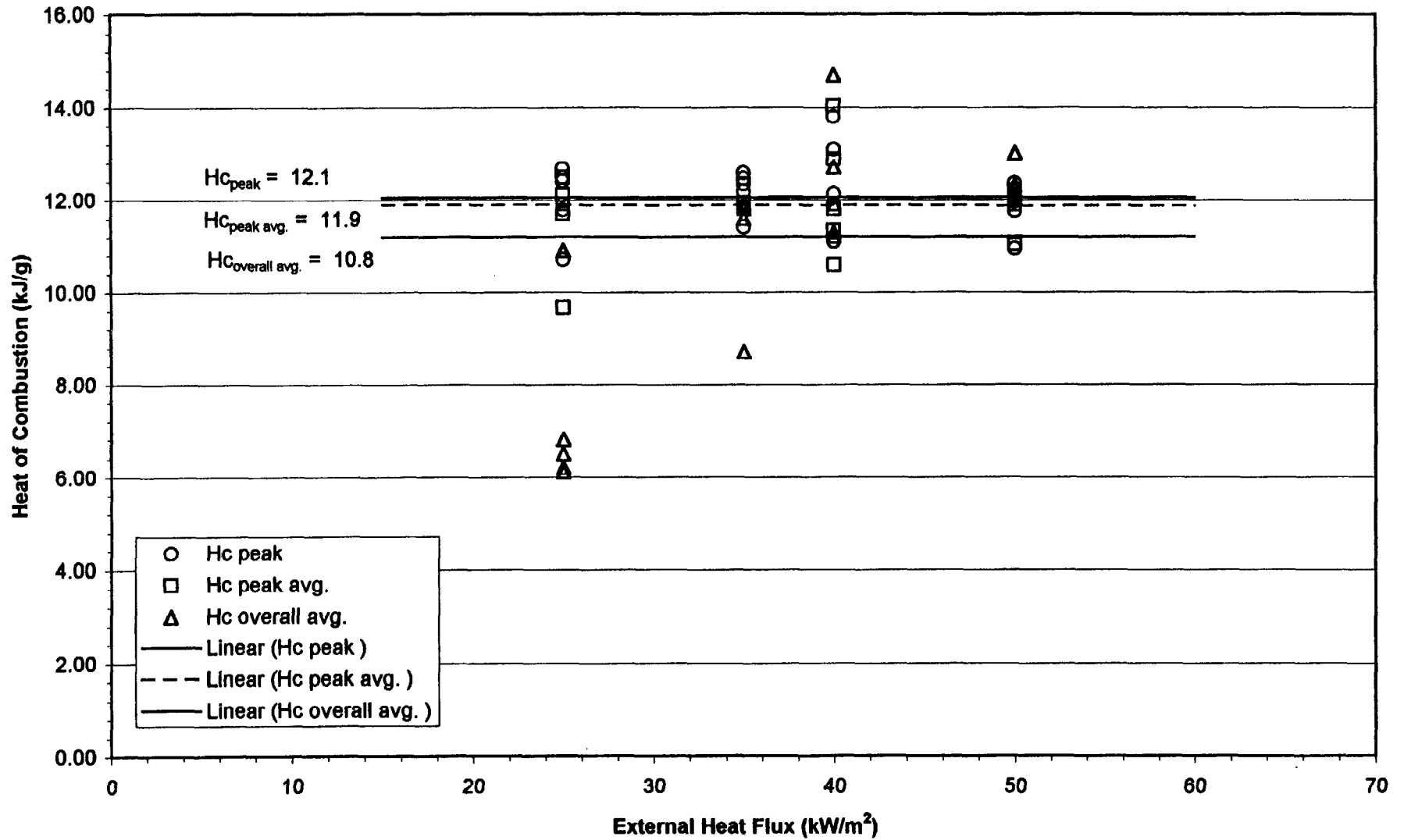
4.09 Varnished Massive Timber: Heat of Combustion vs. External Heat Flux



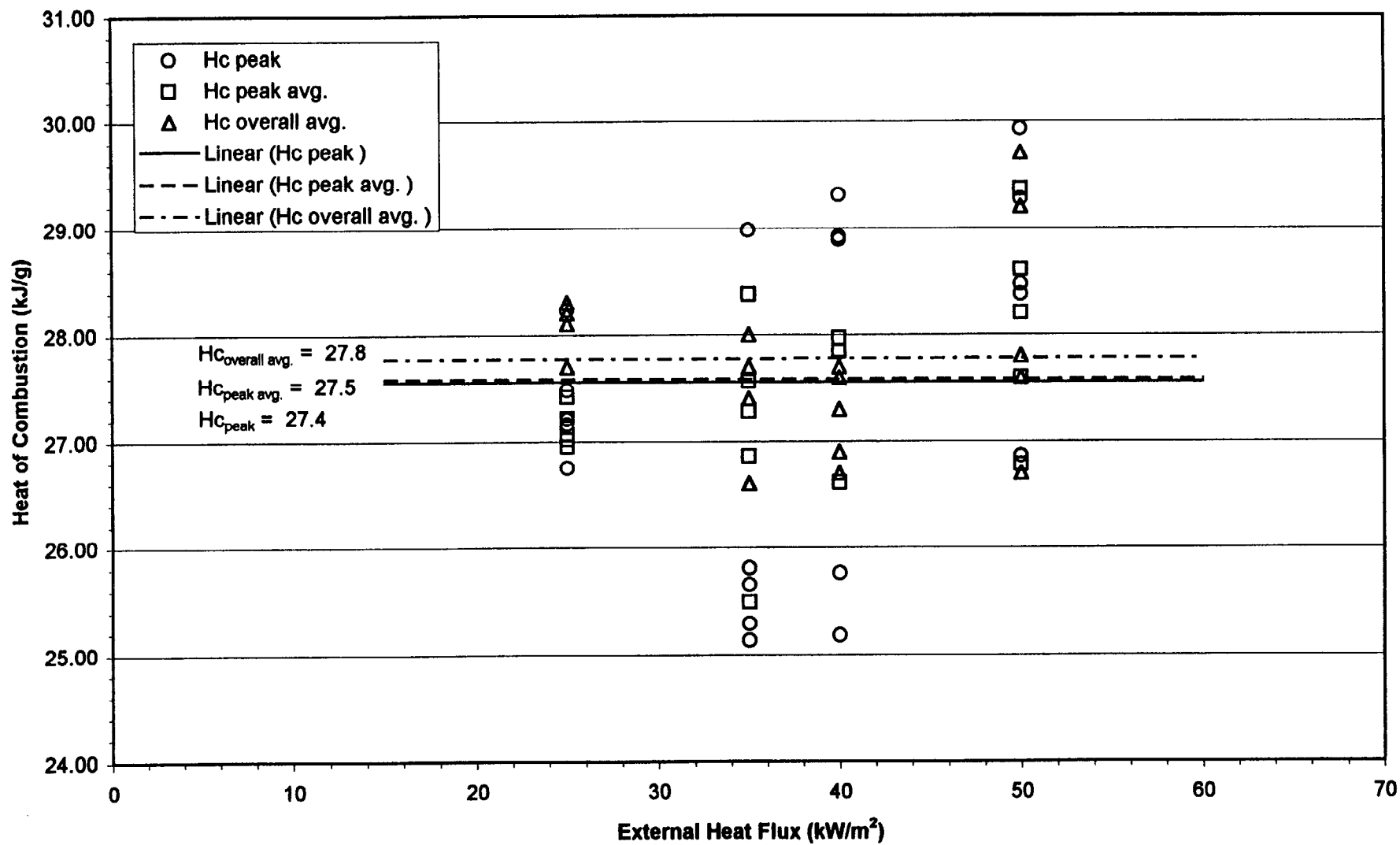
4.10 F.R. Plywood: Heat of Combustion vs. External Heat Flux



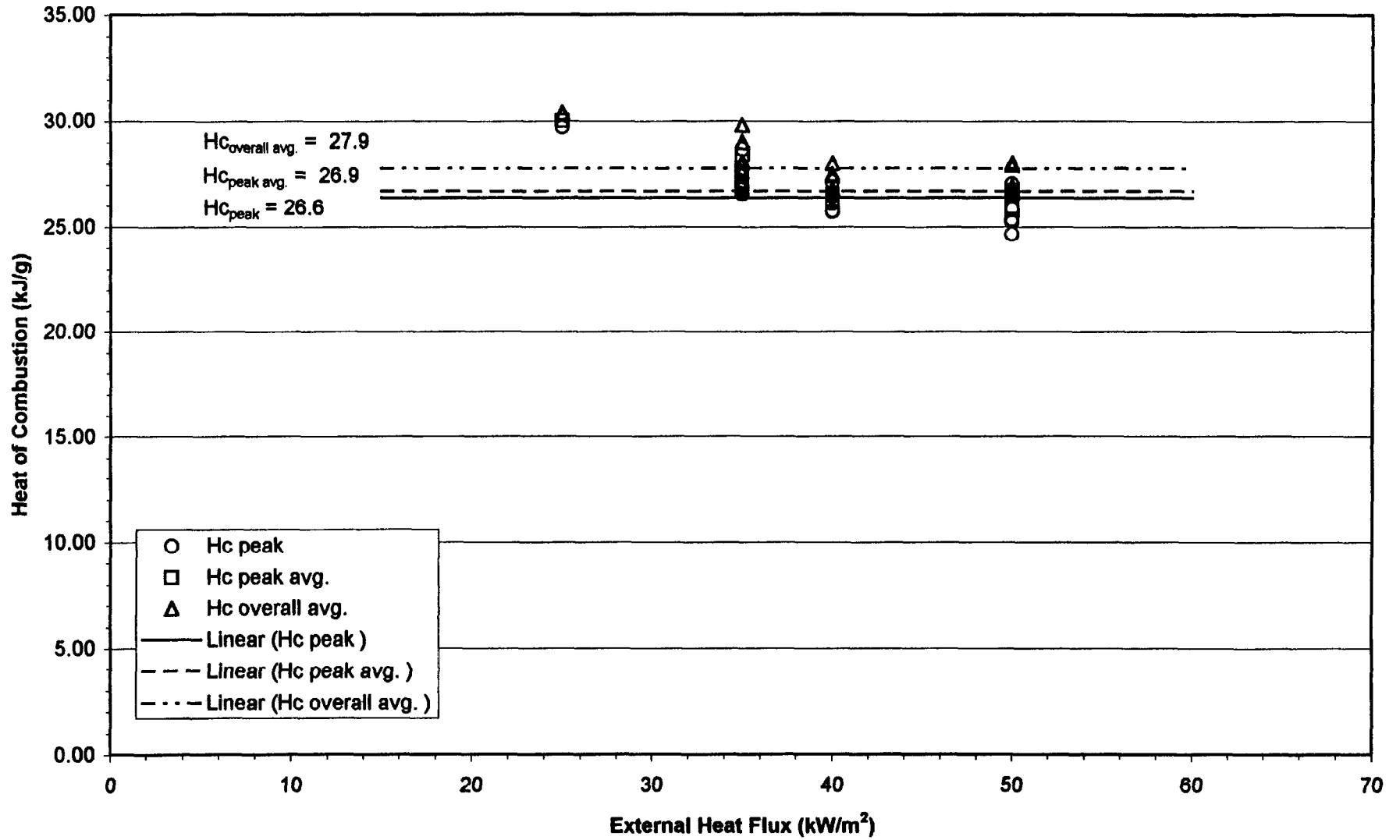
4.11 Normal Plywood: Heat of Combustion vs. External Heat Flux



4.20 F.R. Exp. Polystyrene Board (40 mm): Heat of Combustion vs. External Heat Flux



4.21 F.R. Exp. Polystyrene Board (80 mm): Heat of Combustion vs. External Heat Flux



3.5 Heat of Gasification (L)

Definition

When exposed to a given heat flux, materials will vaporize at a certain rate. The rate of this vaporization can be expressed in terms of the mass loss rate per unit area of material (\dot{m}'') and is dependent on the magnitude of the heat flux. The heat of gasification (L) value is an effective property that describes the energy required to produce the fuel volatiles per unit mass of the material and is typically expressed in the units kJ/g. The effective L value represents the average effects of vaporization of the fuel and does not include transient burning effects. Typical heat of gasification values are presented by Tewarson [27].

The burning of a material is a relatively complex and unsteady process. However, a constant, steady burning rate per unit area can be approximated using constant net heat flux and heat of gasification values by:

$$\dot{m}'' = \frac{\dot{q}''_{net}}{L} \quad (3.16)$$

where \dot{q}''_{net} is the net heat flux to the material (kW/m²). This approximation assumes that at ignition (t_{ig}) the burning rate becomes \dot{q}''_{net}/L and at the burnout time (t_b) it drops to zero. This burning rate approximation is illustrated in Figure 3.7, where the area under the predicted curve is equivalent to the area under the experimental curve. Therefore in order to estimate the steady burning rate of materials, an effective heat of gasification value needs to be determined.

Using mass loss rate data from the Cone Calorimeter, estimations of the heat of gasification can be made. This effective L value can then be used to predict the rate of burning of a material over a range of external heat flux values.

The heat of gasification also allows the energy release rate of a material to be predicted. Equation 3.14 indicates that the energy release rate per unit area can be determined by multiplying the mass loss rate per unit area by the heat of combustion thereby allowing Equation 3.16 to be expressed as:

$$\dot{Q}'' = \dot{q}''_{net} \frac{\Delta H_c}{L} \quad (3.17)$$

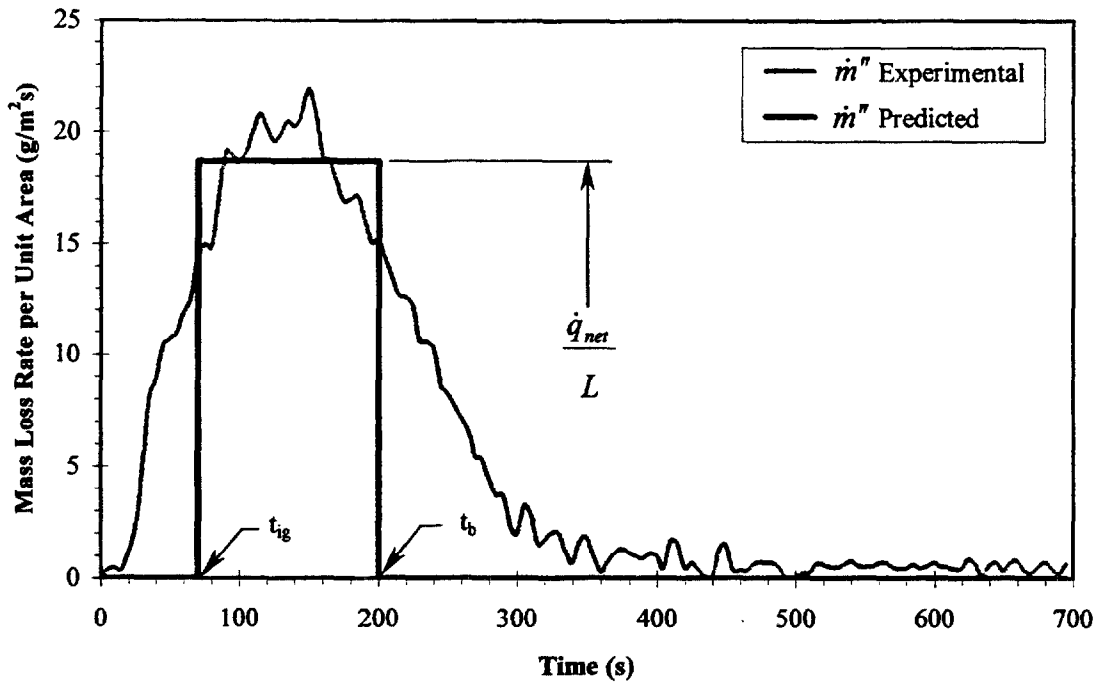


Figure 3. 7: Example of Burning Rate per Unit Area (\dot{m}'') Prediction: R 4.08, 3-Layer Polycarbonate Panel at 50 kW/m².

where \dot{Q}'' is the energy release rate per unit area of burning material (kW/m²) and ΔH_C is the heat of combustion—as calculated above. The predicted energy release rate will become equal to the right hand side of Equation 3.17 at ignition and remain constant over the burning time. Figure 3.8 shows a comparison of a typical predicted energy release rate versus an actual experimentally measured rate. The predicted energy release rate and burnout time, t_{bo} , are calculated such that the area under the predicted curve, \dot{Q}'' , is equivalent to the area under the experimental curve.

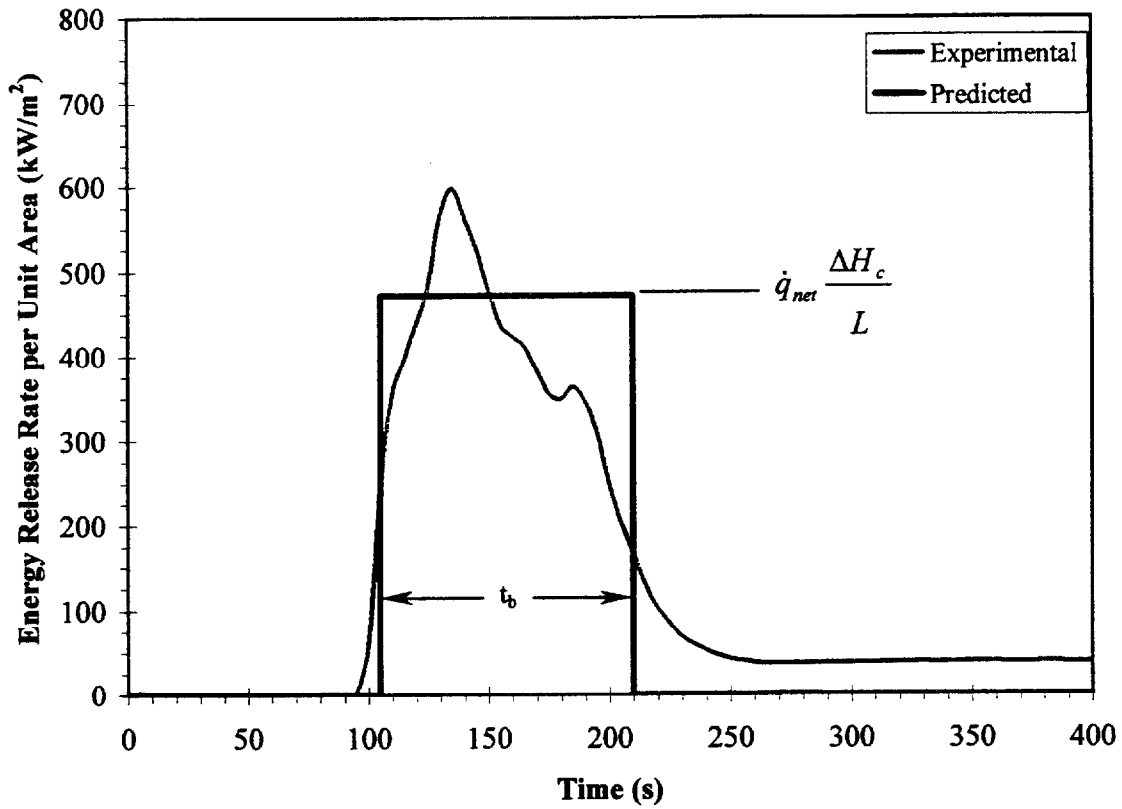


Figure 3. 8: Example of Energy Release Rate per Unit Area (\dot{Q}'') Prediction: R 4.08 at 50 kW/m^2 .

Cone Calorimeter Heat Flux

Equations 3.16 and 3.17 indicate that the mass loss rate and energy release rate per unit area may be linearly dependent on the net heat flux. In the Cone Calorimeter, the net heat flux to the sample is

$$\dot{q}_{net}'' = (1 - \alpha_f) \dot{q}_{ext}'' + \dot{q}_f'' - \dot{q}_{rr}'' \quad (3.18)$$

where α_f is the flame absorptivity, \dot{q}_{ext}'' is the external heat flux provided by the Cone heater (kW/m^2) and \dot{q}_f'' is the total incident heat flux from the flame including radiant and convective heating (kW/m^2):

$$\dot{q}_f'' = \dot{q}_{f,r}'' + \dot{q}_{f,c}''$$

and \dot{q}''_{r} is the heat flux lost due to re-radiation (kW/m) from the heated material surface. Therefore, it would be advantageous if the heat flux from the flame, \dot{q}''_f , and the re-radiant losses, \dot{q}''_{r} , can be determined to be constant over a range of external heat fluxes thereby producing a heat of gasification value that is linearly dependent on the external heat flux alone. This linear dependence will allow effective heat of gasification values to be extracted from the Cone data.

Using Kirchhoff's law [8] we realize that the absorptivity of the flame can be determined to be

$$\alpha_f = \varepsilon_f$$

where ε_f is the emissivity of the flame. Quintiere and Rhodes [24] and Rhodes [25] demonstrated that the flame volume for materials burning in the Cone can be approximated as a tall, vertical cylinder and that the emissivity can be approximated by:

$$\varepsilon_f \cong 1 - e^{-\kappa l_m}$$

where κ is the absorption coefficient (m^{-1}) and l_m is the mean beam length (m). For tall, semi-infinite cylindrical flames with height (H) greater than twice the sample width (D), the mean beam length for radiation to the base of the cylinder (the surface of sample material) is approximately $0.65 \cdot D$ [6]. Therefore for flames of height H greater than $2D$, the flame emissivity is approximately constant and a relatively low value—Rhodes calculates 0.09 for PMMA burning in the Cone Calorimeter. Since the flame emissivity is so low, the flames are very transparent and very little of the external heat flux from the Cone heater is absorbed. Therefore most of the heat flux from the Cone heater is transmitted to the sample material.

Quintiere and Rhodes also indicate that the total flame heat flux (\dot{q}''_f) from thermoplastic materials burning in the Cone Calorimeter can be considered to be constant for different external heat fluxes. The radiant portion of the flame heat flux is

$$\dot{q}''_{f,r} = \varepsilon_f \sigma T_f^4$$

where T_f is the flame temperature (K). The average flame volume temperature for a burning material can be considered to be relatively constant resulting in a constant $\dot{q}''_{f,r}$ value. For example, black PMMA burning in the Cone has a constant flame temperature of approximately 1400 K and an associated radiant flame heat flux of approximately 20 kW/m^2 [25]. This does not imply that all materials have identical radiative heat fluxes from the flames only that for a particular burning material, the radiant heat flux is relatively constant.

Rhodes work also indicates that the convective heat flux to a sample in the Cone Calorimeter is relatively constant as well, but can decrease slightly as the burning rate

increases. An increase in the burning rate will produce a “blocking factor” which acts to effectively reduce the convective heat transfer coefficient. Rhodes determined a convective heat flux of 15 kW/m² for black PMMA in the Cone, assuming a blocking factor of 1 ($\dot{m}'' \rightarrow 0$).

The burning rate of the LSF materials does increase as we increase the external heat flux, however this increase appears to be moderate enough that this decrease in $\dot{q}''_{f,c}$ can be neglected. Therefore, since both the radiative and convective portions of the flame heat flux are approximately constant for tall flames ($H > 2D$), the net flame heat flux incident to materials burning in the Cone Calorimeter, \dot{q}''_f , can be considered to be constant.

The re-radiant heat losses, \dot{q}''_r , from the material surface can be expressed as

$$\dot{q}''_r = \epsilon_s \sigma T_s^4$$

where ϵ_s is the emissivity of the material surface, σ is the Stefan-Boltzmann constant (5.670×10^{-11} kW/m²·K⁴) and T_s is the surface temperature of the material (K). For this analysis the surface emissivities of the burning materials are approximated as being equal to 1. Since most materials will either darken, warp, melt and even char when burning, this is a reasonable approximation.

Rhodes work and work done by Hopkins and Quintiere [7] suggests that the surface temperature for burning thermoplastic materials in the Cone is constant. This surface temperature represents the vaporization temperature of the material (T_v) which is approximately constant and can be approximated as being equal to the ignition temperature of the material (T_{ig}). Although the vaporization temperature is slightly higher than the ignition temperature for most thermoplastic materials, this appears to be a reasonable assumption based on the currently available data for thermoplastics. This implies that the reradiation losses from the sample are constant over different external heat fluxes. However further surface temperature data for non-charring as well as charring materials would help to reinforce this hypothesis. The surface temperature of charring materials is typically much higher than the ignition temperature, especially after a significant char layer has developed and been heated by the incident heat flux. Therefore using the ignition temperature to represent the surface temperature for all materials represents an approximation which may provide some error in the final prediction of the fire growth.

To predict the burning rate per unit area, \dot{m}'' , using Equation 3.16, we need to determine an appropriate L value. In order to do this we consider the flame emissivity, flame heat flux and re-radiant heat loss for each material in the Cone Calorimeter to be constant. We can therefore assume that the \dot{q}''_{net} in Equation 3.18 is only linearly dependent on \dot{q}''_{ext} . Therefore, since the effective heat of combustion and heat of gasification values are also taken to be constant, the burning rate and energy release rate

per unit area will become linearly dependent on the external heat flux from the Cone heater:

$$\dot{m}'' \approx \dot{q}_{ext}'' \frac{1}{L} \quad (3.19)$$

$$\dot{Q}'' \approx \dot{q}_{ext}'' \frac{\Delta H_c}{L} \quad (3.20)$$

This linear dependence of \dot{m}'' and \dot{Q}'' on the external heat flux allows the heat of gasification to be evaluated through methods similar to those for calculating the different ΔH_c values. The exception being that the peak, peak average and overall average energy release rates will be used on both an energy release rate basis as well as a specimen mass loss basis.

Energy Release Rate Methods

The effective heat of gasification values calculated based on energy release rates are based on Equation 3.20. Since ΔH_c and L are constant and are not dependent on the external heat flux, this equation can be differentiated into the following form:

$$\frac{d\dot{Q}''}{d\dot{q}_{ext}''} = \frac{\overline{\Delta H_c}}{L}$$

where $\overline{\Delta H_c}$ indicates an average heat of combustion value, as listed in Table 3.4.

The peak, peak average and overall average energy release rate values (\dot{Q}'') are plotted with respect to the external heat flux (\dot{q}_{ext}'') from the Cone heater. Only the samples where ignition and sustained burning occurred were plotted. Since $d\dot{Q}''/d\dot{q}_{ext}''$ is assumed to be linear, a least squares fit line was drawn through the data points and the slope of the linear fit was determined. The numerical value for the slope is simply equal to $\Delta\dot{Q}''/\Delta\dot{q}_{ext}''$, allowing the effective heat of gasification to be calculated by

$$L = \frac{\overline{\Delta H_c}}{(\Delta\dot{Q}''/\Delta\dot{q}_{ext}'')} \quad (3.21)$$

which can be seen graphically in Figure 3.9.

1. Peak Energy Release Rate (L_{peak})

The \dot{Q}''_{peak} value from each test is taken directly from the LSF data and plotted against the external heat flux from the Cone heater. Using the $\overline{\Delta H_{C, peak}}$ values in Table 3.4, an effective L_{peak} value is calculated for each material based on

$$L_{peak} = \frac{\overline{\Delta H_{C, peak}}}{(\Delta \dot{Q}''_{peak} / \Delta \dot{q}''_{ext})}$$

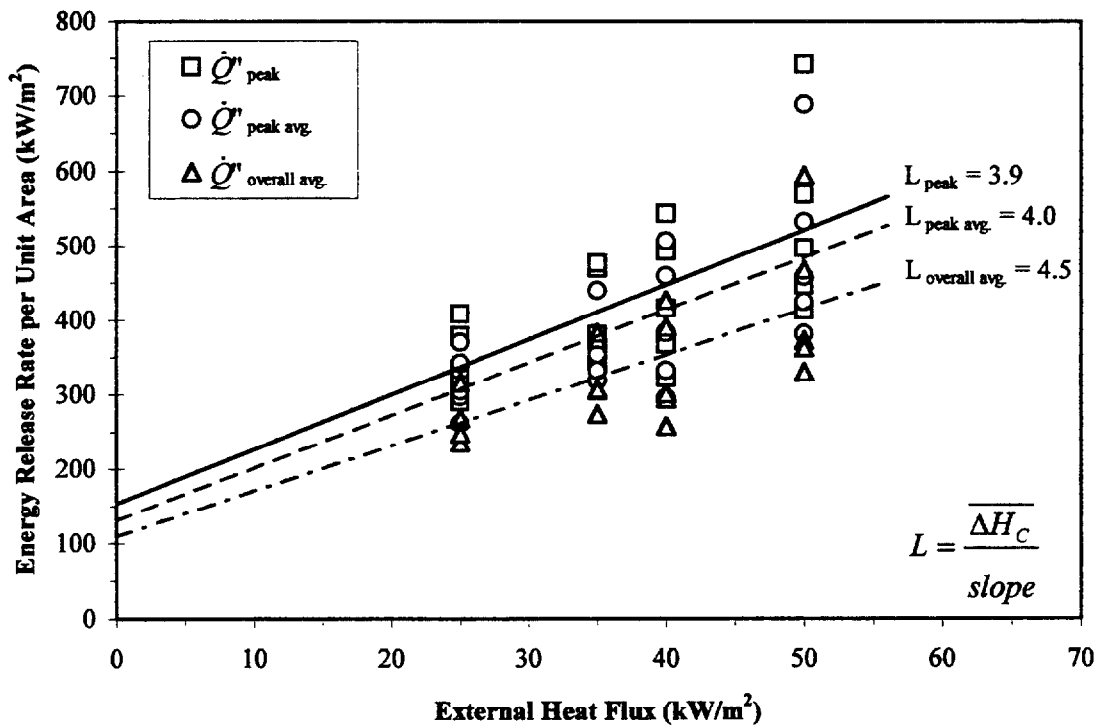


Figure 3. 9: Example of Heat of Gasification (L) Determination Using Energy Release Rates per Unit Area with Respect to the External Heat Flux in the Cone Calorimeter: R 4.05, Fire Retarded Extruded Polystyrene.

2. Average Energy Release Rate Around the Peak ($L_{peak avg.}$)

This method is identical to the one used to determine L_{peak} except that the “peak average” values are used:

$$L_{peak\ avg.} = \frac{\overline{\Delta H_{C\ peak\ avg.}}}{\left(\Delta \dot{Q}''_{peak\ avg.} / \Delta \dot{q}''_{ext} \right)}$$

3. Average Overall Test Results ($L_{overall\ avg.}$)

For this method the total steady burning of the sample material from each test is used to determine the effective heat of gasification value. This results in a more global value as opposed to a value based on an instantaneous or local occurrence. As in the previous two methods, the energy release rate for each test needs to be plotted against the associated external heat flux level from the Cone heater. The overall energy release rate can be determined from

$$\dot{Q}''_{overall\ avg.} = \Delta H_{C, overall\ avg.} \cdot \dot{m}''_{overall\ avg.} \quad (3.22)$$

The overall heat of combustion values used in Equation 3.22 represent values calculated from individual tests as opposed to the average values listed in Table 3.4.

In order to determine a heat of gasification value over the region of steady burning, the total specimen mass loss from the Cone data can not be used. This is done in order to eliminate mass loss from non-burning phenomenon, e.g. moisture evaporation. For example, gypsum wallboard undergoes a rather brief burning period after the paper facing ignites, but the specimen mass will continue to decrease past the point of flame extinction. This continued mass loss is due to the evaporation of the water trapped within the gypsum by the applied heat flux. Therefore, the steady mass loss rate per unit area value ($\dot{m}''_{overall\ avg.}$) will be determined over this sustained burning region.

In order to determine this steady burning mass loss rate, the slope of the specimen mass versus time curve (dm/dt) is determined over the region where sustained burning was believed to occur. The steady burning region is taken as the ignition time until the point at which the mass versus time curve appears to curve towards a horizontal line—indicating a significant reduction in the burning rate. A typical steady burning rate determination can be seen in Figure 3.10.

The times at which the different specimens ignite are provided in the LSF data. The data also includes the time at which flaming ends, but it is unclear if this time represents a sudden end of flaming or a gradual reduction of the flame size until it becomes undistinguishable. There are tests where the reported end of flame time does not reasonably correspond with the end of significant mass loss or energy release. There are also cases where a material underwent ignition and extinguishment several times, and it was unclear as to what end of flaming time to choose. Since these values will be used to predict the burning of materials in actual scenarios, the time at which the burning rate is seriously reduced can be used to represent an approximate point at which steady,

sustained burning might have ended. Therefore the change in the slope of the mass loss versus time curve is implemented here for determining the end of steady burning.

The mass loss rate (\dot{m}) is approximately linear over this steady burning region. Therefore, $\dot{m}''_{overall,avg.}$ can be determined from the slope of the linear fit through the specimen mass versus time curve during steady burning divided by the surface area of the specimen:

$$\dot{m}''_{overall,avg.} = \frac{\dot{m}}{A_s} = \frac{-dm/dt}{A_s}$$

where A_s is the surface area of the sample which is reported by LSF to be 0.0088 m² for all of the samples tested.

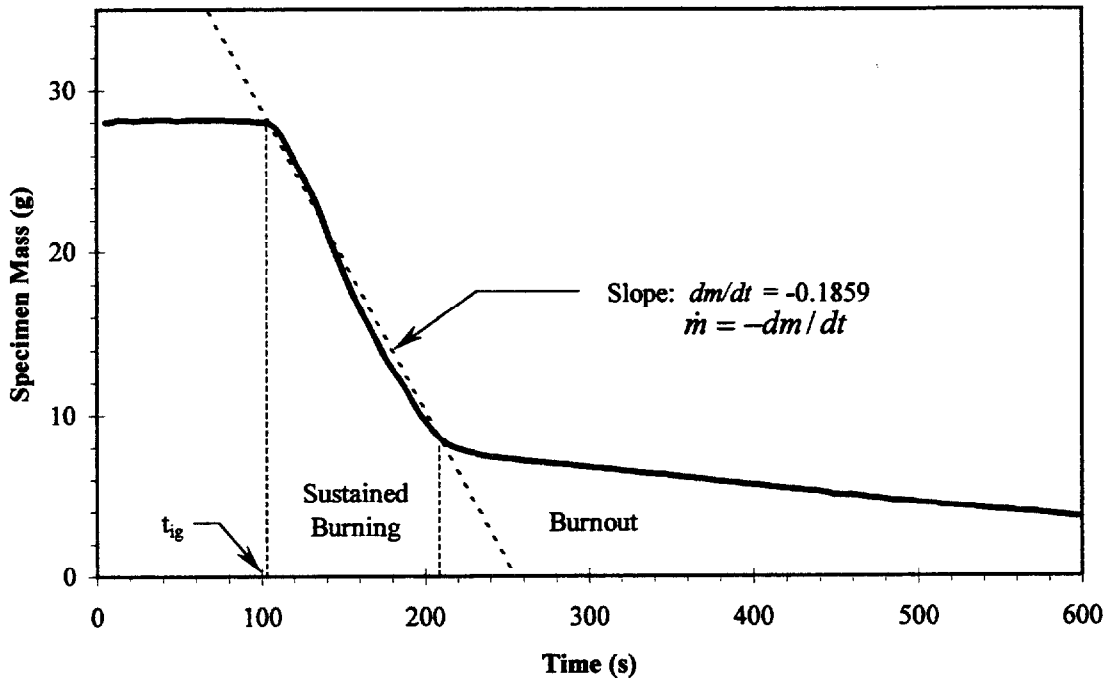


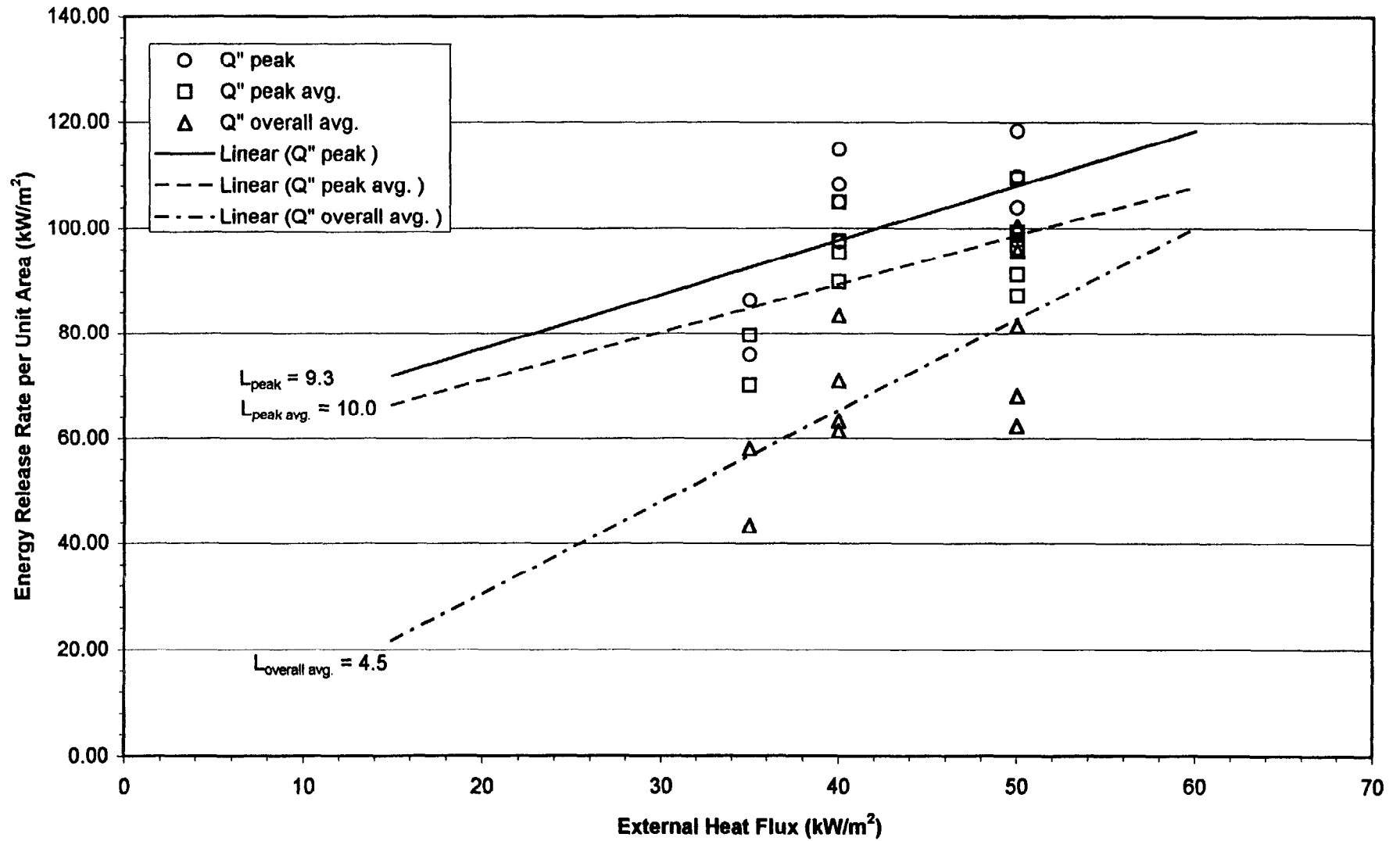
Figure 3. 10: Example of Steady Burning Rate (\dot{m}) Determination: R 4.08, 3-Layer Polycarbonate Panel.

Using $\dot{m}''_{overall,avg.}$, the overall energy release rate per unit area is determined for each test using Equation 3.22 and plotted with respect to the external heat flux from the heater as in Figure 3.9. The slope of the linear fit and $\overline{\Delta H_{C, overall,avg.}}$ are used to determine the L value:

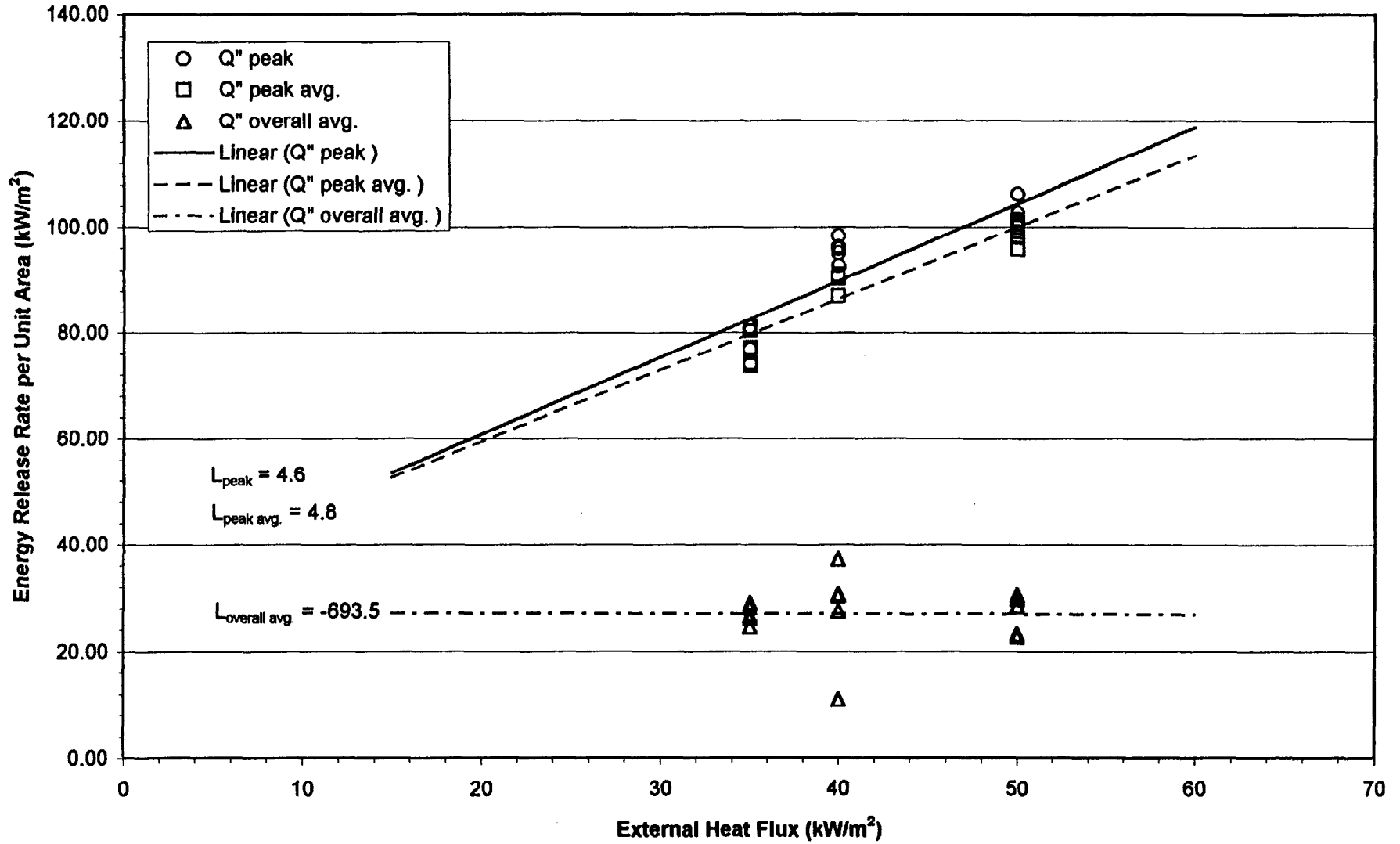
$$L_{\text{overall avg.}} = \frac{\overline{\Delta H}_{C, \text{ overall avg.}}}{\left(\Delta \dot{Q}''_{\text{overall avg.}} / \Delta \dot{q}''_{\text{ext}} \right)}$$

The graphs for determining the heat of gasification by the energy release rate from Appendix A.5 are presented here.

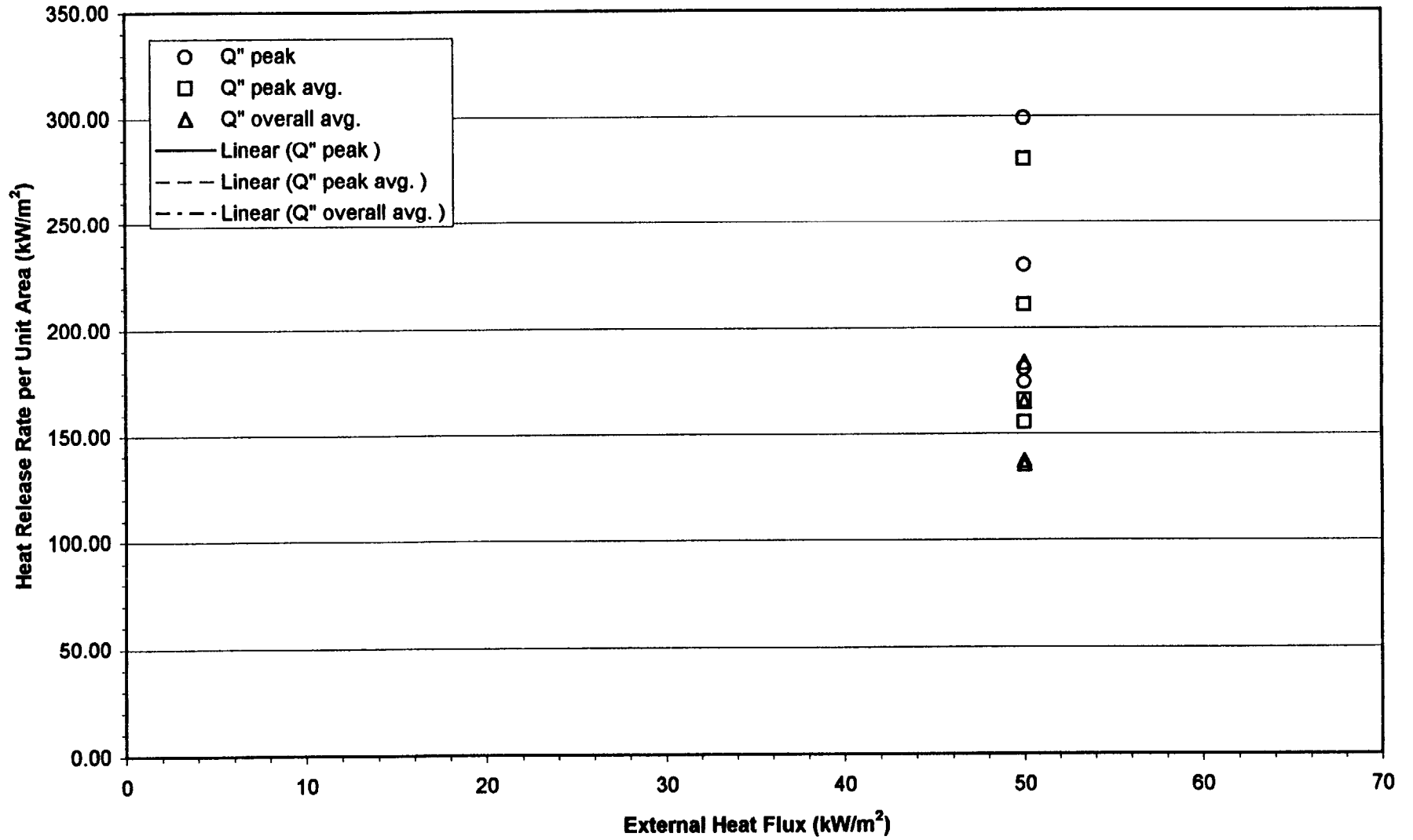
4.01 F.R. Chipboard: Energy Release Rate vs. External Heat Flux



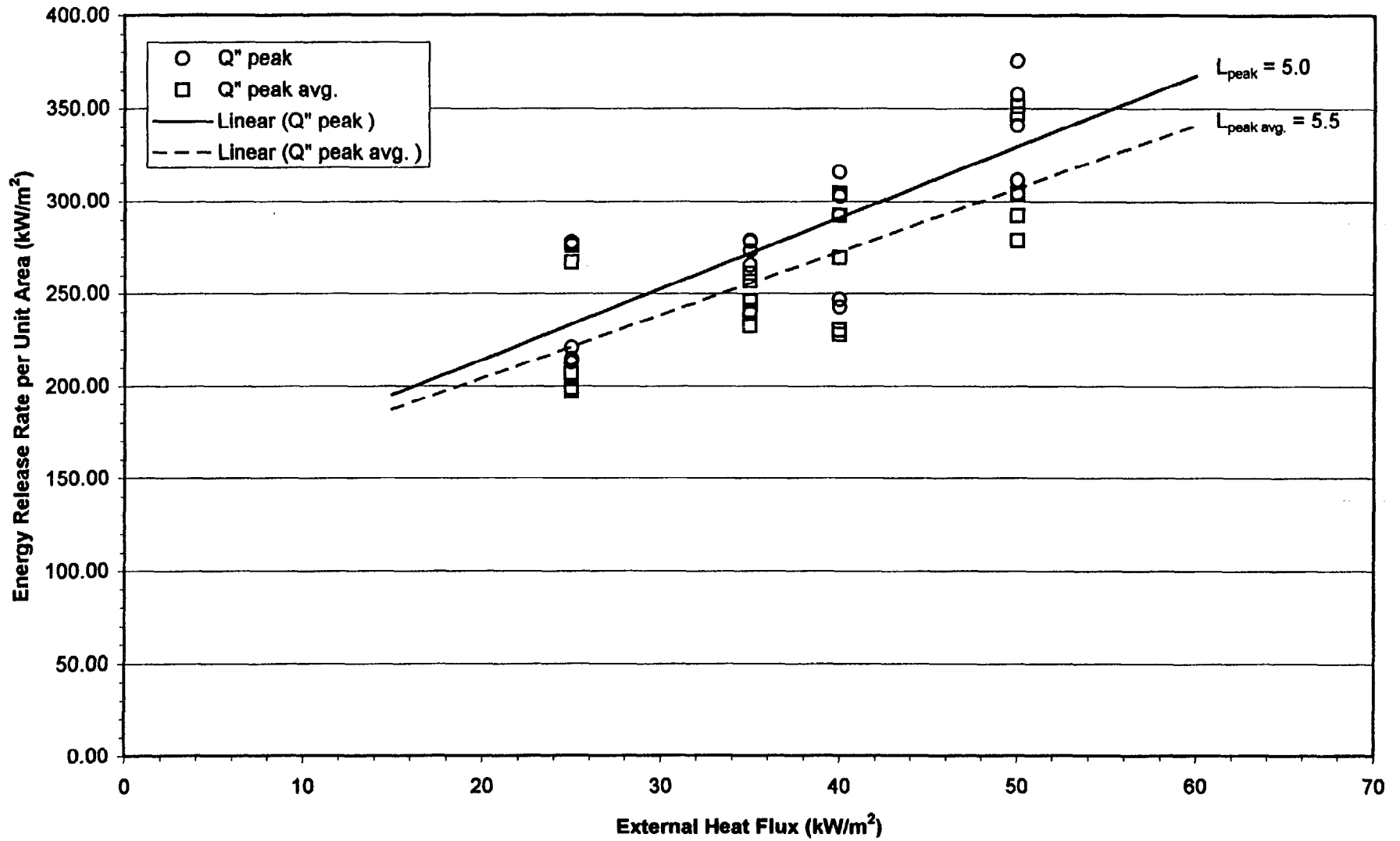
4.02 Paper Faced Gypsum Board: Energy Release Rate vs. External Heat Flux



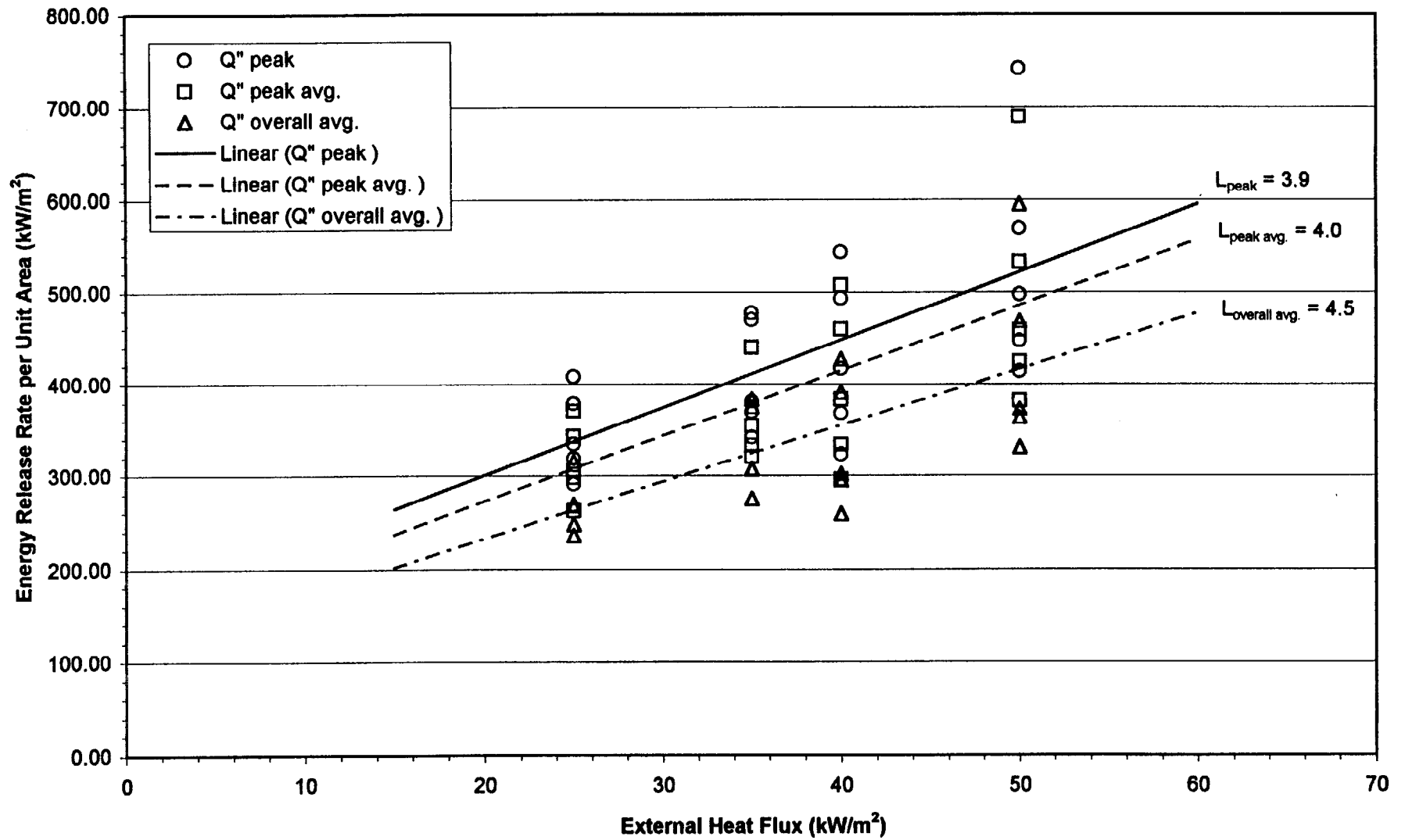
R 4.03 Energy Release Rate vs. External Heat Flux



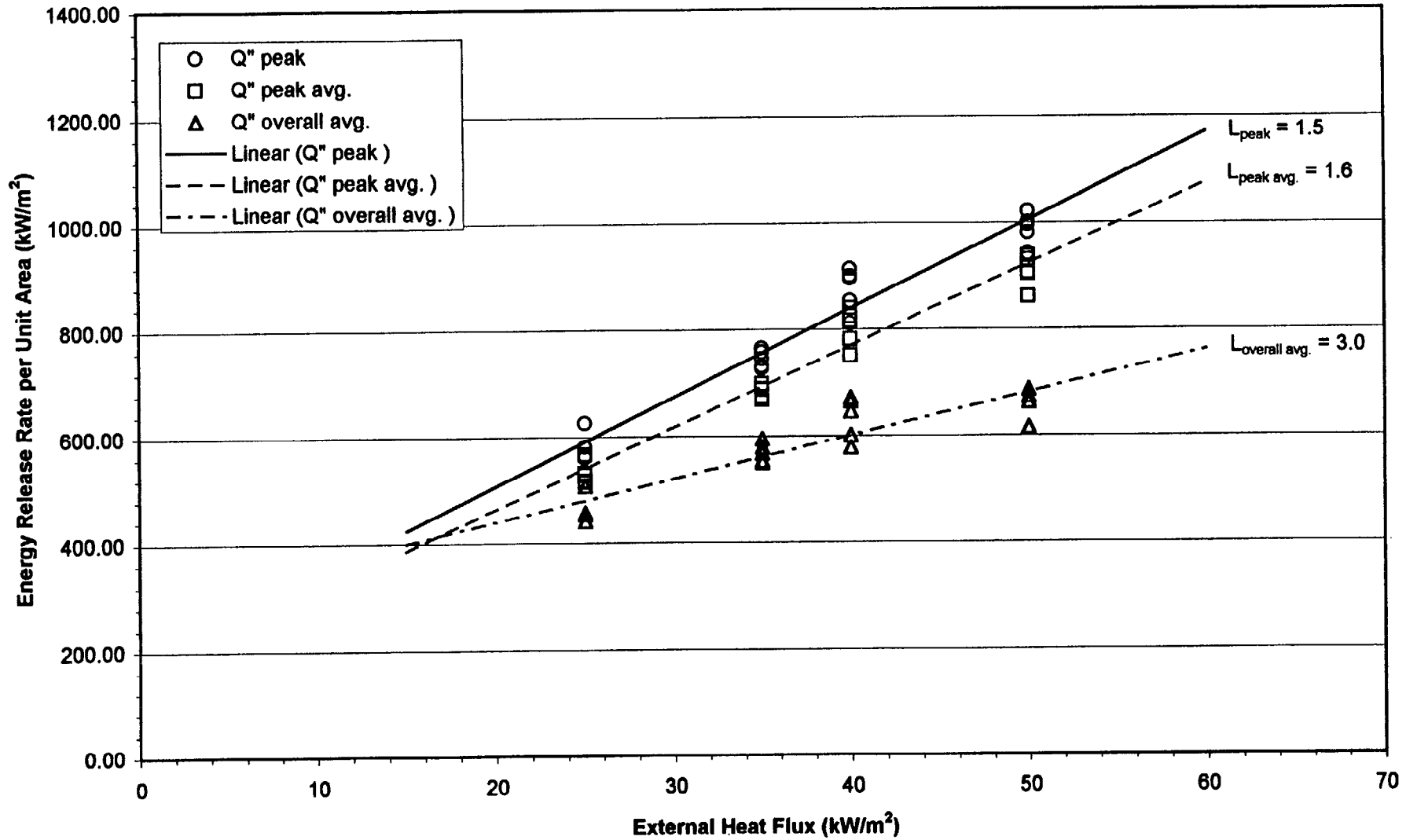
4.04 Polyurethane with Paper Backing: Energy Release Rate vs. External Heat Flux



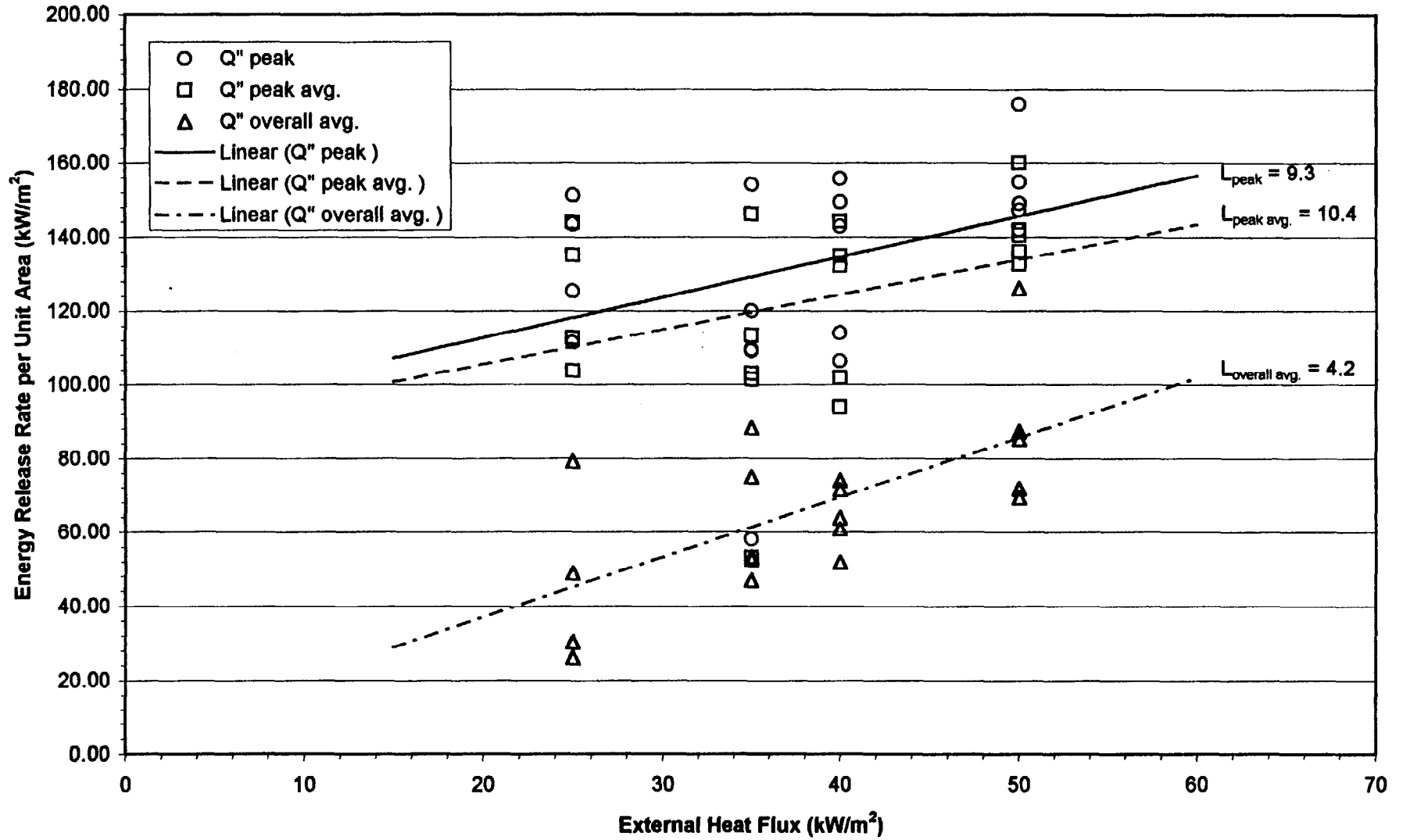
4.05 F.R. Extruded Polystyrene Board (40 mm): Energy Release Rate vs. External Heat Flux



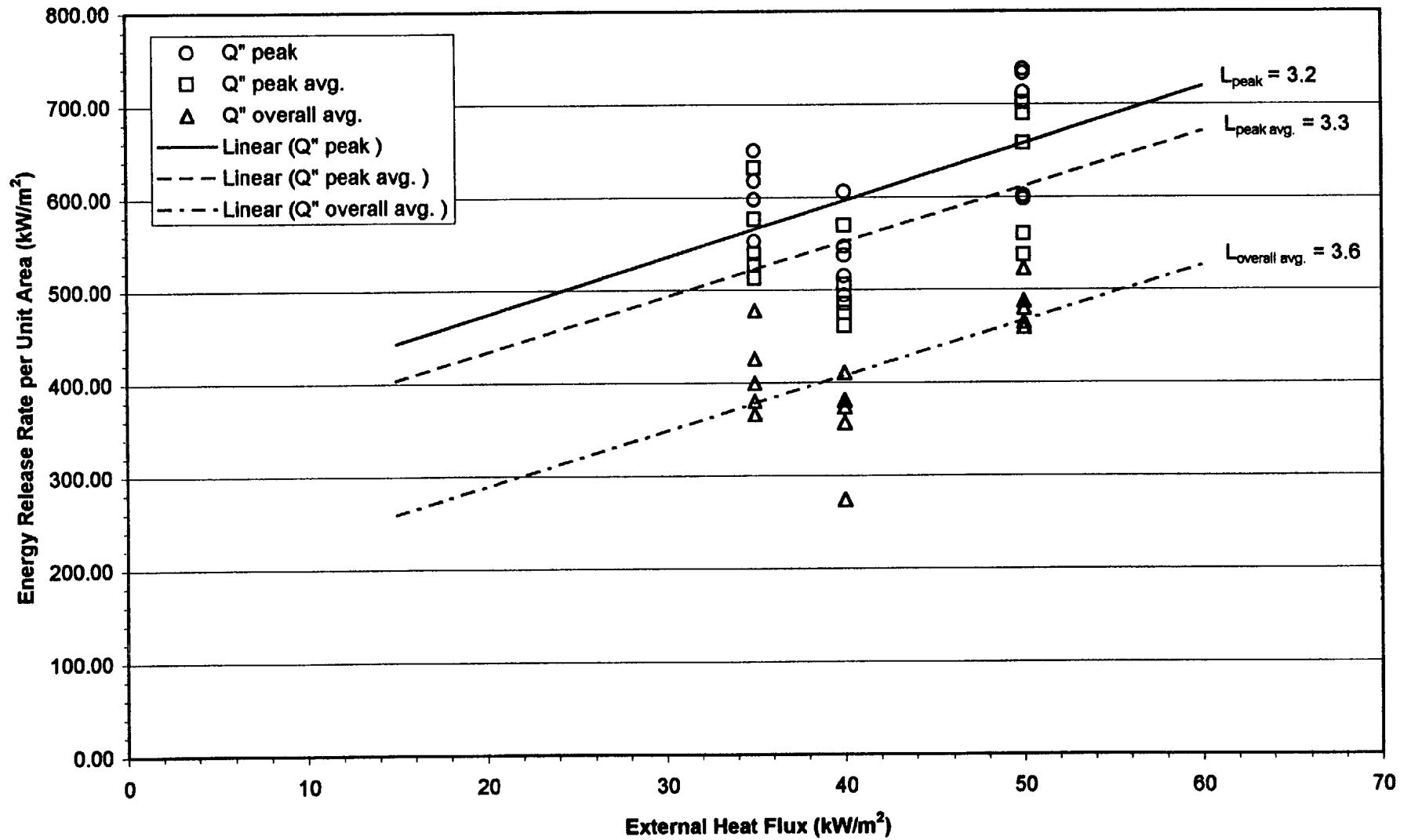
4.06 Acrylic Glazing: Energy Release Rate vs. External Heat Flux



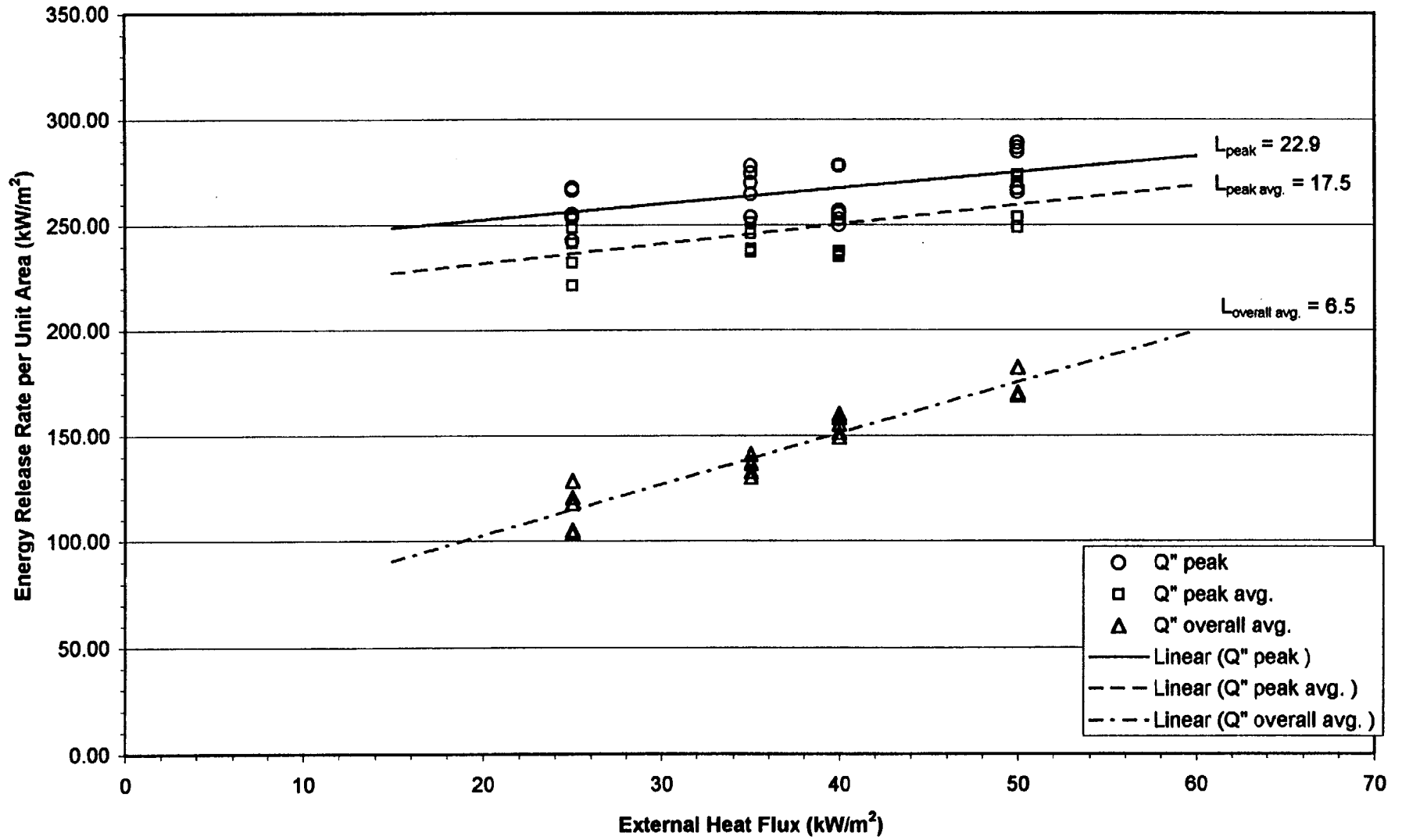
4.07 Energy Release Rate vs. External Heat Flux



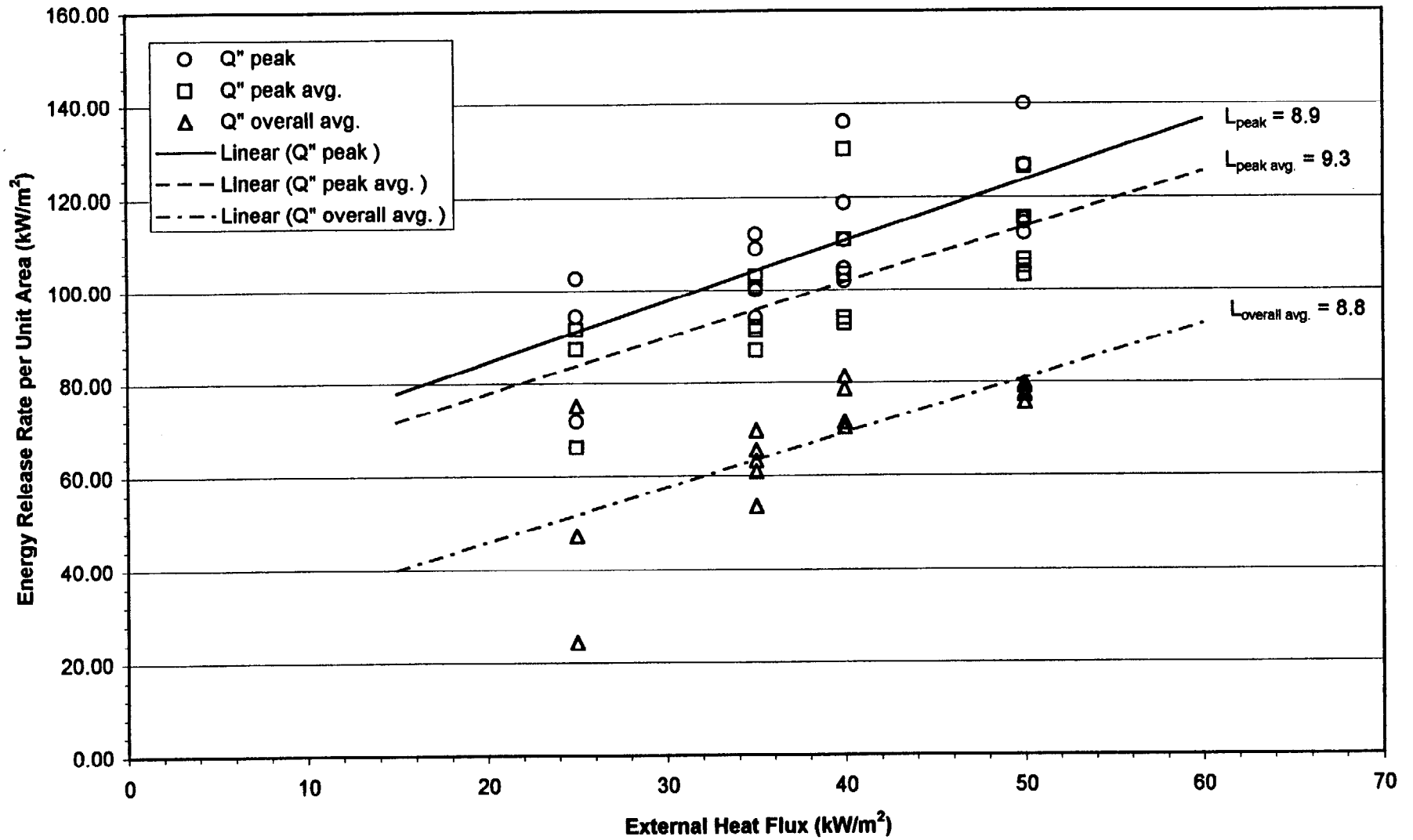
4.08 3-Layered F.R. Polycarbonate Panel: Energy Release Rate vs. External Heat Flux



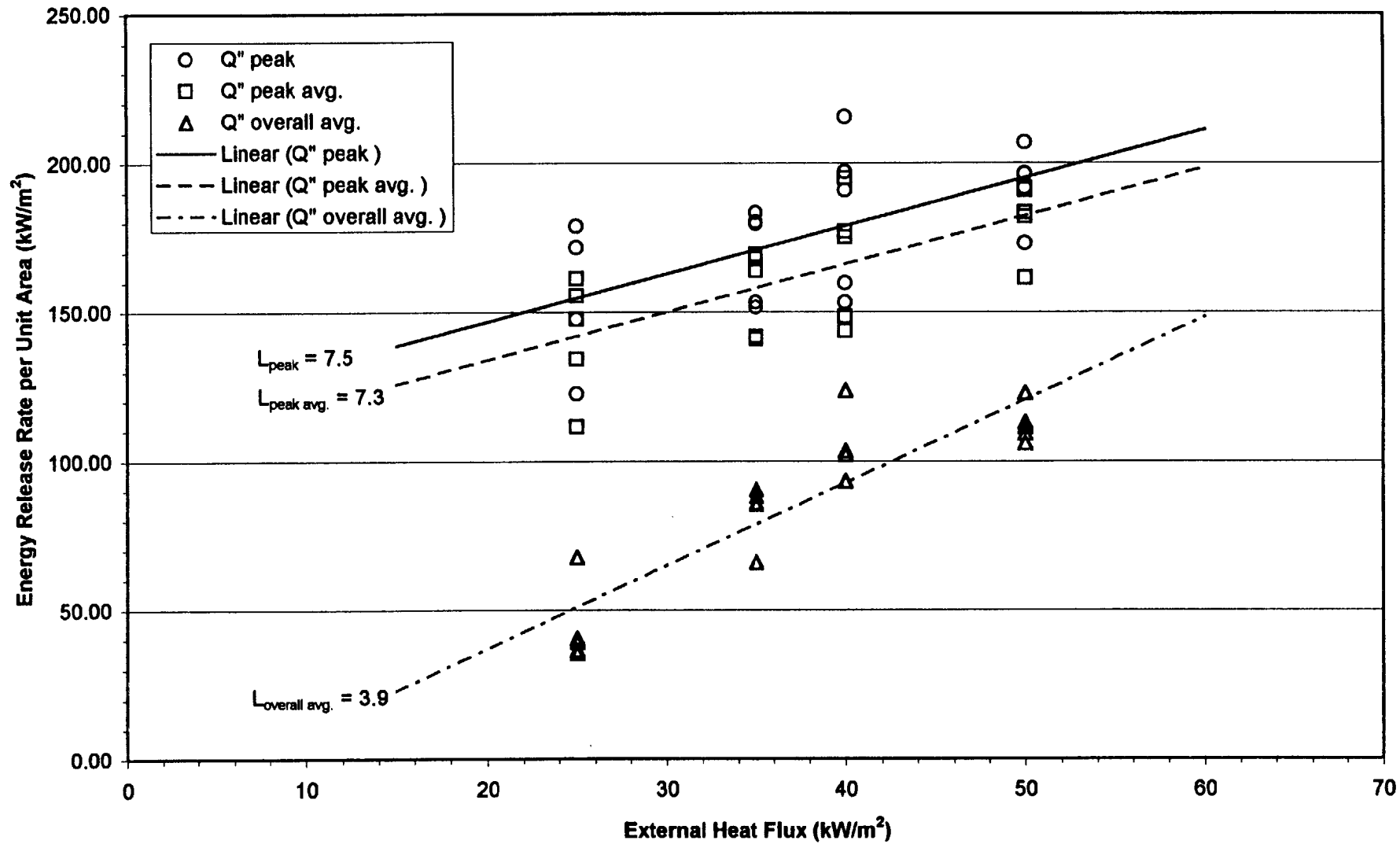
4.09 Varnished Massive Timber: Energy Release Rate vs. External Heat Flux



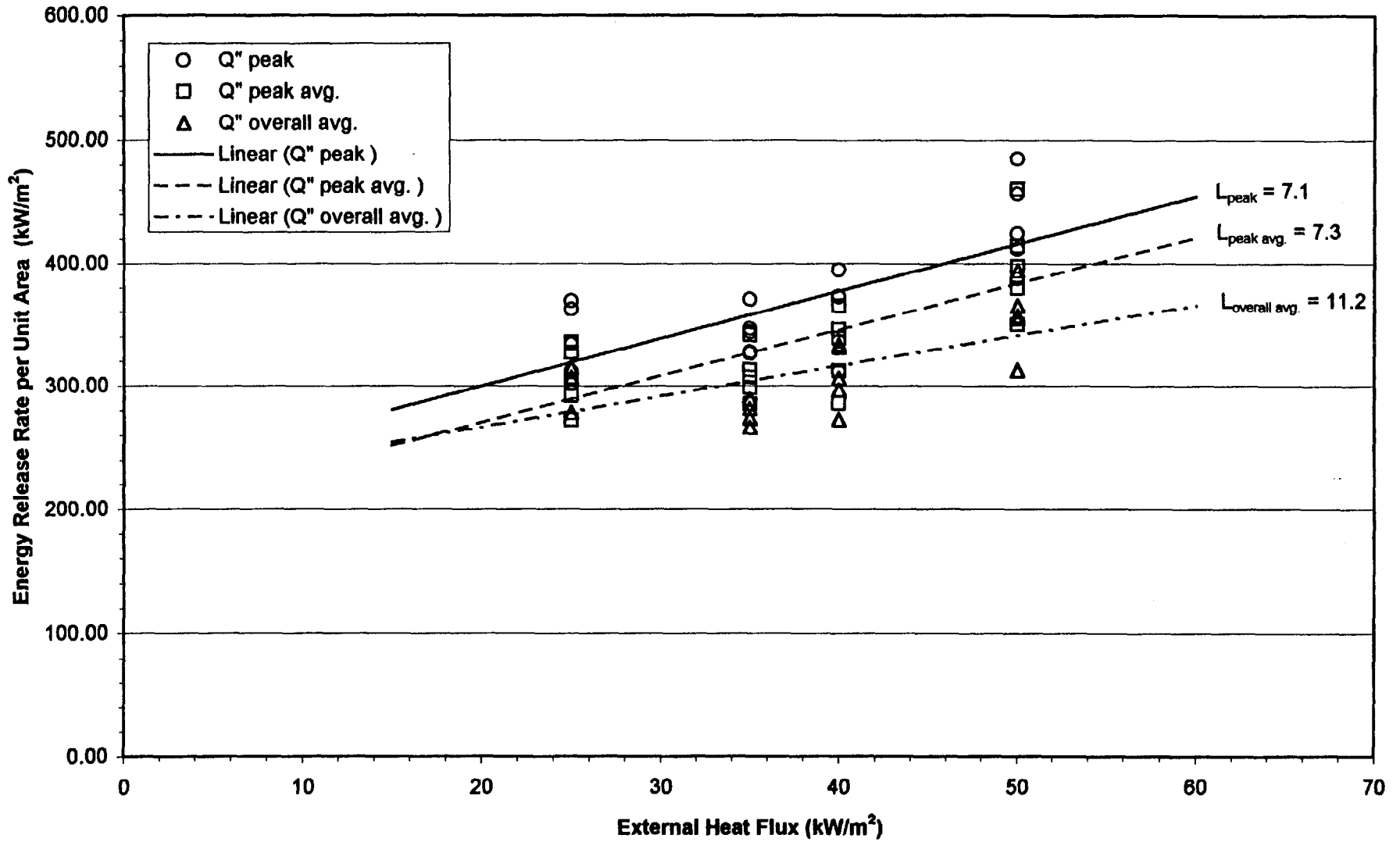
4.10 F.R. Plywood: Energy Release Rate vs. External Heat Flux



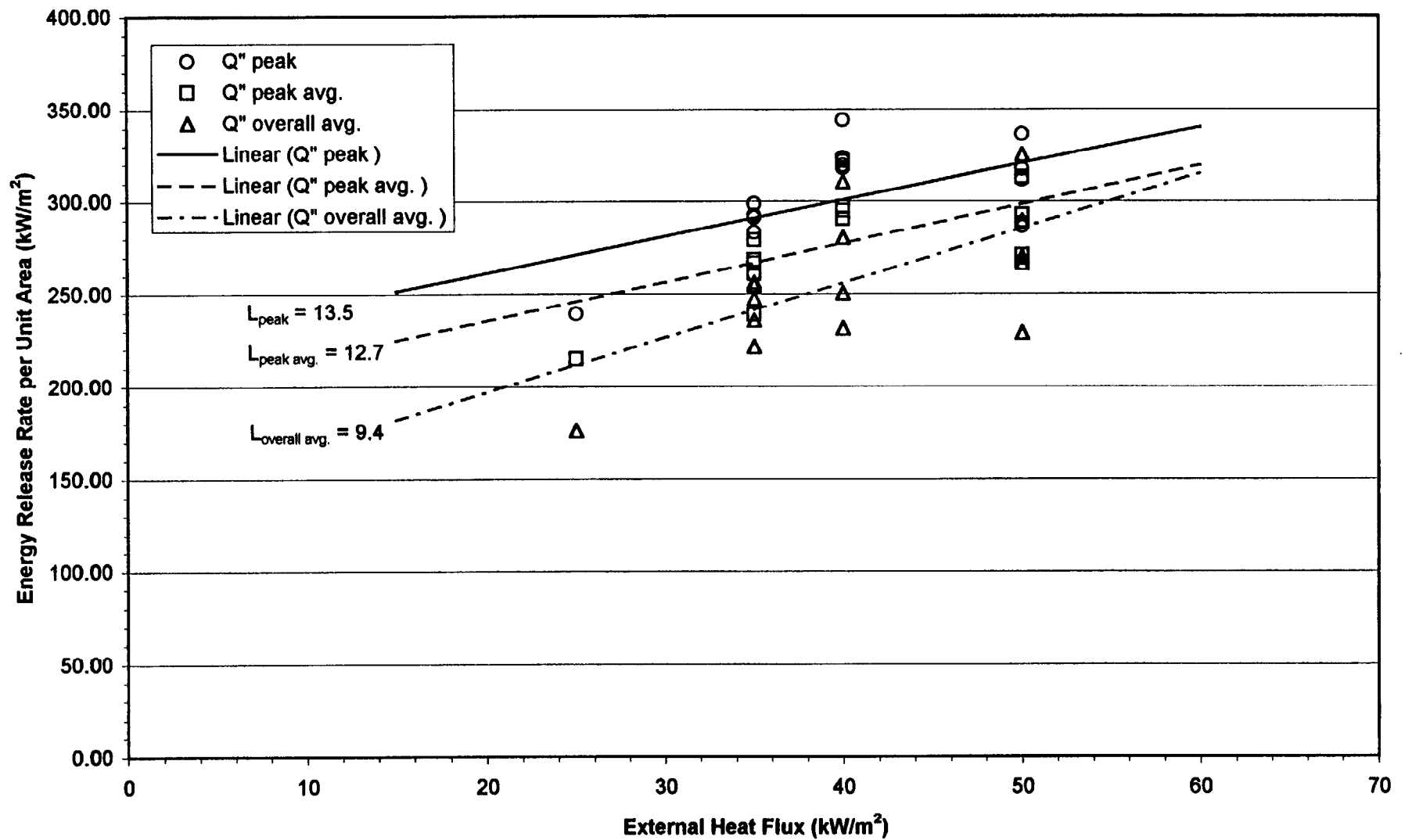
4.11 Normal Plywood: Energy Release Rate vs. External Heat Flux



4.20 F.R. Expanded Polystyrene Board (40 mm): Energy Release Rate vs. External Heat Flux



4.21 F.R. Expanded Polystyrene Board (80 mm): Energy Release Rate vs. External Heat Flux



Specimen Mass Loss Methods

Heat of gasification values determined on a specimen mass loss basis are calculated using Equation 3.19. Differentiation produces

$$\frac{d\dot{m}''}{d\dot{q}_{ext}''} = \frac{1}{L}$$

As with the energy release rate, the mass loss rate per unit area is taken to be linearly dependent on the external heat flux and can be expressed as

$$\frac{\Delta\dot{m}''}{\Delta\dot{q}_{ext}''} = \frac{1}{L} \quad (3.23)$$

Therefore, the effective L value is the inverse of the slope of the linear fit through the specimen mass loss rate per unit area data plotted against the external heat fluxes for each test:

$$L = \frac{1}{(\Delta\dot{m}''/\Delta\dot{q}_{ext}'')} \quad (3.24)$$

A graphical representation of the determination of the heat of gasification using the specimen mass loss rate per unit area is shown in Figure 3.11.

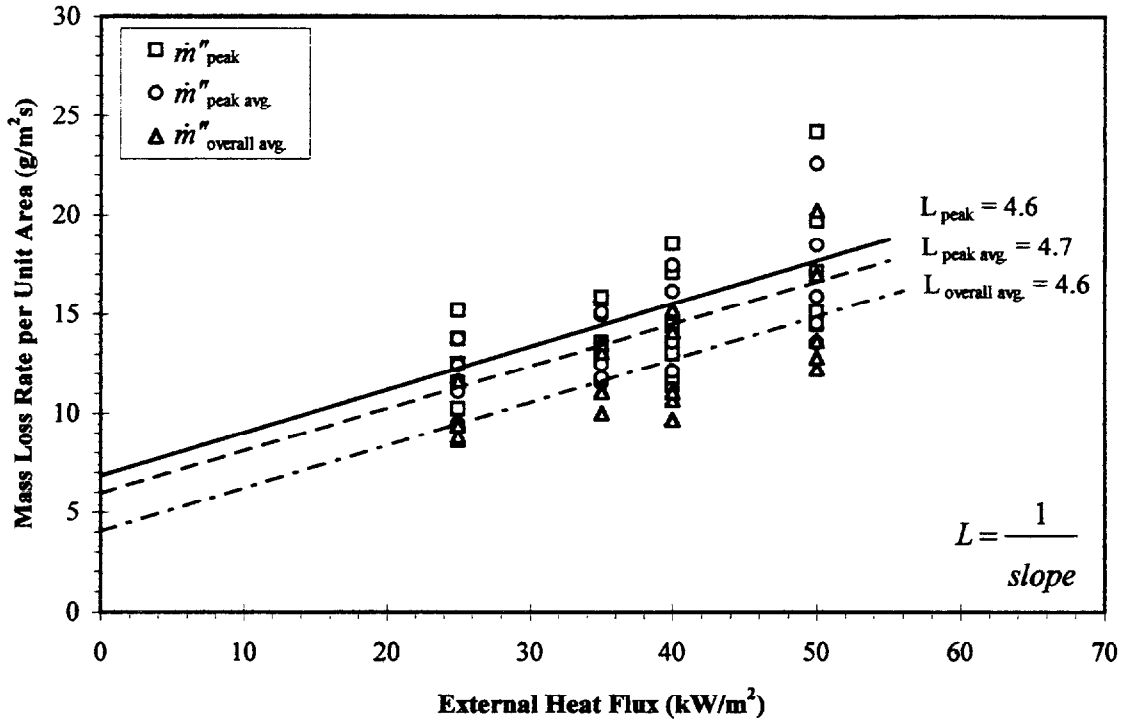


Figure 3. 11: Example of Heat of Gasification (L) Determination Using Specimen Mass Loss Rates per Unit Area with Respect to the External Heat Flux in the Cone Calorimeter: R 4.05, Fire Retarded Extruded Polystyrene.

4. Peak Energy Release Rate (L_{peak}) by Mass Loss

The peak mass loss rate per unit area for each tested specimen was determined by using a form of Equation 3.14:

$$\dot{m}''_{peak} = \frac{\dot{Q}''_{peak}}{\Delta H_{C, peak}} \quad (3.25)$$

The heat of combustion values used here are the actual peak values that were determined for each Cone test (as opposed to the average values from Table 3.4). These peak mass loss rates are then plotted against the external heat fluxes for the test as in Figure 3.11 and the heat of gasification is determined by

$$L_{peak} = \frac{1}{(\Delta \dot{m}''_{peak} / d\Delta \dot{q}''_{ext})}$$

5. Average Energy Release Rate Around the Peak ($L_{peak\ avg.}$) by Mass Loss

This method is the same as the previous method except that $\dot{Q}''_{peak\ avg.}$ and ΔH_C , $\dot{m}''_{peak\ avg.}$ from each test are used in Equation 3.25 to determine the peak average mass loss rate per unit area. The effective heat of gasification is also found in a similar manner:

$$L_{peak\ avg.} = \frac{1}{\left(\Delta \dot{m}''_{peak\ avg.} / \Delta \dot{q}''_{ext} \right)}$$

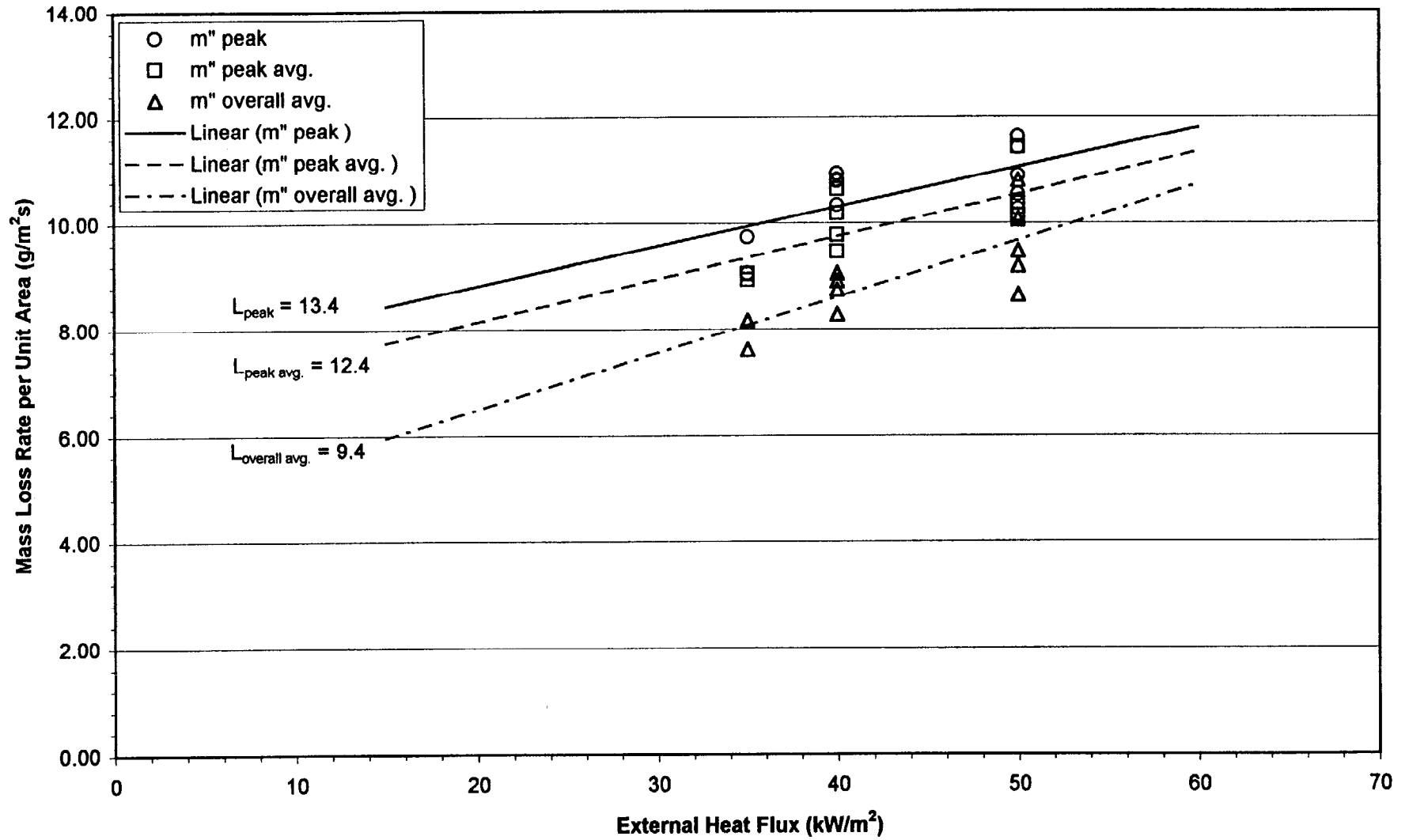
6. Average Overall Test Results ($L_{overall\ avg.}$) by Mass Loss

This method uses the same $\dot{m}''_{overall\ avg.}$ values for the region of steady, sustained burning determined above, in Method #3, plotted against the external heat flux levels.

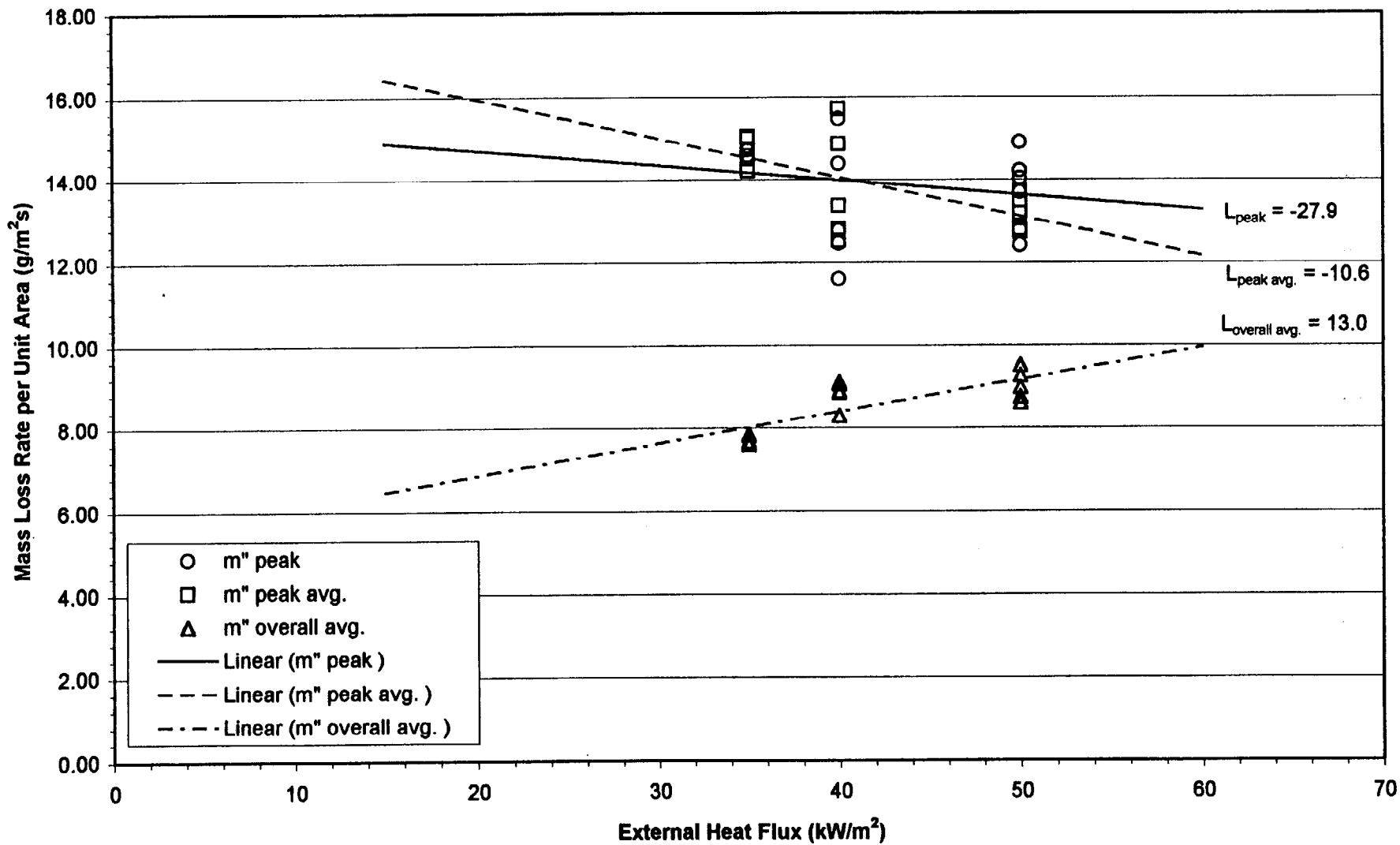
$$L_{overall\ avg.} = \frac{1}{\left(\Delta \dot{m}''_{overall\ avg.} / \Delta \dot{q}''_{ext} \right)}$$

The graphs for determining the heat of gasification by the mass loss rate from Appendix A.5 are presented here.

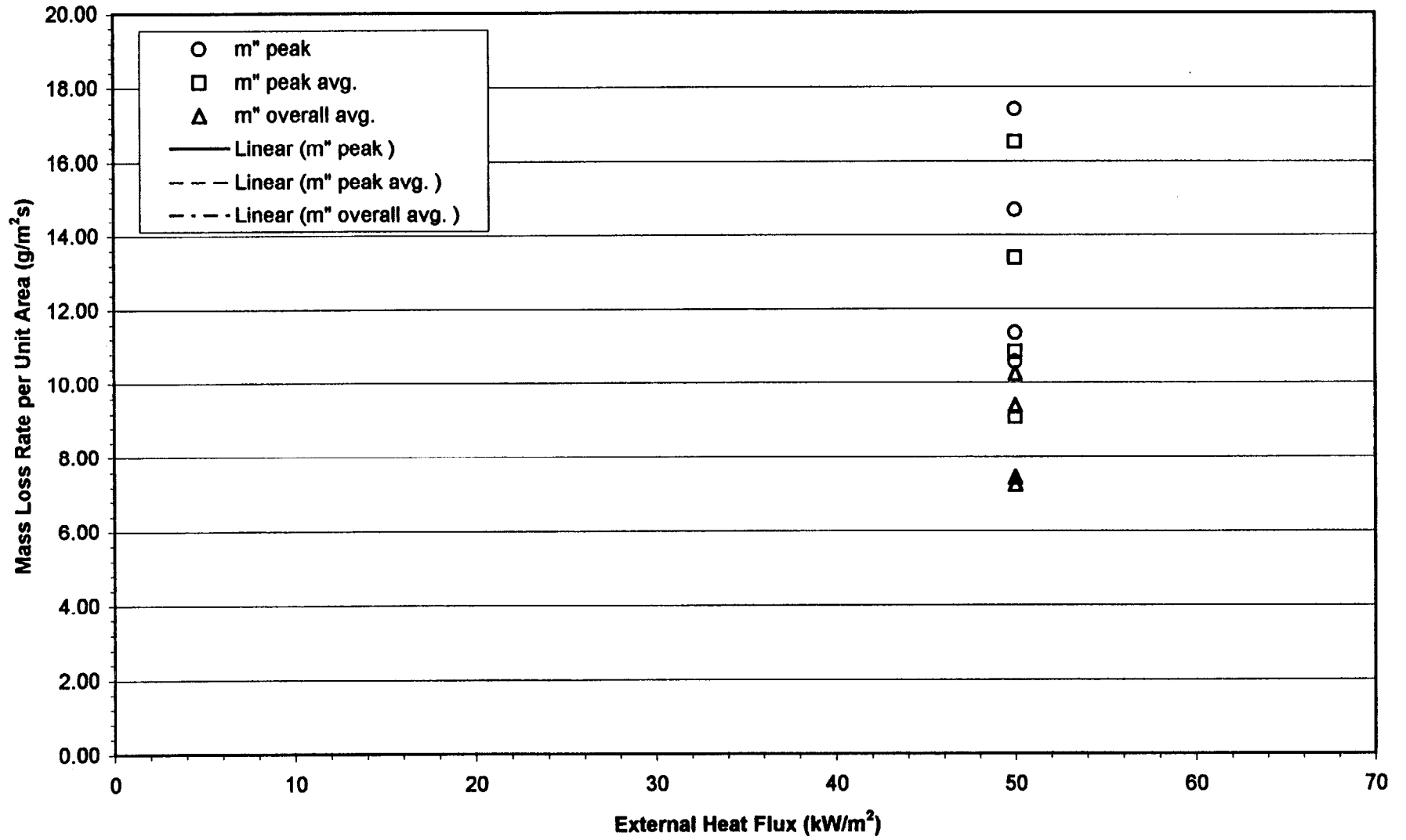
4.01 F.R. Chipboard: Mass Loss Rate vs. External Heat Flux



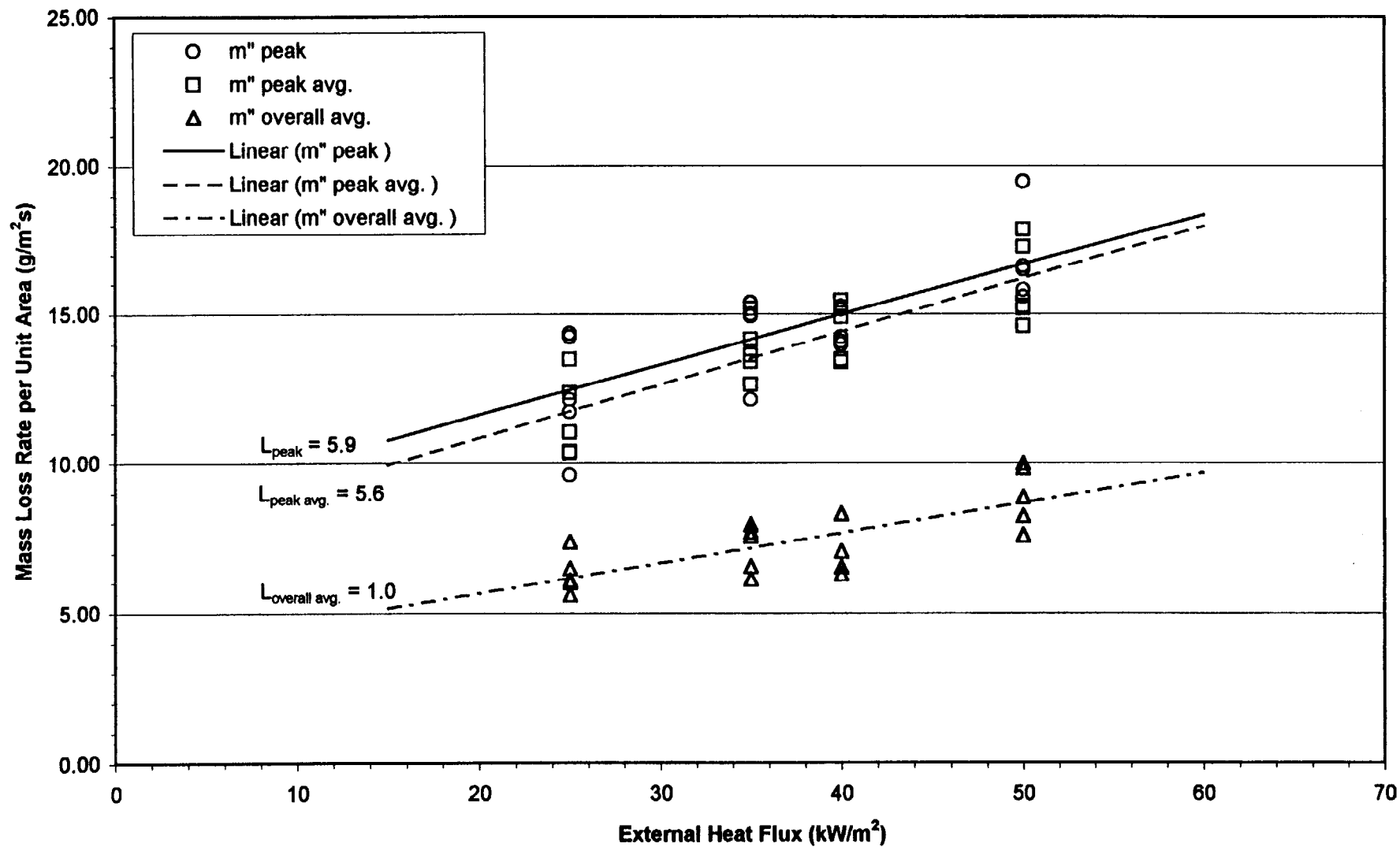
4.02 Paper Faced Gypsum Board: Mass Loss Rate vs. External Heat Flux



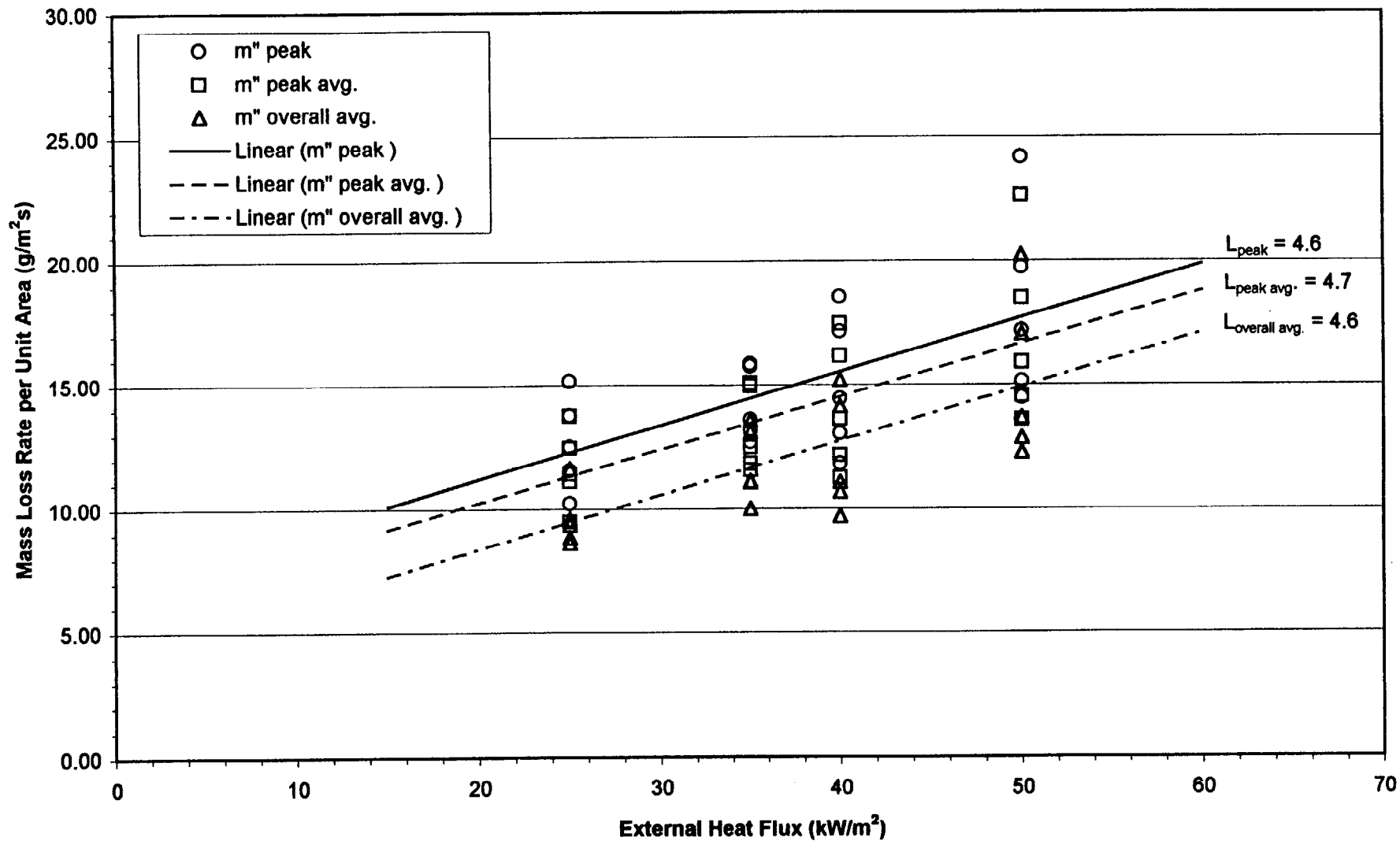
R 4.03 Mass Loss Rate vs. External Heat Flux



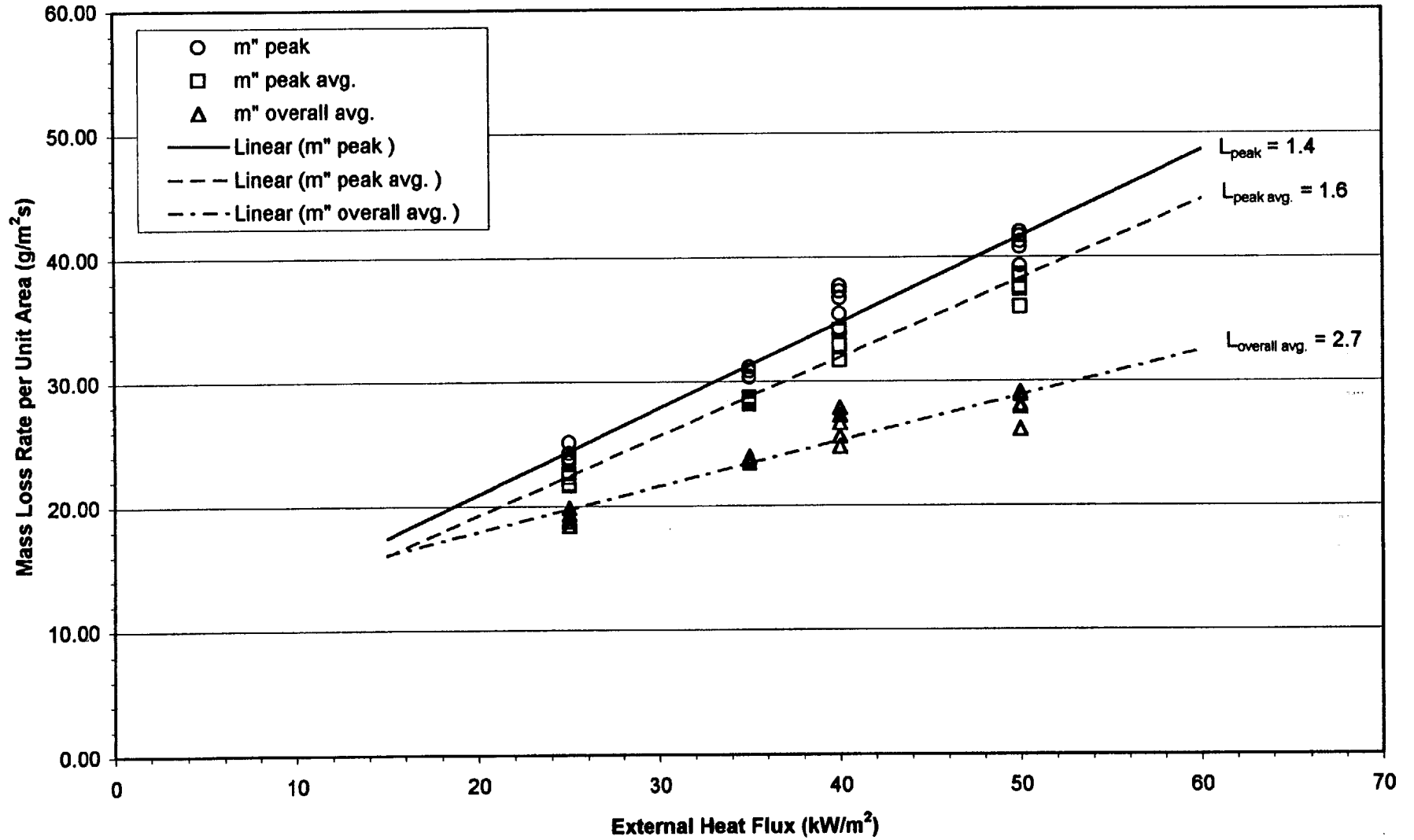
4.04 Polyurethane with Paper Backing: Mass Loss Rate vs. External Heat Flux



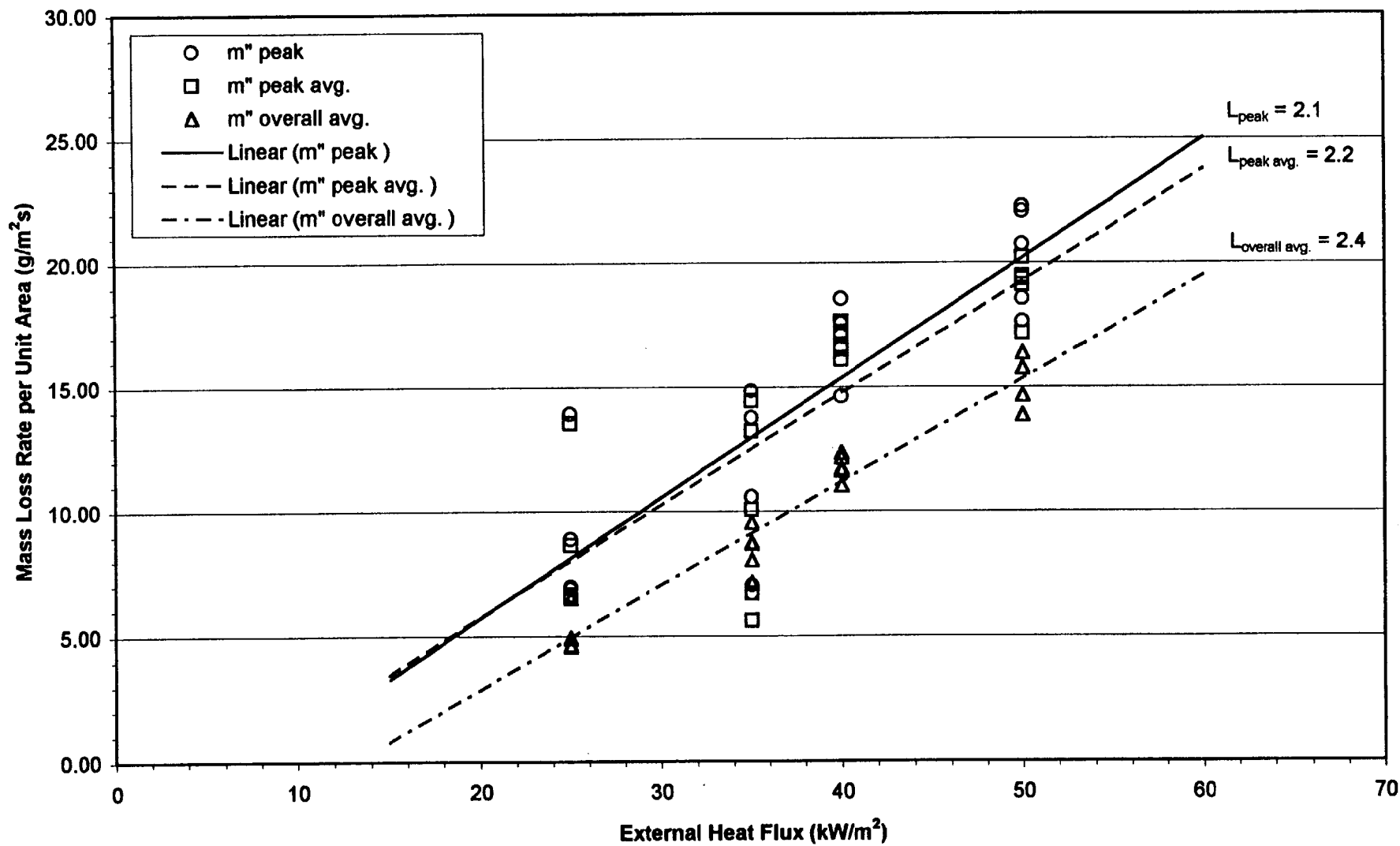
4.05 F.R. Extruded Polystyrene Board (40 mm): Mass Loss Rate vs. External Heat Flux



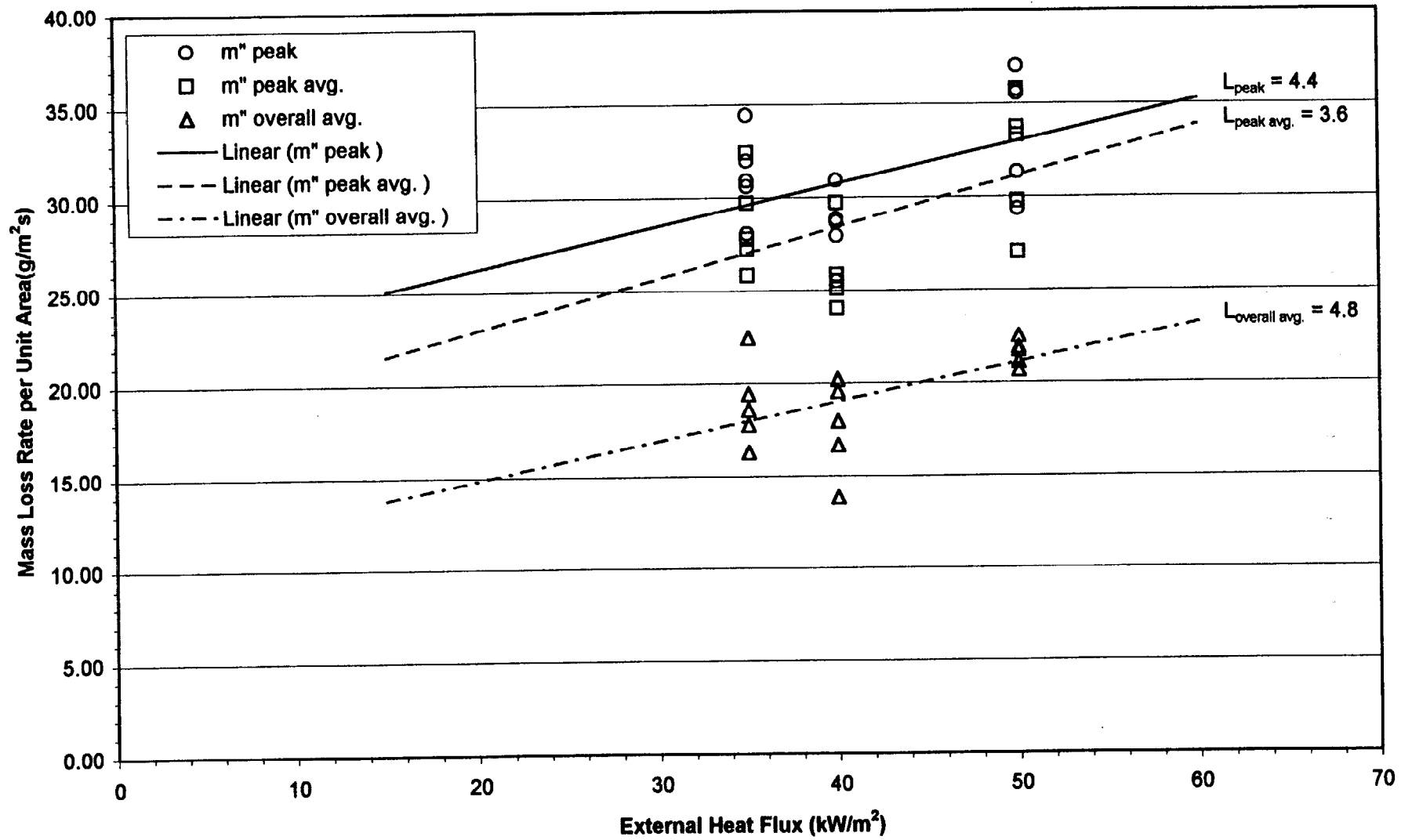
4.06 Acrylic Glazing: Mass Loss Rate vs. External Heat Flux



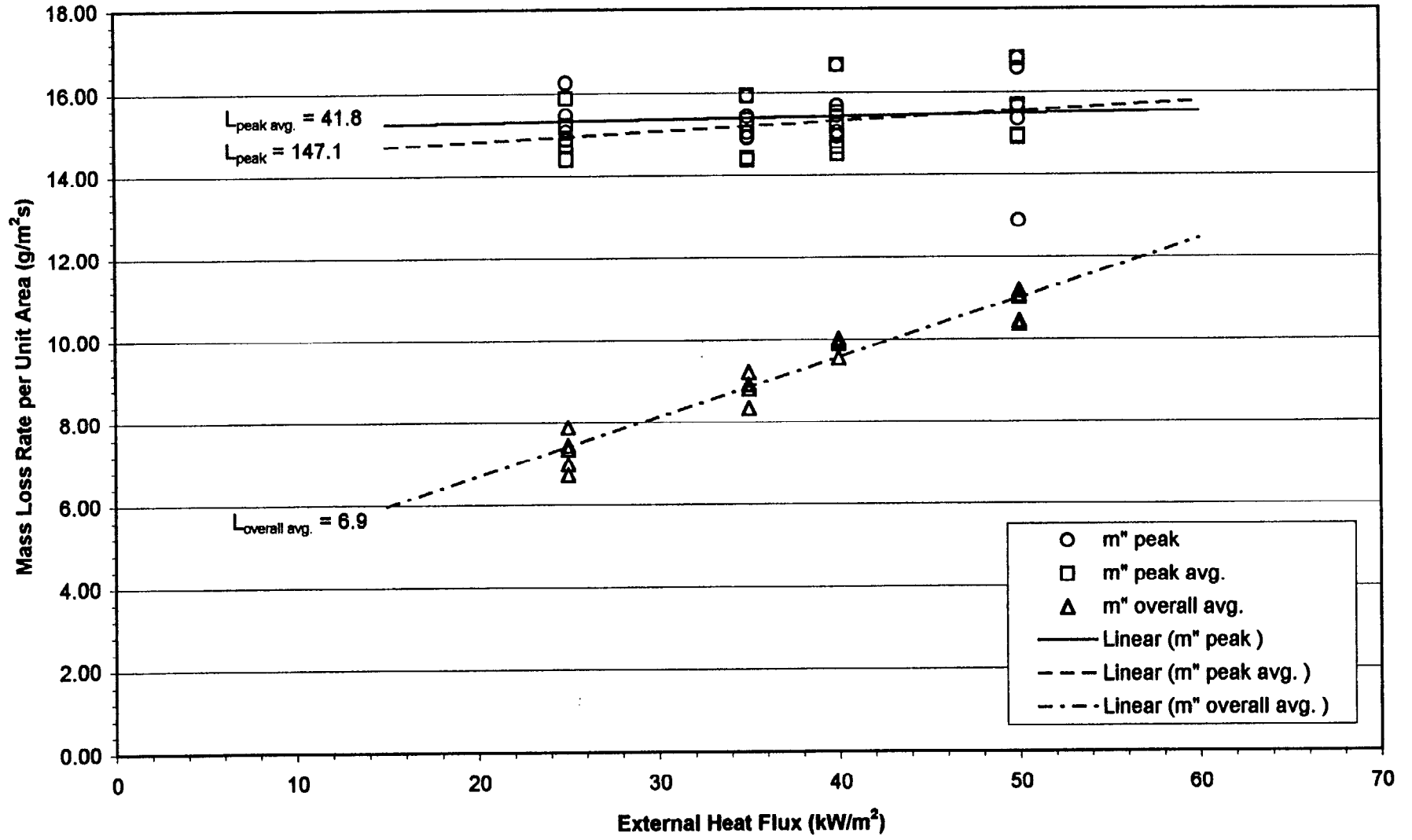
4.07 Mass Loss vs. External Heat Flux



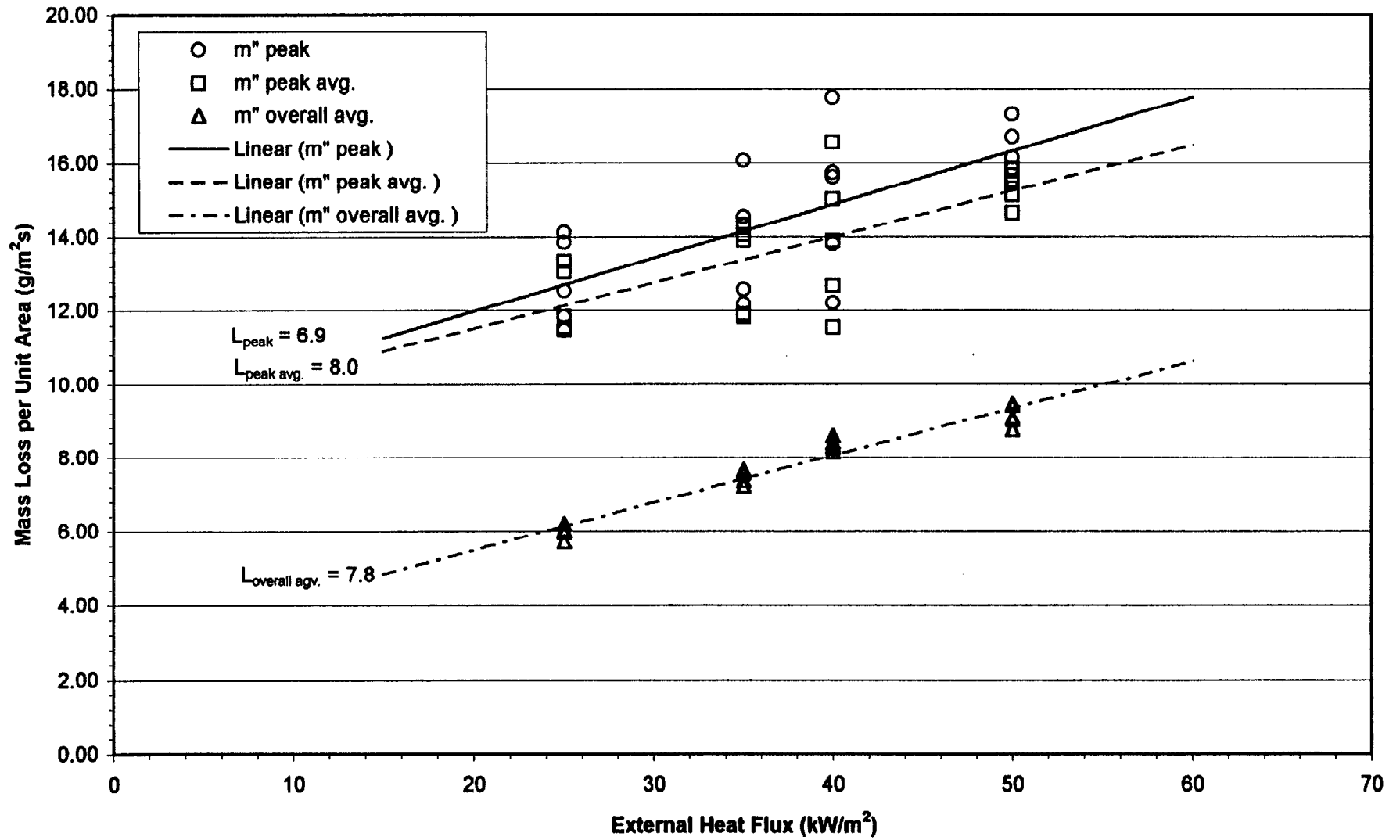
4.08 3-Layered F.R. Polycarbonate Panel: Mass Loss Rate vs. External Heat Flux



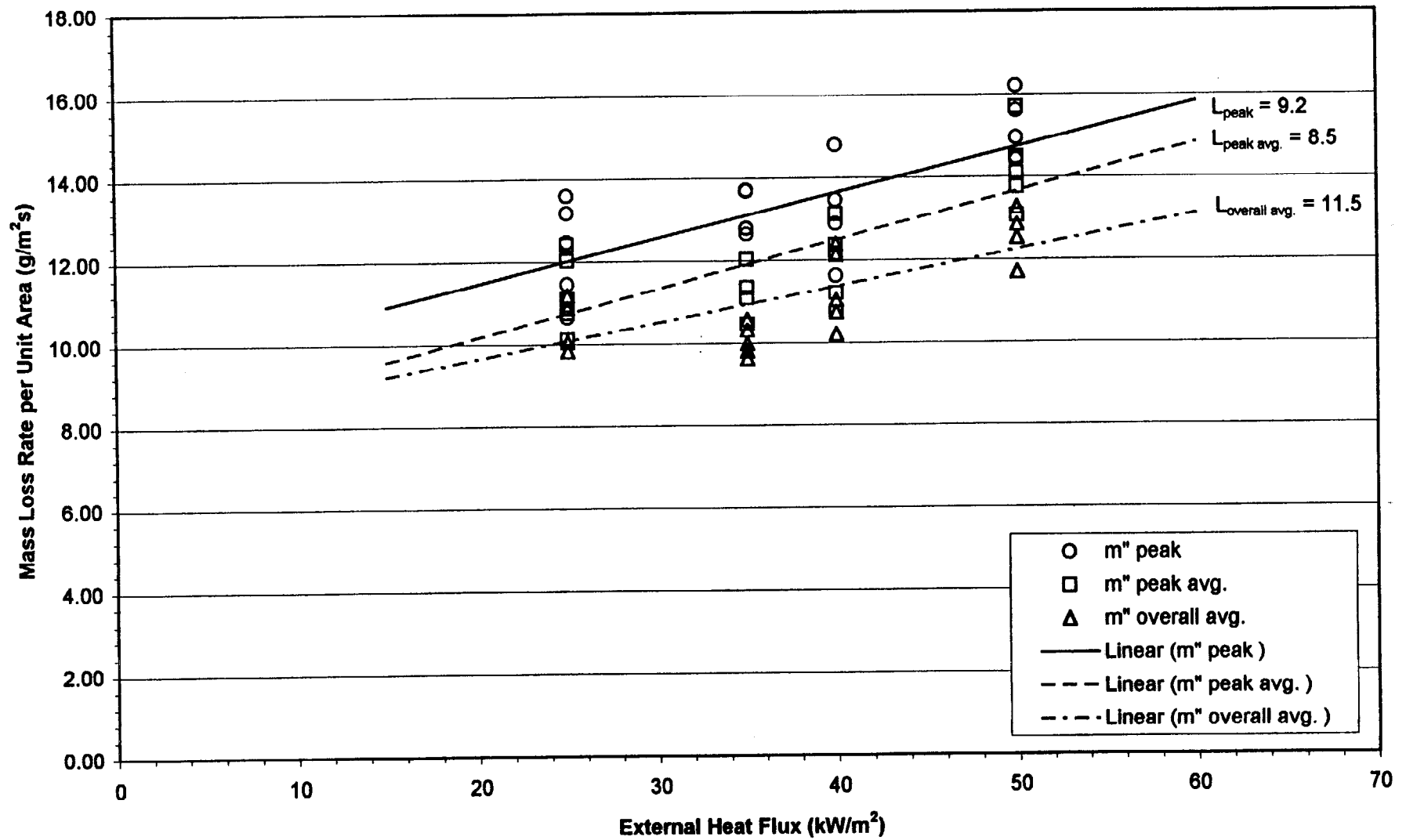
4.09 Varnished Massive Timber: Mass Loss Rate vs. External Heat Flux



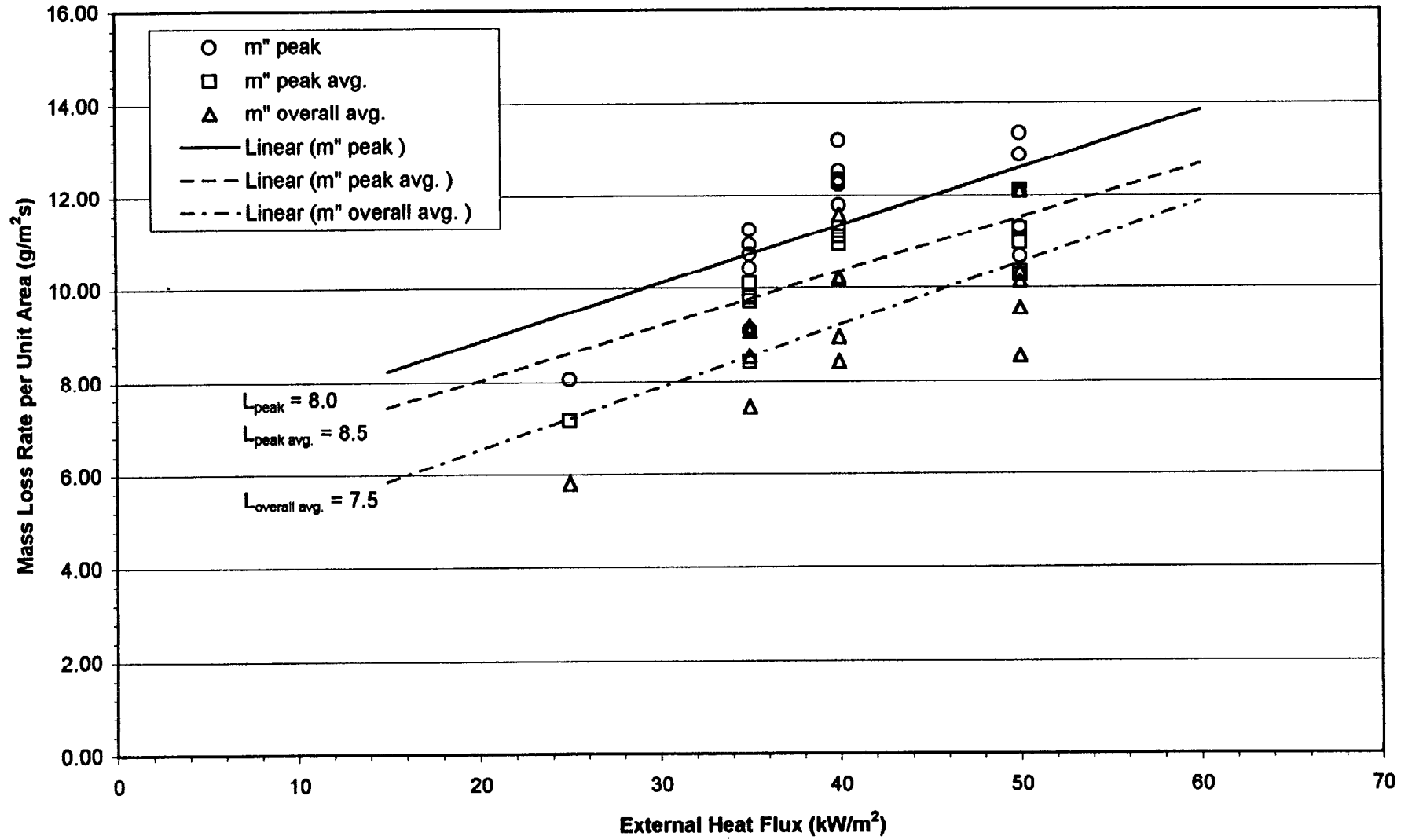
4.11 Normal Plywood: Mass Loss Rate vs. External Heat Flux



4.20 F.R. Expanded Polystyrene Board (40 mm): Mass Loss Rate vs. External Heat Flux



4.21 F.R. Expanded Polystyrene Board (80 mm): Mass Loss Rate vs. External Heat Flux



Heat of Gasification Value Analysis

The six calculated effective heat of gasification values for the different materials are presented in Table 3.5. Theoretically, all six heat of gasification values that have been calculated should be identical. It can be seen that for some materials, the calculated L values are reasonably consistent. However for other materials there is a great deal of discrepancy between the values and some of the values obtained do not make a great deal of sense. These discrepancies are due to moisture evaporation, char formation, unsteady burning rate and difficulties in determining appropriate mass loss rates and will be described in more detail below.

Table 3. 5: Effective Heat of Gasification (L) Values Calculated by Six Methods.

Material	Energy Release Rate			Mass Loss Rate		
	L_{peak} (kJ/g)	$L_{peak\ avg.}$ (kJ/g)	$L_{overall\ avg.}$ (kJ/g)	L_{peak} (kJ/g)	$L_{peak\ avg.}$ (kJ/g)	$L_{overall\ avg.}$ (kJ/g)
R 4.01, FR. Chipboard	9.3	10.0	4.5	13.4	12.4	9.4
R 4.02, Gypsum	4.6	4.8	-693.5	-27.9	-10.6	13.0
R 4.03, PU/Alum. *	---	---	---	---	---	---
R 4.04, PU/Paper	5.0	5.5	---	5.9	5.6	1.0
R 4.05, Ext. PS40	3.9	4.0	4.5	4.6	4.7	4.6
R 4.06, Acrylic	1.5	1.6	3.0	1.4	1.6	2.7
R 4.07, FR. PVC	9.3	10.4	4.2	2.1	2.2	2.4
R 4.08, 3-Layer PC	3.2	3.3	3.6	4.4	3.6	4.8
R 4.09, Mass Timber	22.9	17.5	6.5	147.1	41.8	6.9
R 4.10, FR. Plywood	8.9	9.3	8.8	12.7	13.4	15.5
R 4.11, Plywood	7.5	7.3	3.9	6.9	8.0	7.8
R 4.20, Exp.PS40	7.1	7.3	11.2	9.2	8.5	11.5
R 4.21, Exp.PS80	13.5	12.7	9.4	8.0	8.5	7.5

* Material properties could not be extrapolated from the test data

Negative heat of gasification values were calculated for the Paper Faced Gypsum Board (R 4.02). This is most likely due to the effects of the rapid burning of the paper facing followed by the evaporation of the moisture trapped within the gypsum itself. The continuous mass loss causes the effects of the burning paper to become relatively insignificant to the mass loss rate when determining $L_{overall, avg.}$ by the energy release method. The rapid burning of the paper facing produces very low energy release rate ($\approx 100 \text{ kW/m}^2$) and a minimal increase in the mass loss rate over a very short time period as can be seen in Figure 3.12. Therefore, inconsistencies appear in the determination of the peak and peak average mass loss rates leading to errors in the development of L due to the linear fit through the data.

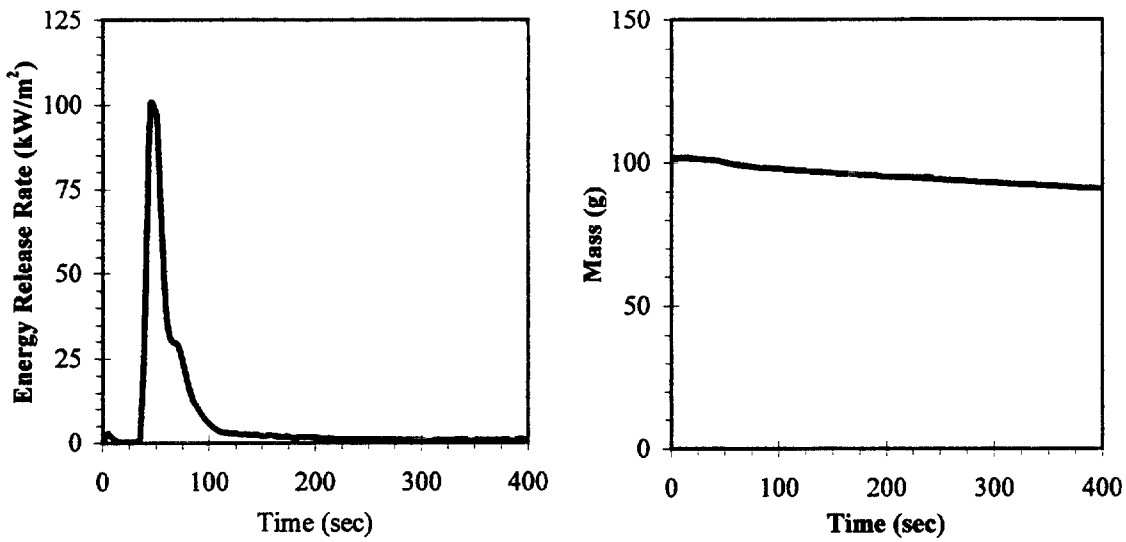


Figure 3. 12: Typical Energy Release Rate per Unit Area and Specimen Mass for Gypsum Board, R 4.02, in the Cone Calorimeter.

The $L_{overall\ avg.}$ value by the energy release rate method for the polyurethane foam panel with paper facing, R 4.04, is missing due to missing data from LSF. Without the $\Delta H_{C, overall\ avg.}$ values, this value could not be calculated. The $L_{overall\ avg.}$ value by the mass loss rate also appears to be very low while the other four values are relatively consistent. This was due to difficulties in determining the region of steady mass loss in Method #3 above. For most other materials the region of steady burning is clearly marked by a steady specimen mass loss followed by a sharp transition in the specimen mass with respect to time graph. However as Figure 3.13 indicates, the specimen mass follows more of a curve with respect to time therefore making it difficult to accurately determine this transition point. Using the point at which the energy release rate begins to rapidly decline (≈ 115 seconds in Figure 3.13) as the end of steady burning would have provided a line with a higher mass loss rate. This may provide a more appropriate L value when a linear fit is drawn through the mass loss rate per unit area data plotted versus the external heat flux.

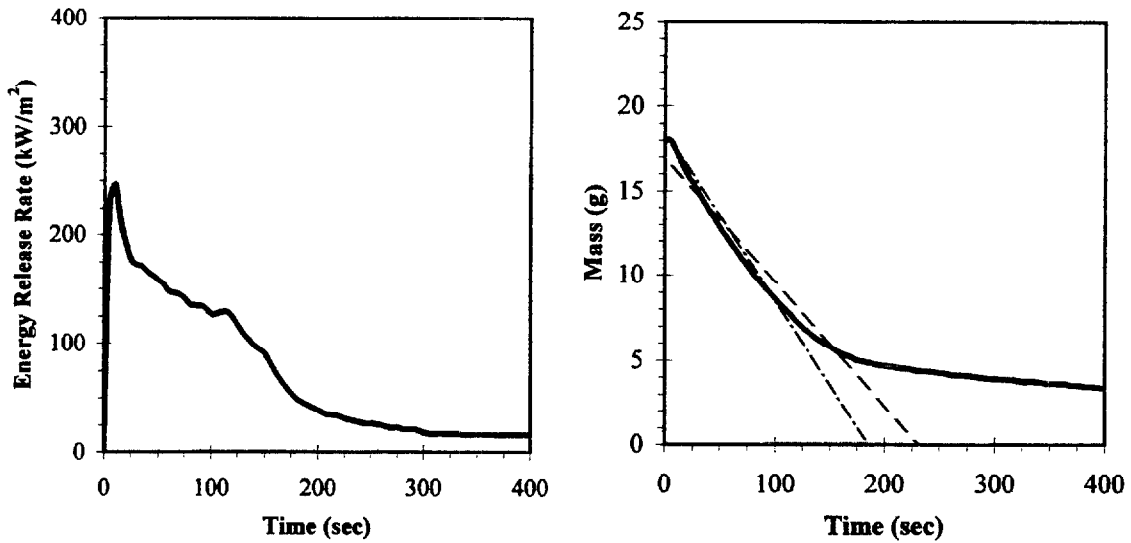


Figure 3. 13: Typical Energy Release Rate and Specimen Mass for Polyurethane Foam Board with Paper Facing, R 4.04, in the Cone Calorimeter.

The L values determined by the energy release rate method for fire retarded PVC, R 4.07, are much higher and less consistent than those calculated by the mass loss rate method. These high values are most likely due to the large amount of scatter that exists for the heat of combustion values, especially for the peak and peak average values at low external heat flux levels (see Figure 3.14). This type of scatter was not seen in the analysis of the other materials. The reason for this scatter is most likely due to the inconsistent burning characteristics of PVC as seen in Figure 3.15. The existence of both single and multiple peak energy release rates produces inconsistent data which therefore produces higher average ΔH_C values thereby producing high L values. The overall average heat of combustion has a lower, more constant value which explains why the $L_{overall\ avg.}$ value is closer to the mass loss rate values. The use of a lower heat of combustion value may be appropriate for determining L as well as for predicting the performance of fire retarded PVC.

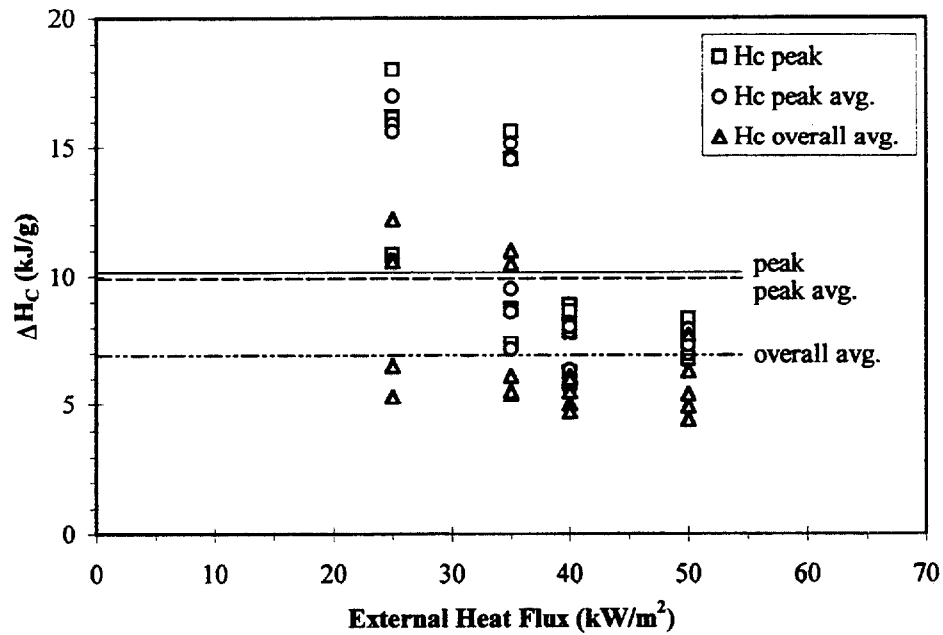


Figure 3. 14: Average Heat of Combustion Values for Fire Retarded PVC, R 4.07.

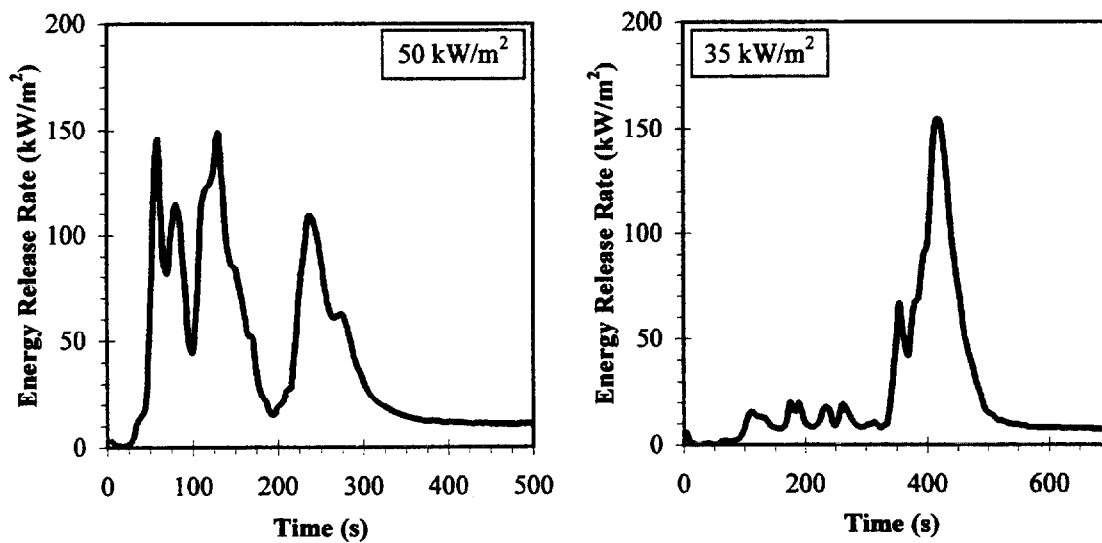


Figure 3. 15: Various Energy Release Rates for Fire Retarded PVC, R 4.07, in the Cone Calorimeter

The heat of gasification values for varnished massive timber, R 4.09, indicate a great deal of fluctuation. The L_{peak} and $L_{peak avg.}$ by mass loss rate values seem particularly high. Upon ignition the massive timber rapidly releases a large amount of

energy, which is most likely due to the varnish burning away. This peak energy release rate is relatively constant for different external heat flux levels and the mass loss rate associated with this peak appears to be constant as well (see Figure 3.16). This type of burning is atypical for wood samples burning in the Cone Calorimeter and confirms that the burning varnish has a constant energy release rate and mass loss rate regardless of the external heat flux. Typically the initial and secondary energy release rate peaks are proportional to the external heat flux.

Constant peak energy release and mass loss rates results in a linear fit through the peak and peak average mass loss rate data that is almost horizontal. Therefore, the inverse of the slope of this fit produces a high L value that does not appear to be appropriate for the material. The relatively high peak and peak average values by the energy release method are also most likely due to the high energy release rate associated with the burning of the varnish.

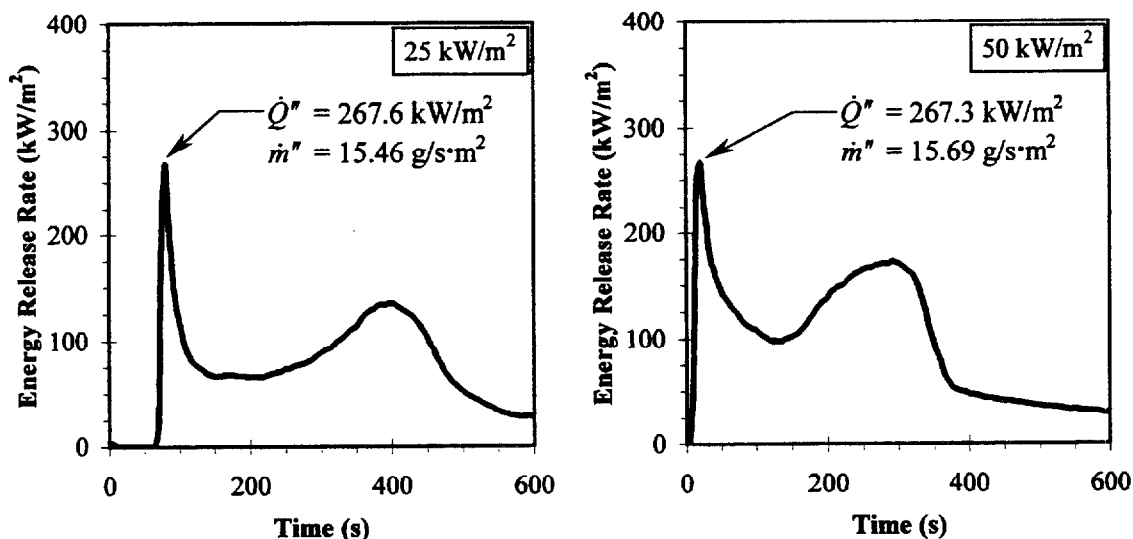


Figure 3. 16: Peak Energy Release and Mass Loss Rates for Varnished Massive Timber, R 4.09, at Different External Heat Flux Levels in the Cone Calorimeter.

Fire retarded chipboard, R 4.01, and normal plywood, R 4.11, demonstrate slightly reduced $L_{overall\ avg.}$ by energy release values. This seems to be typical for cellulosic-type materials and is most likely due to char formation. At lower heat fluxes, a layer of char can develop over the surface of normal charring materials, like wood, long before ignition. However, as the wood is continually heated, it pyrolyzes and continues to lose mass even though there is no flame present. At much higher heat fluxes, ignition usually occurs before a significant char layer can develop. Due to the mass loss prior to ignition at lower heat fluxes, the overall energy release rate will be reduced, therefore producing a linear fit through the data that has a higher slope. The inverse of this higher slope will produce a reduced L value as can be seen in Table 3.5. The fire retarded

plywood does not show this significantly low $L_{overall\ avg.}$ value mostly due to only some of the samples igniting at 25 kW/m² and less importance being placed on these data points when taking a linear fit through the data. It is important to note that charring materials will show this sort of char layer development dependence at different low heat flux levels and this level will depend on sample orientation, fire retardant additives and material properties (critical heat flux for ignition, density, thermal conductivity, etc.).

3.6 Total Energy Per Unit Area (Q'')

Samples tested in the Cone Calorimeter release a certain amount of energy (Q) over the duration of the test. In order to predict the performance of materials in full-scale scenarios, this total evolved energy term is needed. However, it is desirable to eliminate thickness and density factors in the expression of this energy. Therefore the total amount of energy that can be released from a material when it is burning is expressed in terms of a unit area (Q''). The total energy per unit area can be calculated by:

$$Q'' = \frac{Q}{A_s}$$

where Q is the total heat evolved from the sample material and A_s is 0.0088 m². The total heat evolved for each tested sample is provided in Appendix A.6.

Like the heat of combustion and heat of gasification, Q'' is regarded as a material property that is independent of the incident heat flux. It expresses the total amount of energy present per unit area of material. Therefore in order to calculate an effective Q'' value for a material, the numerical average of all the Q'' values measured in the Cone is calculated. This average value effectively represents the total energy available from a square meter of the material and is expressed graphically in Figure 3.17—the horizontal line indicating the average Q'' value. The average values determined for all of the materials are presented in Table 3.6 and the graphs from Appendix A.6 are also presented for convenience.

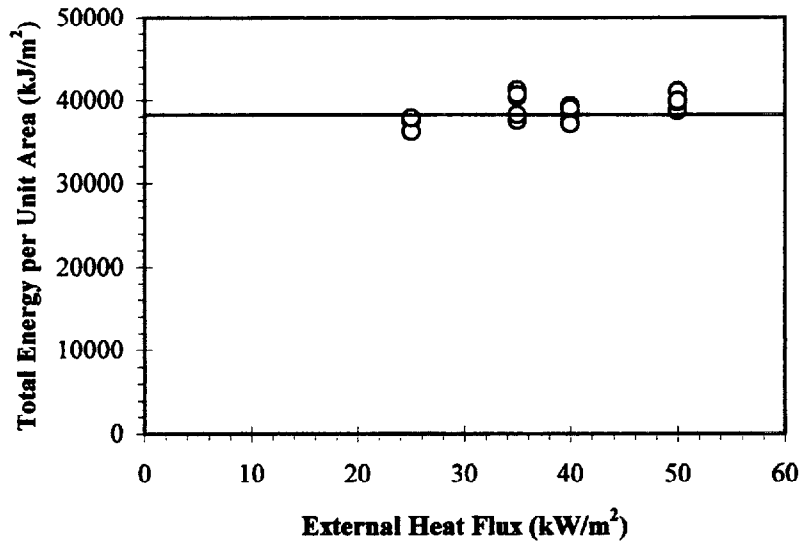
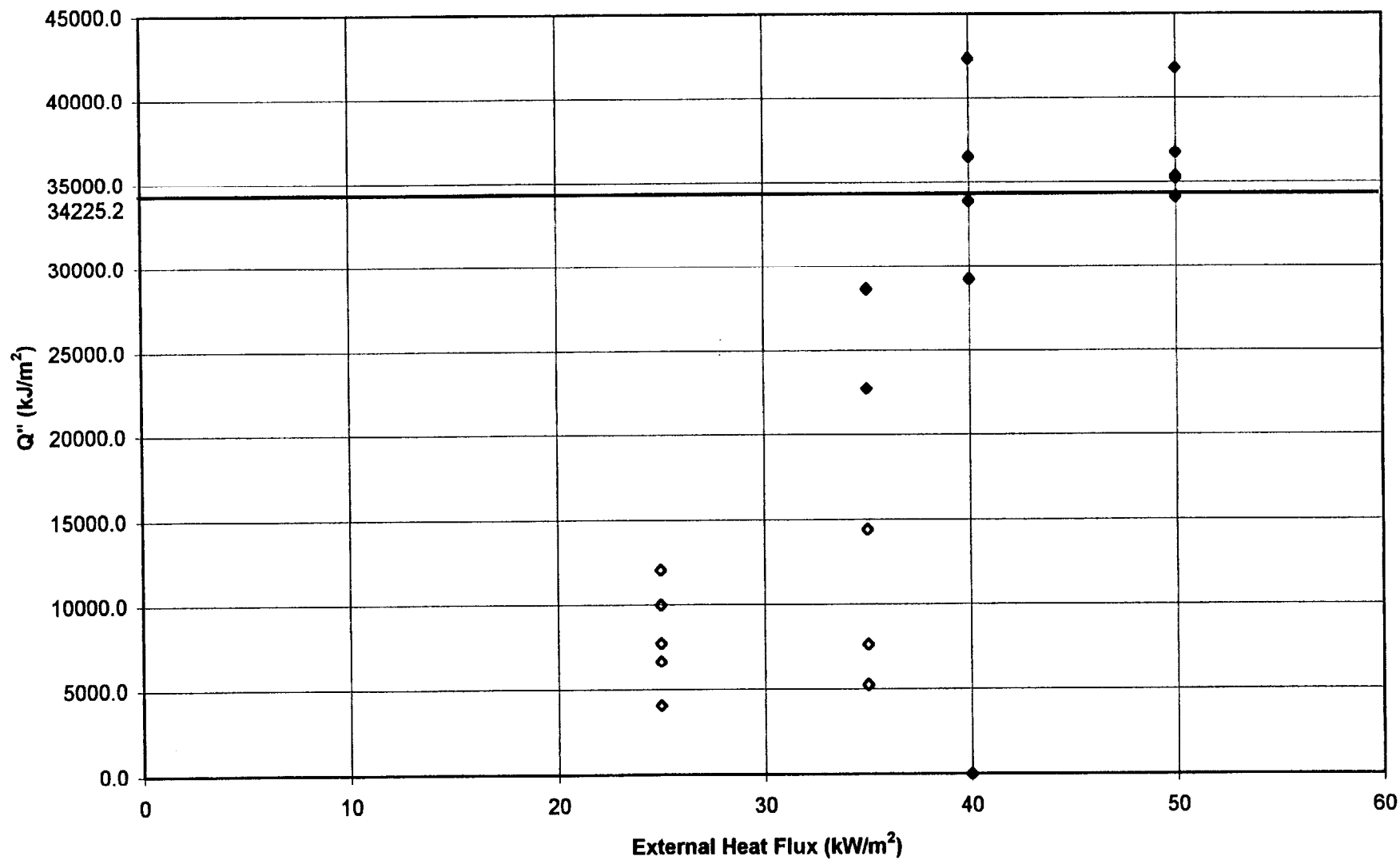


Figure 3. 17: Typical Total Energy per Unit Area (Q'') Determination: R 4.05, Extruded Polystyrene Board.

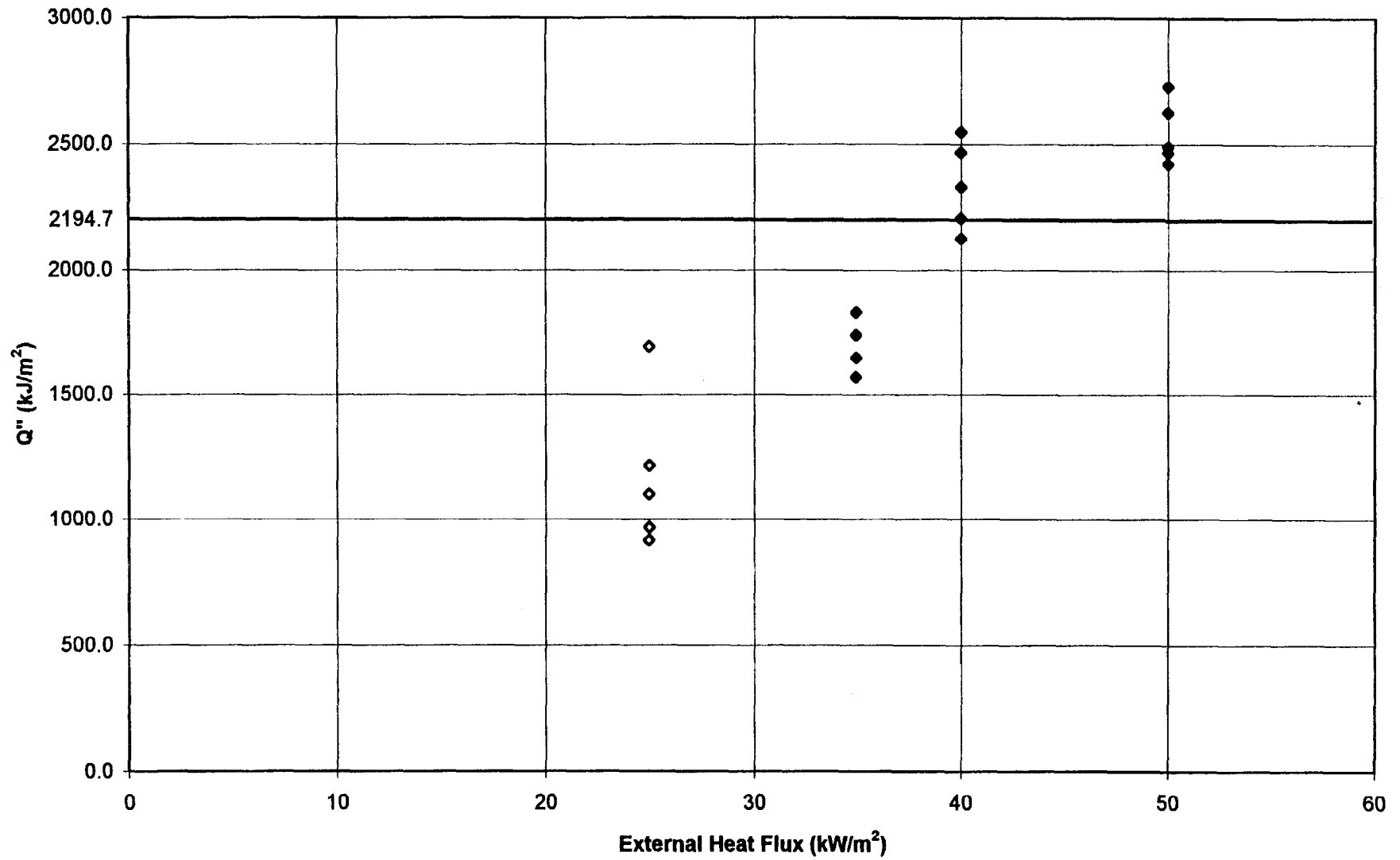
Table 3. 6: Energy Release per Unit Area of Material.

Material	Q'' (MJ/m ²)
R 4.01, FR. Chipboard	34.2
R 4.02, Gypsum	2.2
R 4.03, PU/Alum.	32.9
R 4.04, PU/Paper	30.8
R 4.05, Ext. PS40	38.7
R 4.06, Acrylic	89.5
R 4.07, FR. PVC	16.1
R 4.08, 3-Layer PC	58.1
R 4.09, Mass Timber	68.2
R 4.10, FR. Plywood	51.8
R 4.11, Plywood	64.6
R 4.20, Exp. PS40	33.9
R 4.21, Exp. PS80	25.5

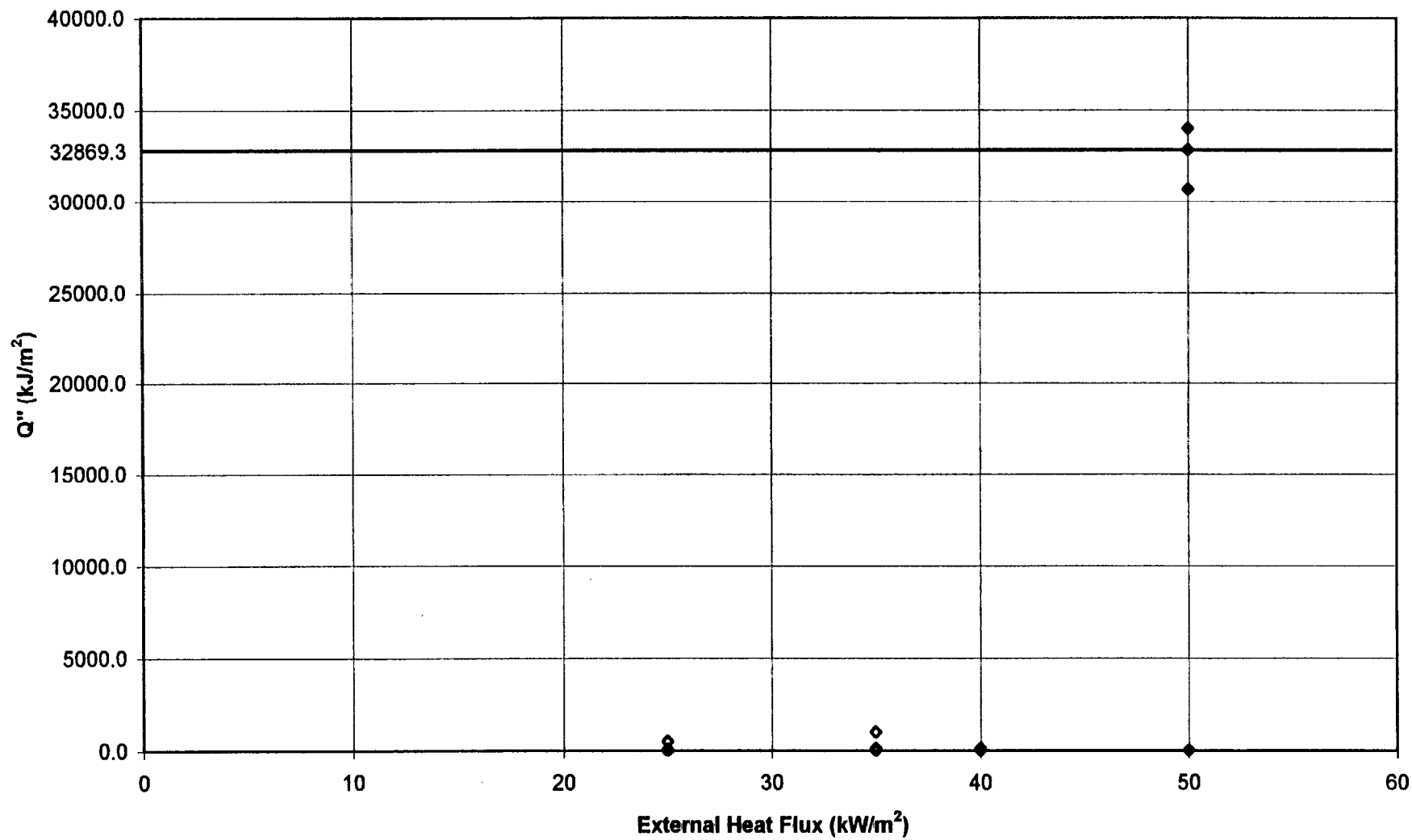
R 4.01 F.R. Chipboard: Total Heat Evolved vs. External Heat Flux



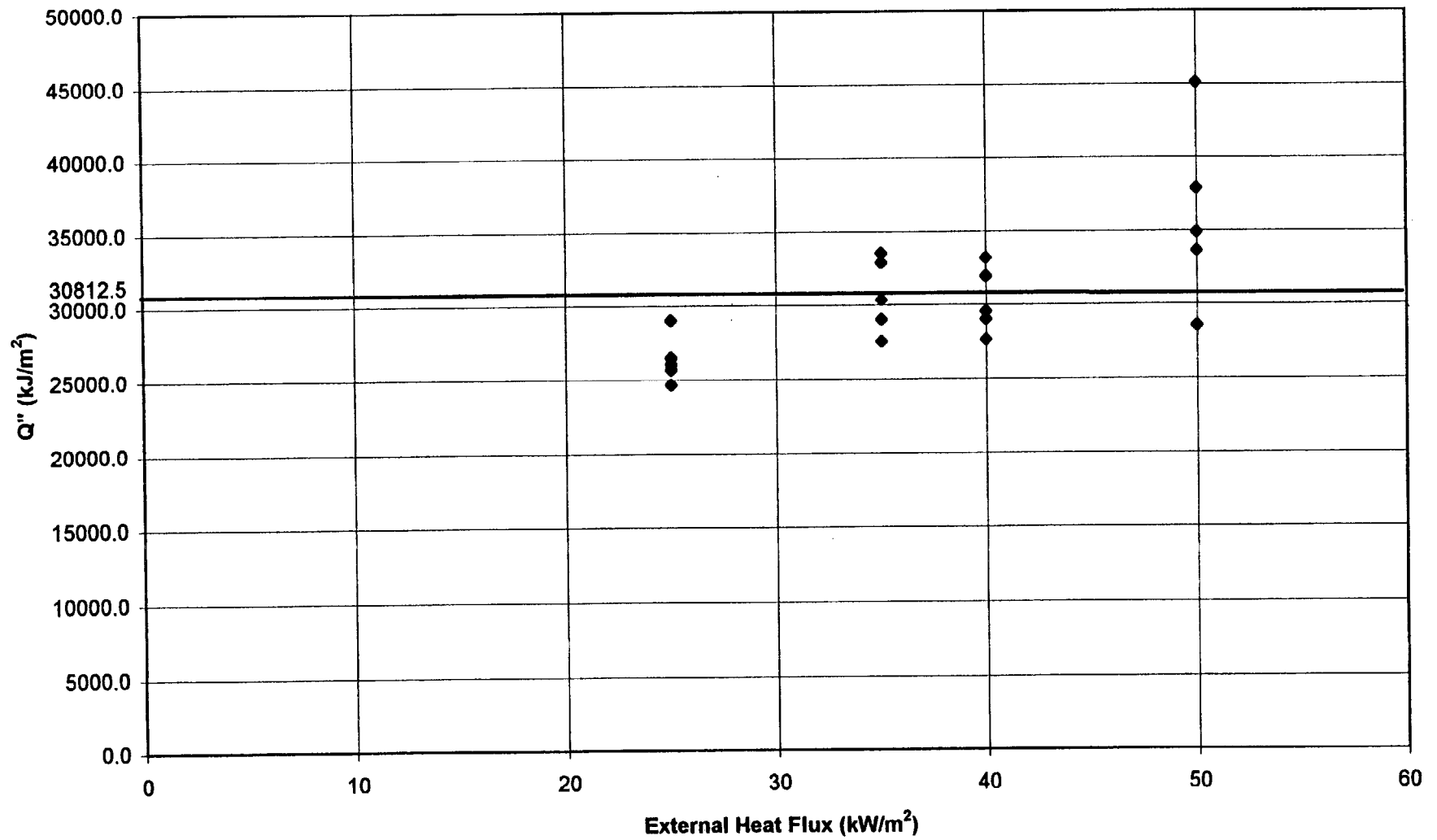
R 4.02 Paper Faced Gypsum Board: Total Heat Evolved vs. External Heat Flux



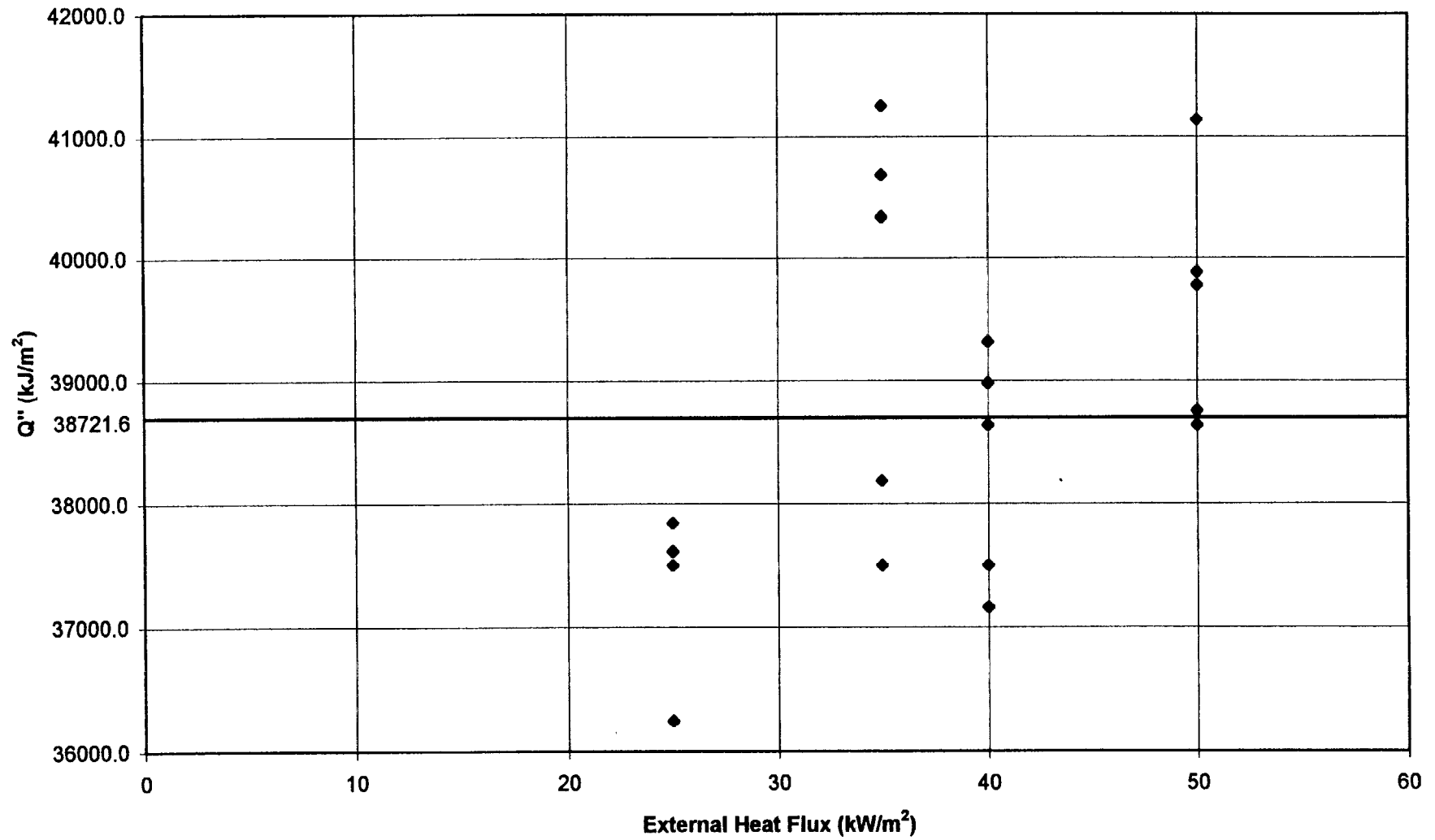
**R 4.03 Polyurethane Foam Panel with Aluminum Faced Paper:
Total Heat Evolved vs. External Heat Flux**



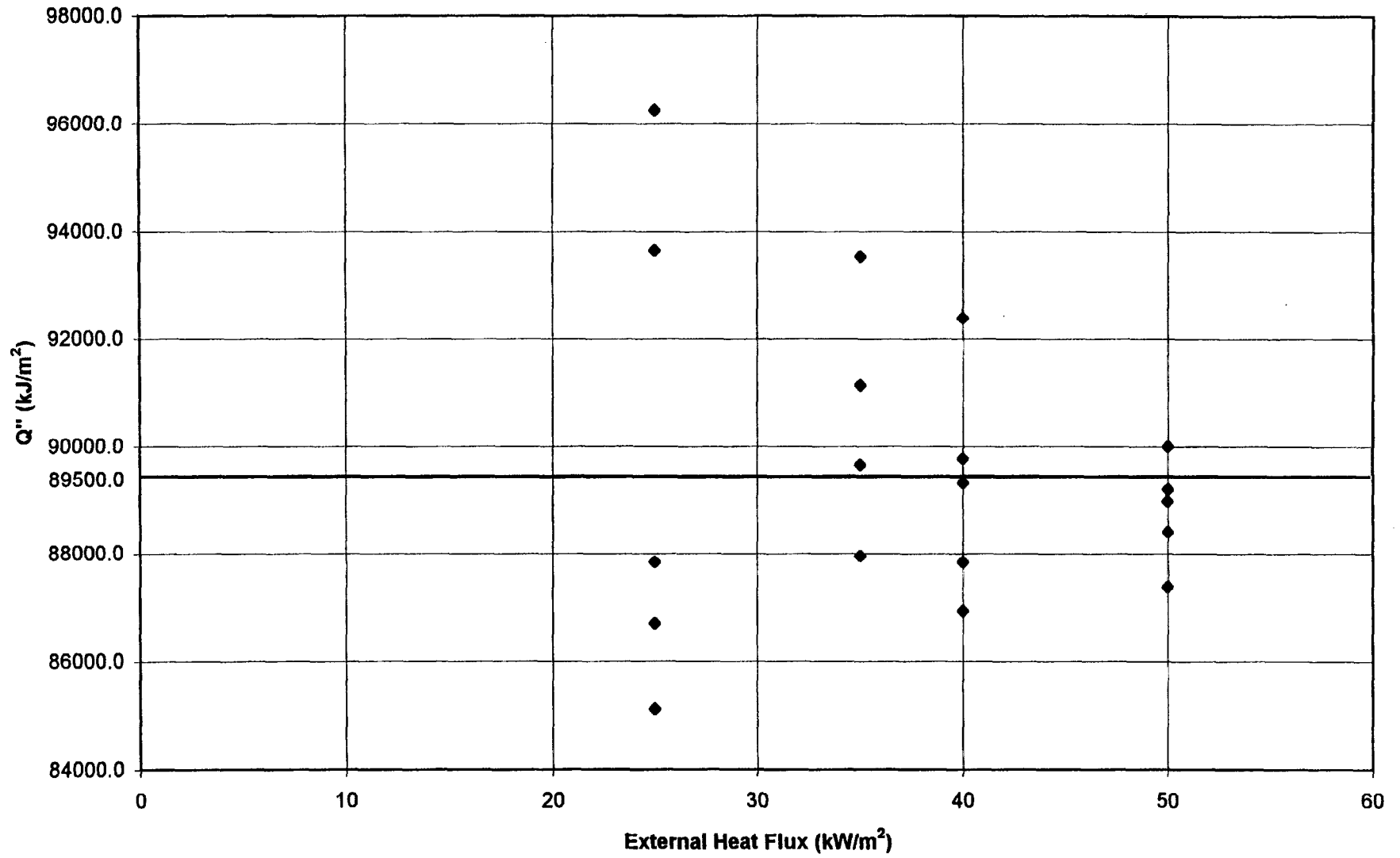
**R 4.04 Polyurethane Foam Panel with Paper Backing:
Total Heat Evolved vs. External Heat Flux**



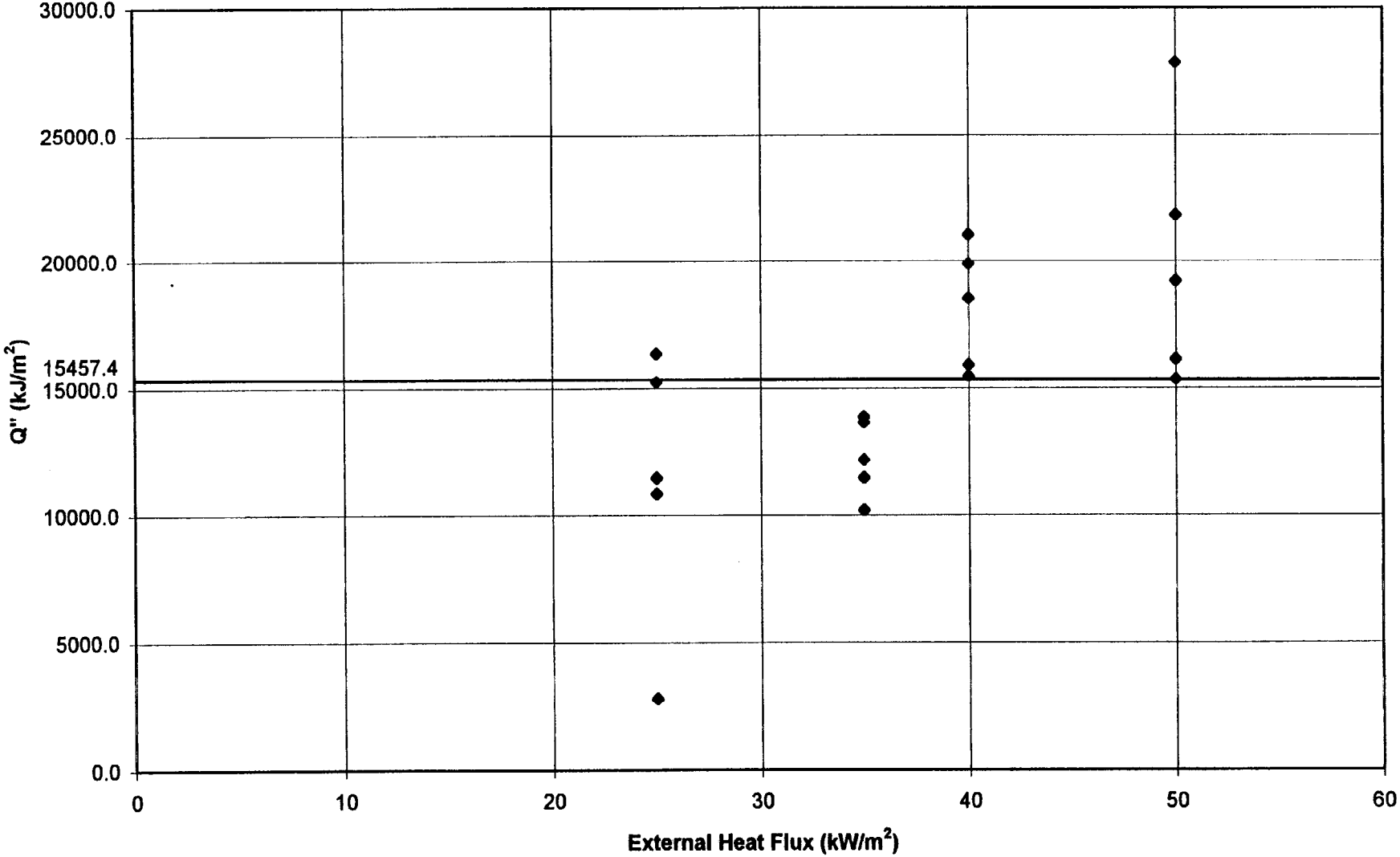
**R 4.05 Extruded Polystyrene Board (40 mm):
Total Heat Evolved vs. External Heat Flux**



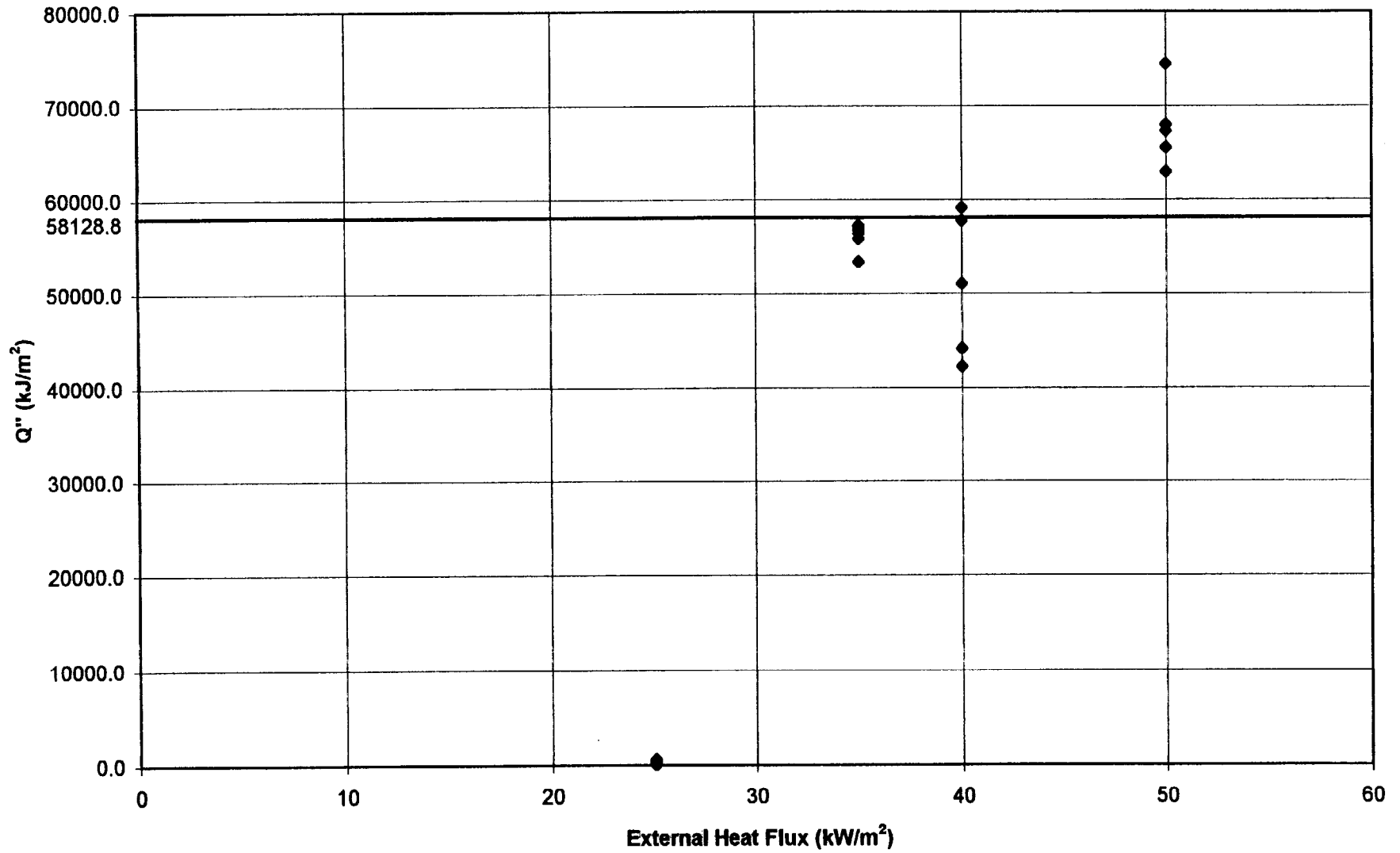
R 4.06 Acrylic Glazing: Total Heat Evolved vs. External Heat Flux



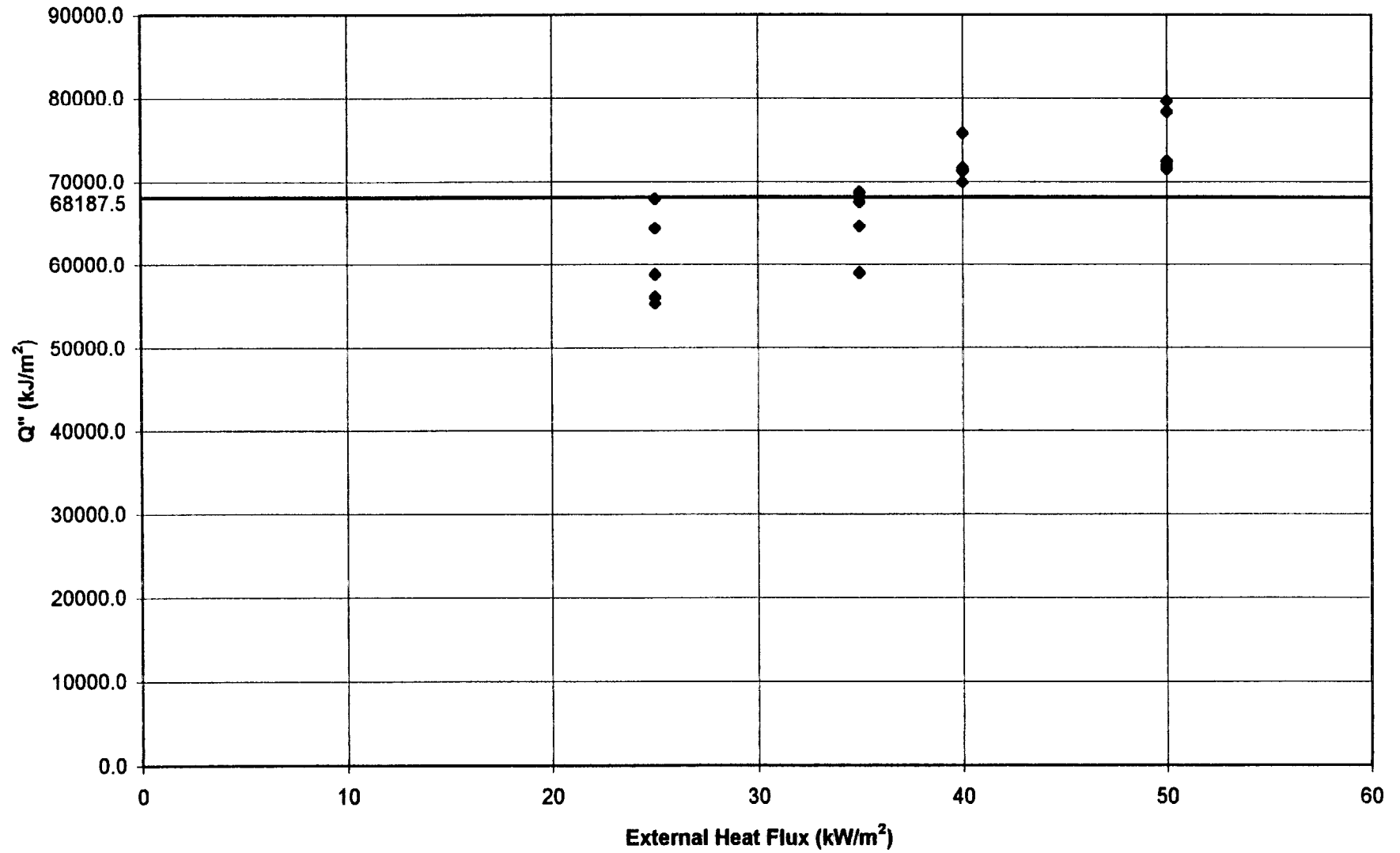
R 4.07 F.R. PVC: Total Heat Evolved vs. External Heat Flux



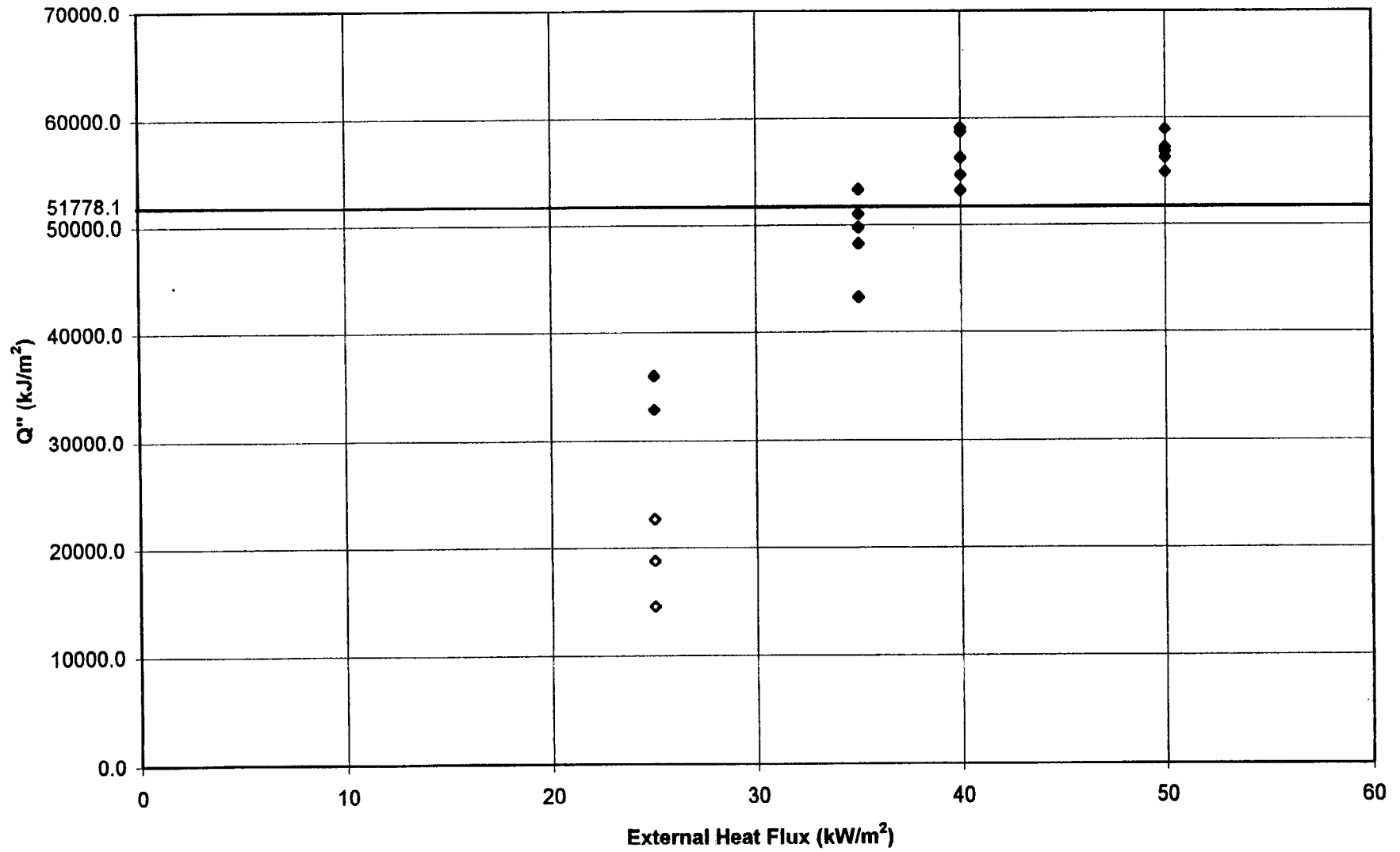
R 4.08 3-Layered F.R. Polycarbonate Panel: Total Heat Evolved vs. External Heat Flux



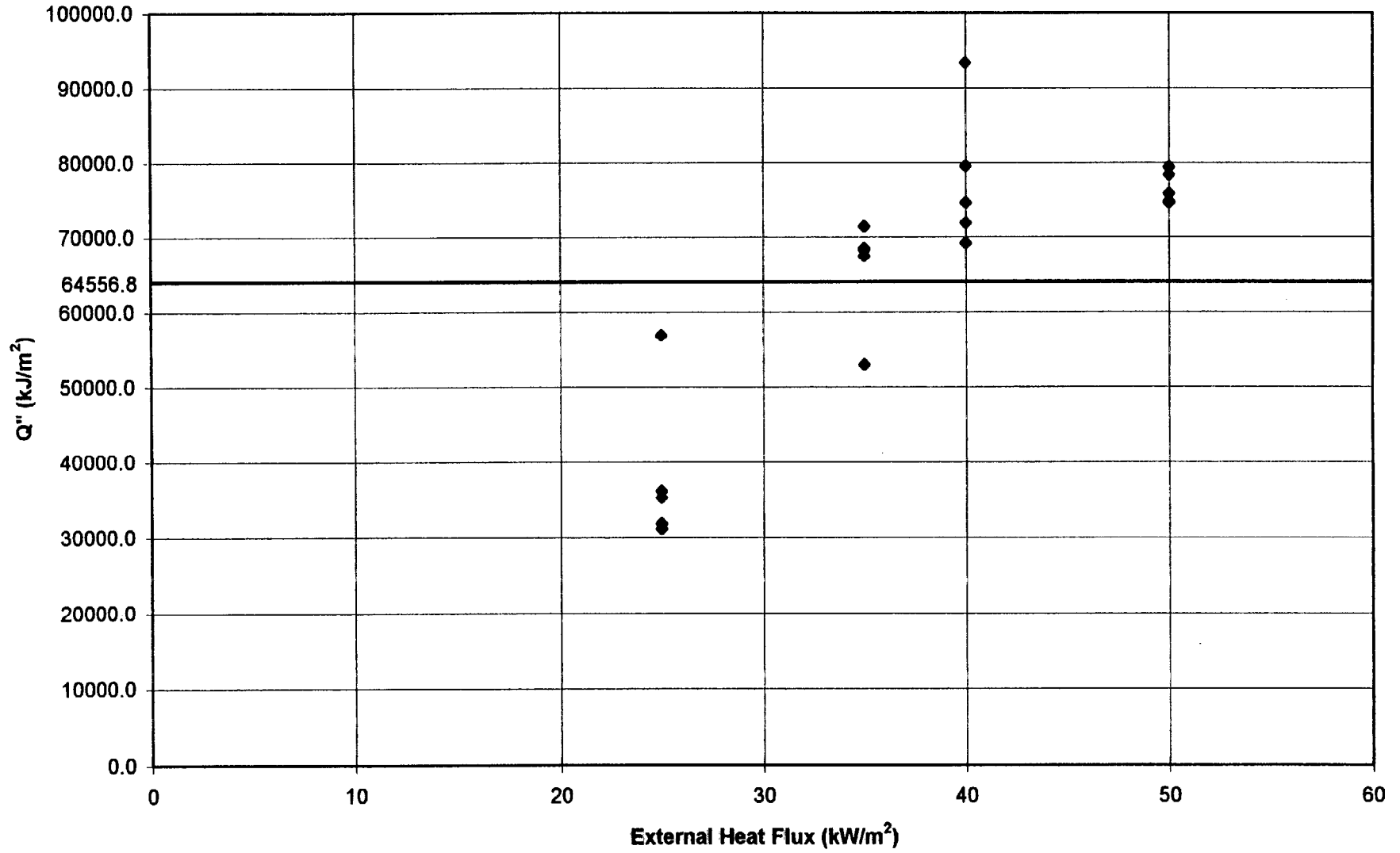
R 4.09 Varnished Massive Timber: Total Heat Evolved vs. External Heat Flux



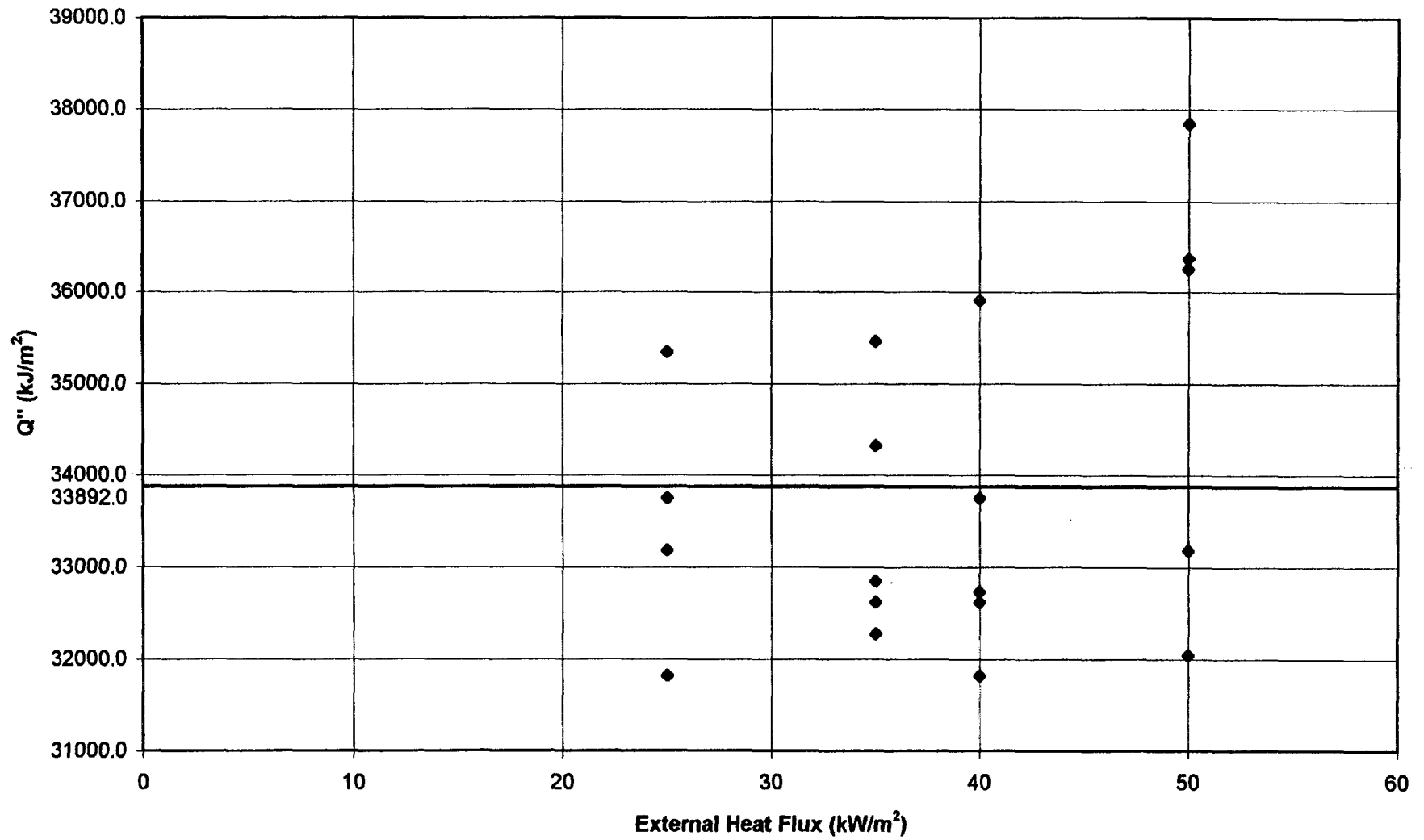
R 4.10 F.R. Plywood: Total Heat Evolved vs. External Heat Flux



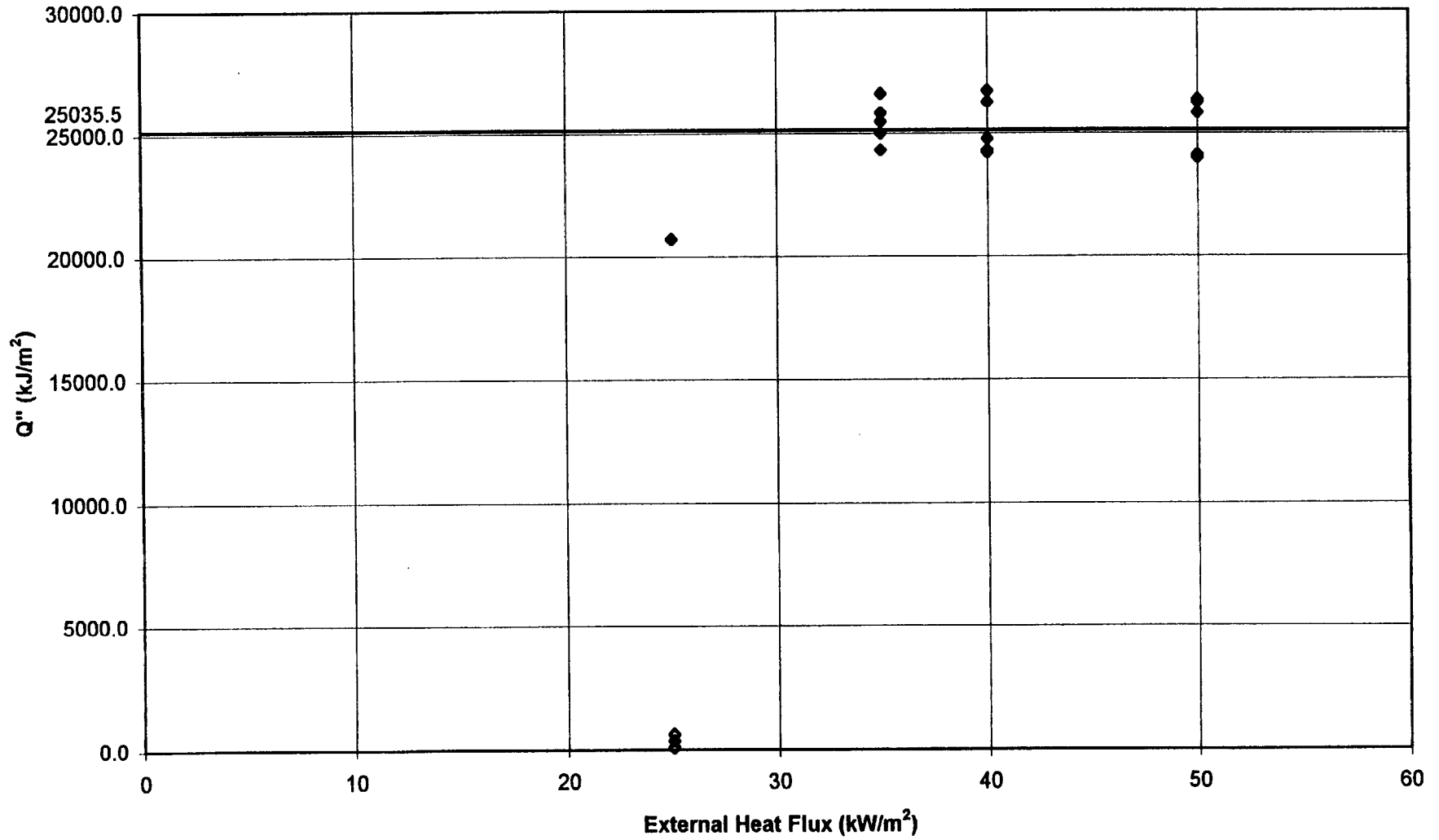
R 4.11 Normal Plywood: Total Heat Evolved vs. External Heat Flux



**R 4.20 F.R. Expanded Polystyrene Board (40 mm):
Total Heat Evolved vs. External Heat Flux**



R 4.21 F.R. Expanded Polystyrene Board (80 mm):
Total Heat Evolved vs. External Heat Flux



3.7 Material Property Conclusion

In order to appropriately model the performance of the materials, the properties that best represent the burning characteristics under actual conditions must be determined. It is also desirable to determine these properties in a systematic manner that will allow consistent predictions of material properties. For this analysis, the “peak average” heat of combustion and heat of gasification by the energy release rate method appear to be the most appropriate. This was a judgement that was made based on the desire to most accurately represent full-scale conditions with the model. The “peak” values were not used because it was believed that instantaneous burning effects would not be consistent with actual material performance. The peak values may also produce an energy release rate from the material that is too high and will cause excessive, unrealistic flame spread and fire growth. The “overall average” values were not chosen because non-burning effects such as moisture evaporation could have caused errors in the determination of the material properties. A comparison of some typical energy release rate predictions for a thermoplastic and charring material in the Cone are presented in Figures 3.14 and 3.15, respectively. As the figures indicate, the peak average values appear to give the best representation of the energy release rate for both types materials. Therefore, the peak average properties for all materials were used.

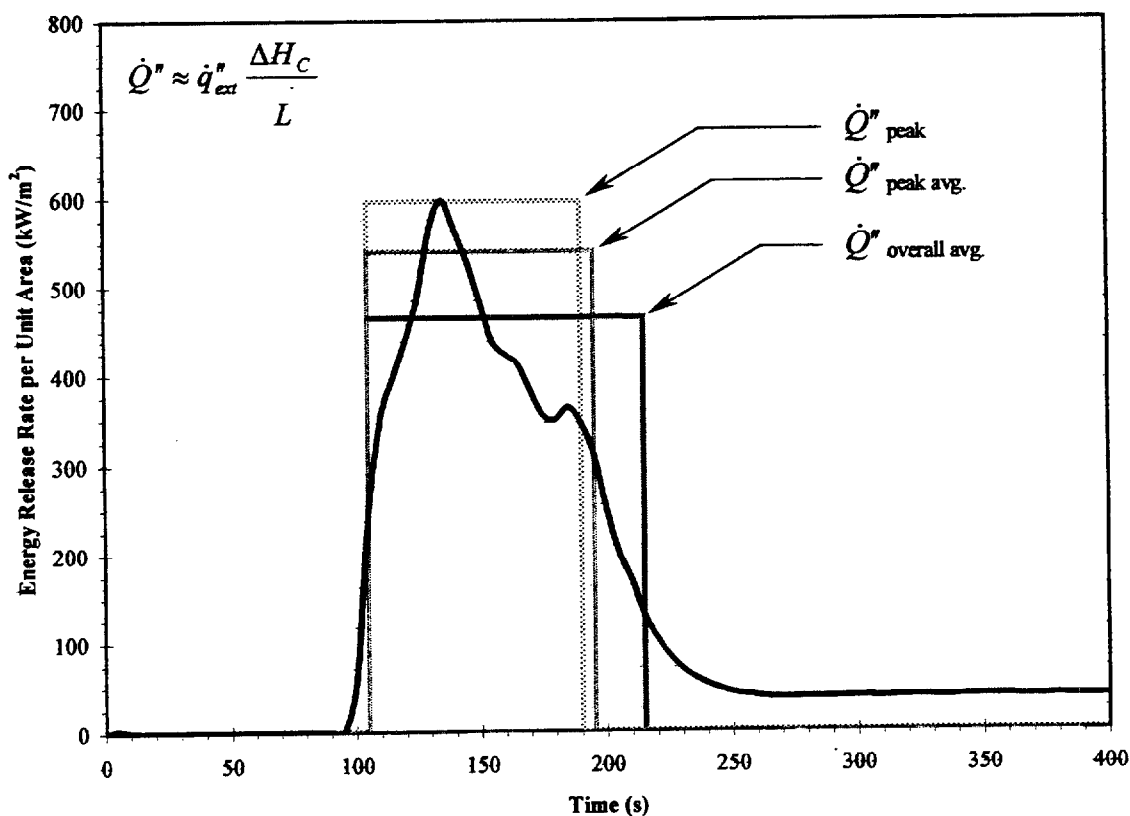


Figure 3. 18: Comparison of Methods for Predicting the Energy Release Rate of a Thermoplastic Material in the Cone Calorimeter: R 4.08.

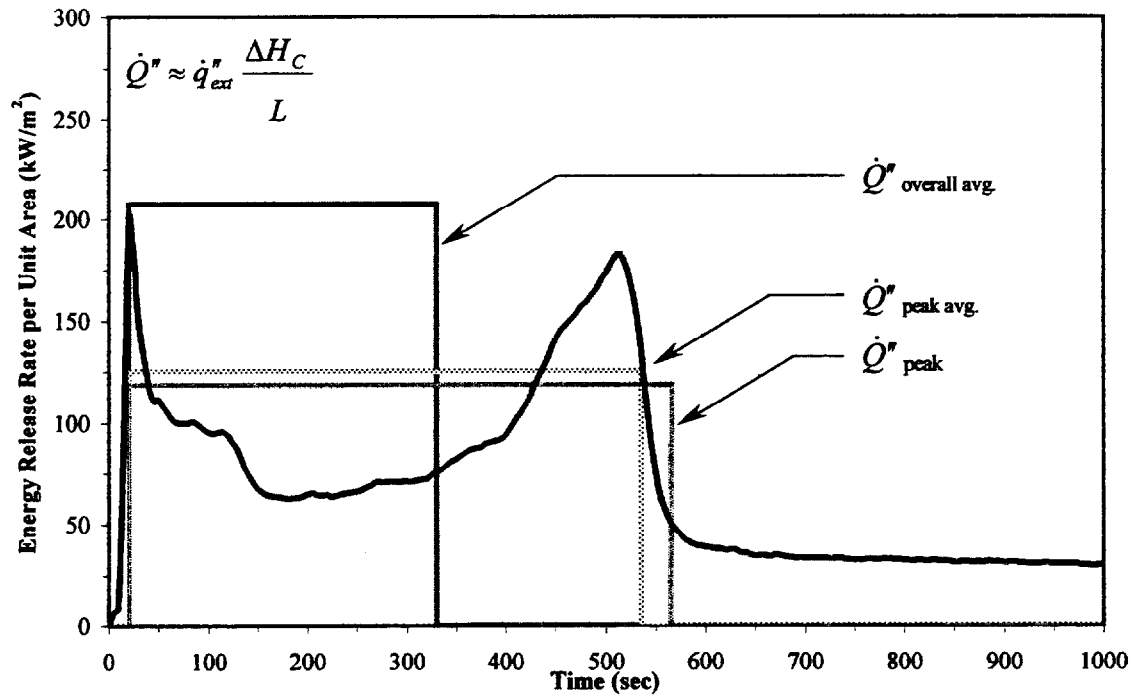


Figure 3. 19: Comparison of Methods for Predicting the Energy Release Rate of a Charring Material in the Cone Calorimeter: R 4.11, Normal Plywood.

4. FIRE GROWTH PREDICTIONS

4.1 Fire Growth Model

The model used for predicting the performance of the LSF materials in the room/corner test was developed by Quintiere. Previous literature has been published which describes the physics of model and its application [5, 15, 18, 19] and a brief description is provided in Section 1.2, therefore a detailed description will not be provided here. However, important aspects of the model that were taken into consideration in the analysis of these materials will be provided at the appropriate points. The model requires input data regarding the following:

- Initial room temperature: 20 °C
- Room geometry: 2.4 m x 3.6 m x 2.4 m high with a 2.0m x 0.8 m door/vent.
- Ignition burner output: 100 kW for 10 minutes followed by 300 kW for an additional 10 minutes.
- Model precision
- Material Property Data

A copy of the Fortran source code for the model is provided in Appendix D.

4.2 Material Properties Used

The material properties used for modeling the flame spread are presented in Table 4.1. There is no lateral flame spread parameter, Φ , for the acrylic glazing (R 4.06) since the ignition temperature and minimum temperature for spread are the same. The lack of data for the polyurethane foam panel with aluminum facing, R 4.03, is due to the lack of material ignition at all incident heat fluxes except 50 kW/m². Due to the reflective nature of the aluminum facing ignition only occurred at the highest external heat flux in the Cone Calorimeter and material properties could not be extrapolated. Therefore the material properties developed for the polyurethane foam panel with paper facing, R 4.04, were used to predict the performance of the aluminum faced foam in the full-scale test. The room/corner test ignition burner will quickly coat the aluminum facing with soot thereby causing a significant increase in the absorptivity of the aluminum and an increase in the heat transfer to the polyurethane. This will cause the aluminum faced foam to perform much like the paper faced foam and allows for a fire growth prediction to be made. Observations from the full-scale test indicate that the aluminum facing began to become damaged in the region around the ignition burner after approximately 14 seconds. This damage to the aluminum facing allowed the polyurethane foam to be exposed to the igniter flames and which allowed rapid ignition, unlike in the Cone Calorimeter.

As mentioned in the previous section, the “peak average” heat of combustion and heat of gasification values are used for the basic material performance prediction

However, modifications to the properties will be made to account for potential errors in the properties (as discussed in Section 3.5) and unusual performance in the room/corner test, i.e., melting.

Adjusted Properties for Melting/Dripping Materials

In order to account for the melting of thermoplastic materials the burnout time of the material (t_b) can be approximated as being the time at which the material began to melt in the full scale tests. This approximation assumes that when a material melts, drips and/or falls from the walls and ceiling in the room/corner test, it is burned away and no longer present and available to burn. The model calculates the burnout time of a material by

$$t_b = \frac{Q''}{\dot{Q}''} \quad (4.1)$$

where Q'' is the total energy per unit area of the material (kJ/m^2) and \dot{Q}'' is the energy release rate per unit area (kW/m^2) which can be calculated by

$$\dot{Q}'' = \dot{q}_{net}'' \frac{\Delta H_c}{L} \quad (4.2)$$

where \dot{q}_{net}'' represents the net heat flux to the material which is approximated as the total heat flux from the flame minus any re-radiation from the material surface:

$$\dot{q}_{net}'' = \dot{q}_f'' - \dot{q}_{rr}'' \quad (4.3)$$

Quintiere [19] considers the flame heat flux to be constant over the pyrolysis (burning) region and over the extended flame length. The net flame heat flux over the pyrolysis zone is taken as being 60 kW/m^2 . This represents the heat flux to the material surface over the height of the ignition burner flame and the heat flux from the flames over the region of material that is burning. The value used by Quintiere is consistent with values reported by Kokkala [11] for a similar ignition burner in a corner: 50 to 60 kW/m^2 over 60% of the average flame height. Quintiere also selects the extended wall flame heat flux to the unburned material above the pyrolysis region to have a constant value of approximately 30 kW/m^2 . The idealized heat flux distributions from the ignition burner and the extended wall flame can be seen in Figure 4.1.

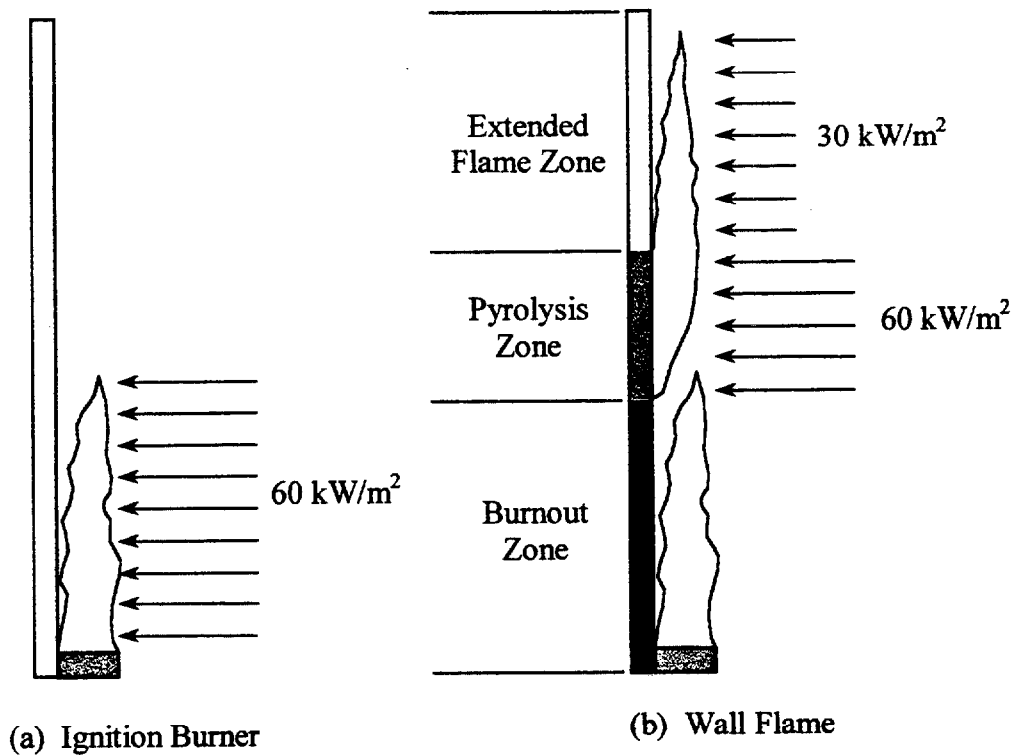


Figure 4. 1: Idealized Heat Flux Distributions.

Using Equations 4.1 to 4.3, an approximate burnout time for the material can be calculated. The model treats the burnout time as the time at which the material is no longer present and available to burn, which is also the case when the material melts or falls off of the wall and the ceiling in full-scale tests. Therefore the time for a material to begin melting in the full-scale experiments were then taken to be “effective burnout times”. In order to achieve these effective times, the total energy per unit area of material (Q'') was reduced by a fraction which caused the burnout time to be similar to the melting time. This reduced Q'' is then taken to be an approximation of the actual energy available from melting materials.

This approximation method seems to work relatively well. However, for some materials the reduced Q'' prediction did not produce enough of a reduction in the heat release to simulate the full-scale test. For those materials, the Q'' value was further decreased until a representative prediction was achieved. Therefore, it can be seen that this method is not a completely accurate method of approximating the melting of actual materials, but it does help in showing the sensitivity of the model and identifying the hazards and processes that are involved in melting materials.

4.3 Results

The material performance predictions by Quintiere's fire growth model were compared with full-scale ISO 9705 room/corner tests performed at the Swedish National Testing and Research Institute [28]. Graphical comparisons of the predicted and full-scale test energy release rates are presented in Figures 4.2 through 4.13.

A key factor for determining material performance in the room/corner test is the amount of time that it takes the burning material to take the room to flashover. Because flashover is a complex phenomenon, the time to onset in the 9705 room/corner test is associated with an energy release rate of 1,000 kW based on flames emerging from the door and floor heat flux. This 1 MW criterion is for the most part independent of the material and only a property of the room geometry. Other factors effect the overall performance of a material, but for the most party the time for the energy release rate to reach 1,000 kW will be analyzed.

Predictions made by the model using the properties presented in Table 4.1 are simply identified in the figures as "Prediction". For some materials, especially thermoplastic materials that tended to melt and drip, key observations from the full-scale tests are presented in these figures. The figures also show predictions that were made using adjusted material properties, which will be discussed below. The adjusted properties for these predictions are identified in the legends of the appropriate figures.

It should be noted that for the full-scale test results there appears to be a consistent lag between the beginning of the test and the time at which 100 kW from the ignition burner is measured. This lag is between 20 and 60 seconds for each test (see Figure 4.2 to 4.13) and indicates an important characteristic of the SP oxygen consumption calorimeter. This lag time has some significance in the result comparisons which follow.

Table 4. 1: Ignition, Flame Spread and Energy Release Properties of the LSF Materials used for Modeling.

Material	T_{ig} (°C)	$T_{s,min}$ (°C)	$k\rho c$ [(kW/m ² K) ² s]	Φ (kW ² /m ³)	ΔH_c (kJ/g)	L (kJ/g)	Q'' (MJ/m ²)
R 4.01, FR. Chipboard	505	507	4.024	0.0	9.2	10.0	34.2
R 4.02, Gypsum	515	517	0.549	0.0	6.4	4.8	2.2
R 4.03, PU/Alum.	---	---	---	0.0	16.3	---	32.9
R 4.04, PU/Paper	250	77	0.199	8.7	18.9	5.5	30.8
R 4.05, Ext. PS40	275	77	1.983	1.2	27.8	4.0	38.7
R 4.06, Acrylic	195	195	2.957	---	24.1	1.6	89.5
R 4.07, FR. PVC	415	352	1.306	0.2	9.9	10.4	16.1
R 4.08, 3-Layer PC	495	167	1.472	0.0	19.5	3.3	58.1
R 4.09, Mass Timber	330	77	0.530	6.9	16.3	17.5	68.2
R 4.10, FR. Plywood	480	197	0.105	0.7	11.2	9.3	51.8
R 4.11, Plywood	290	147	0.633	2.2	11.9	7.3	64.6
R 4.20, Exp. PS40	295	77	1.594	4.2	27.5	7.3	33.9
R 4.21, Exp. PS80	490	77	0.557	7.1	26.9	12.7	25.5

R 4.01, Fire Retarded Chipboard.

The results of the room/corner test show a low energy release rate with minimal flame spread for the first ten minutes. After the ignition burner was increased to 300 kW, the energy release increased to approximately 700 kW after about 5 minutes. However, a flashover energy release rate of 1,000 kW was never achieved. The model prediction shows a similar trend as the full-scale prediction except that the maximum predicted energy release rate is approximately 400 kW. The general performance of the fire retarded chipboard is predicted, however the amount of energy release is substantially under predicted.

The under prediction by the model may be a direct result of the calculation of the heat of gasification. If the $L_{peak\ avg.}$ value used for the basic prediction (10.0 kJ/g) is too high, the energy release rate may be lower than expected:

$$\dot{Q}'' = \dot{q}''_{net} \frac{\Delta H_c}{L}$$

Therefore the overall average value, 4.5 kJ/g, was input into the model. As Figure 4.2 indicates, this L value allows the fire retarded chipboard to reach 1 MW. This indicates that a lower heat of gasification value may be more appropriate for the chipboard, but that the overall value is far too low.

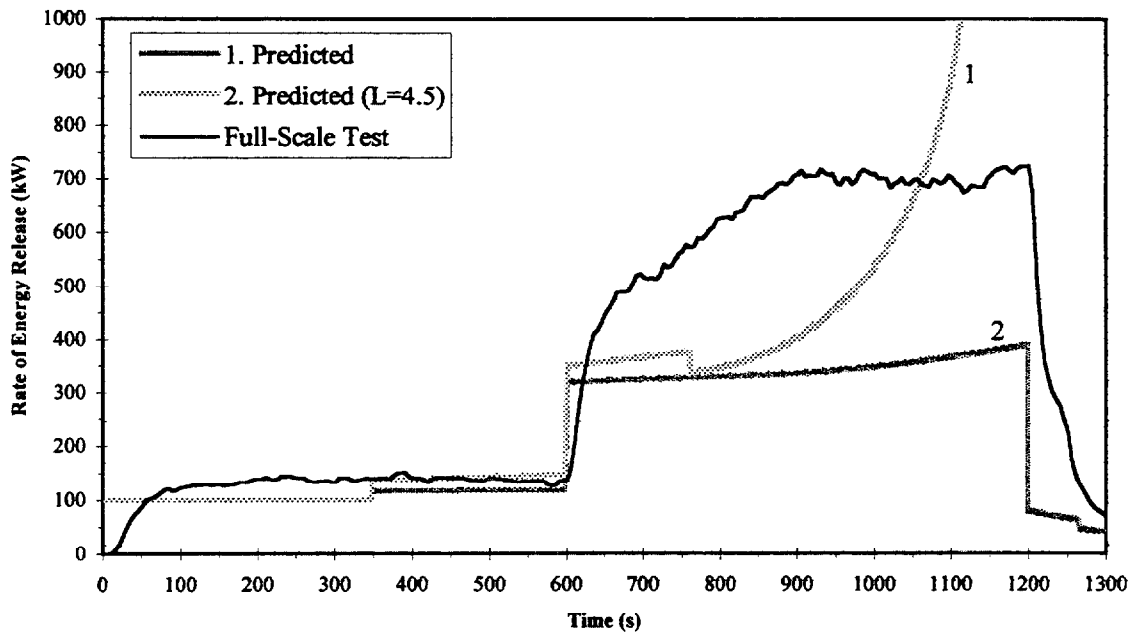


Figure 4. 2: Full-Scale Energy Release Rate for Fire Retarded Chipboard, R 4.01.

R 4.02 Paper Faced Gypsum Board.

Observations from the full-scale test indicate minimal heat release and flame spread during the first ten minutes. After the ignition burner was increased to 300 kW, there was some flame spread along the ceiling resulting in a slight increase in energy release. However, this diminished as the paper facing stopped burning.

The basic prediction shows minimal energy release during the first ten minutes followed by a tremendous increase in the energy release rate approximately 1 minute after the ignition burner is increased. As mentioned previously, thin materials are difficult to predict and the paper facing is basically a thin covering over a non-combustible material. Furthermore, the rapid burning of the paper and the slow, steady moisture evaporation make paper faced gypsum board an extremely difficult material to model.

In order to predict the performance of the gypsum board the heat of gasification (L) is increased by 50% (i.e. $1.5 \cdot L$) and the total energy per unit area (Q'') is reduced by 50% (i.e. $0.5 \cdot L$). Figure 4.3 indicates that both adjustments provide similar predictions of the performance. However, these adjustments were arbitrarily determined and were merely an attempt to measure the sensitivity of the model for such a complex material.

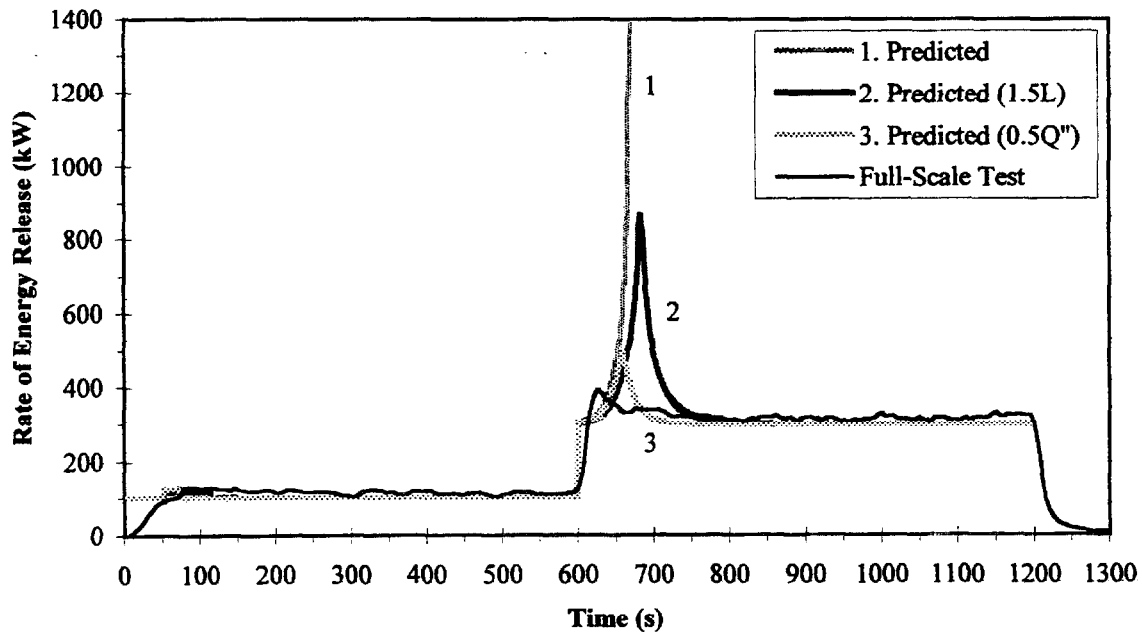


Figure 4. 3: Full-Scale Energy Release Rate for Paper Faced Gypsum Board, R 4.02.

R 4.03 Polyurethane Foam Panel with Aluminum Facing

Since material properties could not be extrapolated from the Cone tests for the aluminum faced foam, paper faced foam per faced foam properties are used.

In the room/corner test, the aluminum facing near the ignition burner became damaged after about 14 seconds. This allowed the polyurethane to become exposed to direct flame impingement by the ignition burner. After 27 seconds large portions of the ceiling were ignited and after about 40 seconds the energy release rate reached 1 MW and flames were observed coming out the doorway.

The model predicts the ignition of the material after about 2 to 3 seconds and after 9 seconds the energy release rate is above 1,000 kW. To account for the melting of the foam, the total energy per unit area (Q'') is reduced by 70% to 9.9 MJ/m² and the model predicts a similar fire growth. This indicates that even with a large portion of the material gone, the fire will still tend to grow at an amazingly fast rate.

The heat of gasification is then increased by a factor of 2 in order to possibly account for some of the initial reflection of the incident heat flux by the aluminum facing. As Figure 4.4 indicates, this prediction produces a 1 MW energy release rate after 22 seconds. This, therefore indicates that although the calculated heat of gasification values for the paper faced foam are very consistent, they may be too low to predict the performance of the aluminum faced polyurethane foam. These discrepancies are most likely due to the use of the paper faced foam properties to predict performance in the full-scale test. The aluminum facing no doubt delayed the ignition of the foam producing some of the differences seen in the Figure.

R 4.05, Fire Retarded Extruded Polystyrene Board

The 40 mm thick extruded polystyrene board ignited after 20 seconds in the room/corner test. After 85 seconds, the material on the ceiling was melting and dripping onto the floor. Fifteen seconds later the energy release rate reached 1 MW. Flames could not be seen coming from the doorway, however thick, black smoke emanating from the room may have obscured them. After about 2 minutes, the energy release rate began to reduce and after 3 minutes only the flames from the corner ignition burner were present. The burner heat output was increased to 300 kW at 10 minutes. Twenty seconds later the energy release rate was above 1,500 kW and melted, burning polystyrene droplets were falling from the ceiling. Flames could still not be observed out the doorway, but thick black smoke was once again emanating from the opening. After the fire was extinguished almost all of the material was either burned or melted.

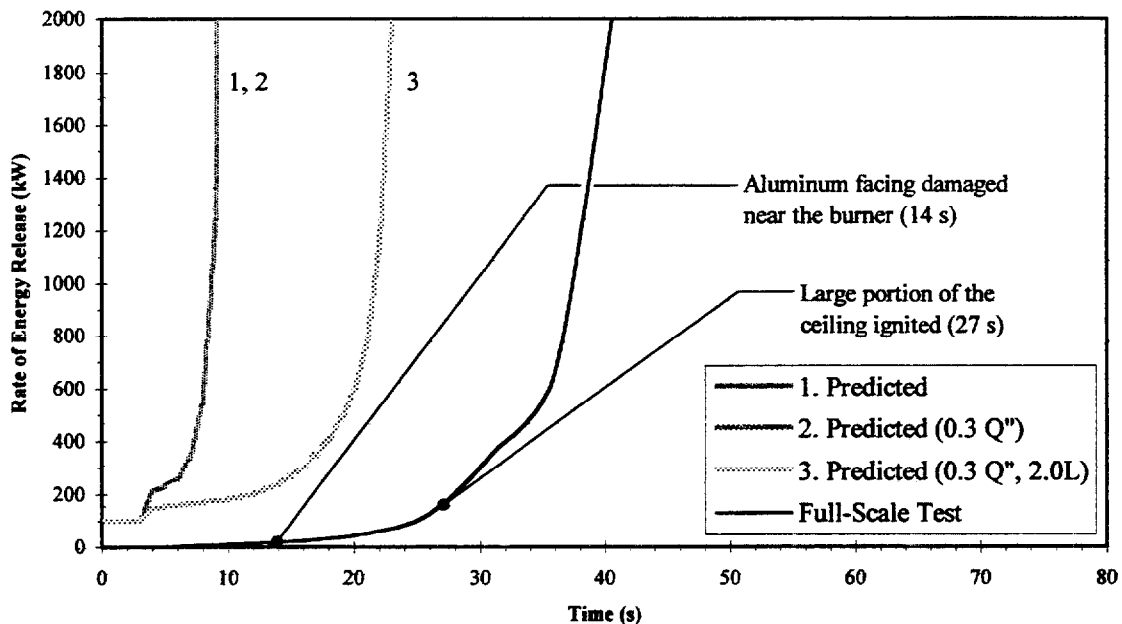


Figure 4. 4: Full-Scale Energy Release Rate for Polyurethane Foam Panel with Aluminum Facing, R 4.03, Using Material Properties for Polyurethane Panel with Paper Facing, R 4.04.

The polystyrene foam clearly indicates a material that melts and drips from the walls and ceiling. However as Figure 4.5 indicates, the model prediction with the unadjusted Cone properties appears to do a reasonable job of predicting the initial peak in the energy release rate. There is approximately 30 seconds difference between the prediction and experimental test results.

To simulate melting, the total energy per unit area is reduced to 30% of the original value: 11.6 MJ/m^2 . This adjusted prediction provided the same rapid fire growth as the original. The total energy is then further reduced by a factor of 1/2, to 15% of the original value. This adjustment indicates a slight rise in the energy release rate immediately after ignition followed by a decay to the baseline energy release rate from the burner. As in the full-scale test when the ignition burner output is increased, there is a tremendous increase in the energy release rate and 1,000 kW is reached at 614 seconds.

In an attempt to better predict the actual performance of the material a total energy per unit area value between the previous two is chosen: 22%. This value predicts the initial energy release rate peak extremely well, but does not indicate the decrease in energy release or the increase associated with the burner output increase.

The vigorous melting of polystyrene foam indicates that it is extremely difficult to model. However, by reducing the total energy per unit area in order to simulate melting effects, reasonable predictions can be achieved.

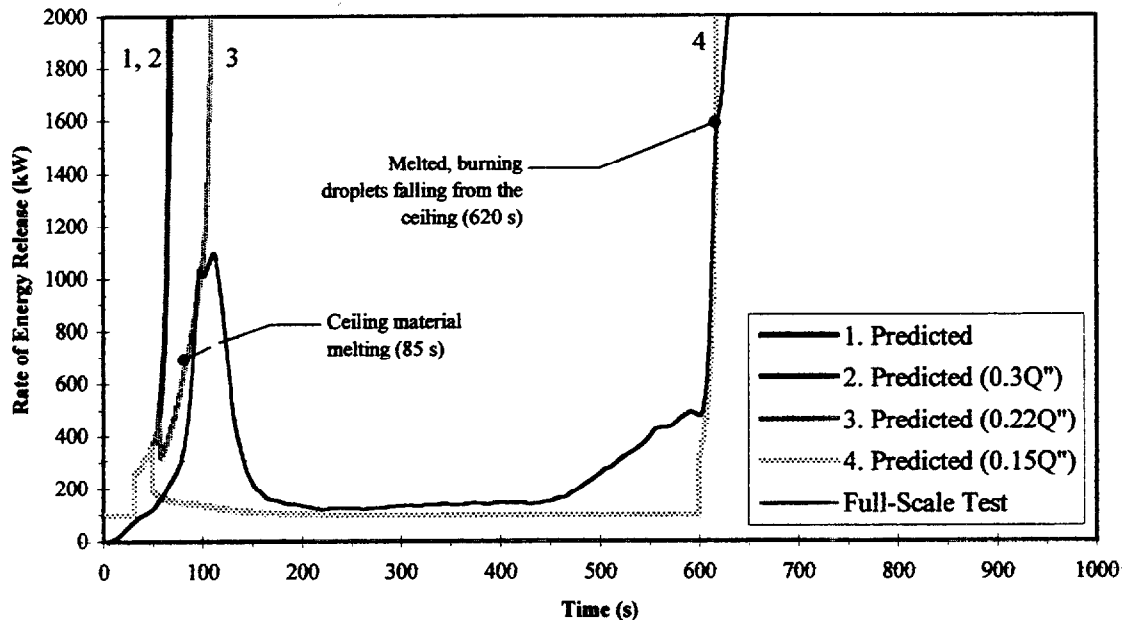


Figure 4. 5: Full-Scale Energy Release Rate for Extruded Polystyrene Board, R 4.05.

R 4.06, Clear Acrylic Glazing

The sheets of acrylic glazing ignited after 1 minute in the full-scale room/corner test. Once ignited, the acrylic began to melt and form a small burning pool near the burner. After 90 seconds the ceiling material had ignited and 15 seconds later burning, melted droplets were falling to the floor. After 130 seconds, an approximately 2 m² pool of melted acrylic was burning on the floor near the ignition burner. About 5 seconds later the energy release rate reached 1 MW. After extinguishment it was observed that most of the material was burnt or melted and melted acrylic covered about half of the floor area. Unlike the extruded polystyrene which had a tendency to melt and form droplets, the acrylic mostly appeared to melt and flow away from the wall and ceiling in sheets.

This material also represents a significant challenge for the fire growth model. The basic prediction identifies ignition after 21 seconds and a 1 MW energy release rate 6 seconds later. This prediction underestimates the “flashover” of the space by about 2 minutes. Therefore, the Q” value is reduced to 25% of the original value in order to simulate the significant melting that occurred. As Figure 4.6 indicates, this reduction of the amount of energy available from the acrylic had no effect on the prediction. This indicates that even with 75% of the material gone, the model still predicts the same rapid fire growth and flashover. The heat of gasification value is then arbitrarily increased by a

factor of 3 to determine the sensitivity of the model and to determine if a more appropriate L value should be used. This increased L value provides the same rapid fire growth only it takes 50 seconds to reach 1,000 kW, indicating that the calculated L value may in fact be lower than that of the actual material. However the highest calculated value from Table 3.5 is only twice as large as the peak average value used. This discrepancy remains unexplained although the rapid flashover of the acrylic glazing is predicted and represents a worst-case scenario.

Although the full-scale fire growth for acrylic is rapid by typical room/corner test standards, the predicted growth is much more rapid. The more gradual growth in the test is no doubt due to the melting and falling away of the acrylic. Materials such as this are even more difficult to model due to the very rapid reduction in material available for burning. It is difficult to accurately determine when a section of acrylic will begin to melt and then to predict how much of the material will ooze from the walls and ceiling. The current predictions are reasonable and identify the potential for rapid fire growth. However, they do not necessarily account for the actual performance of acrylic glazing. With repeated full-scale testing and modeling of similar materials a method of determining the material properties may be developed which will allow for a more appropriate prediction. At this time no further conclusions regarding the material properties of the acrylic glazing and there applicability to this type of modeling can be made.

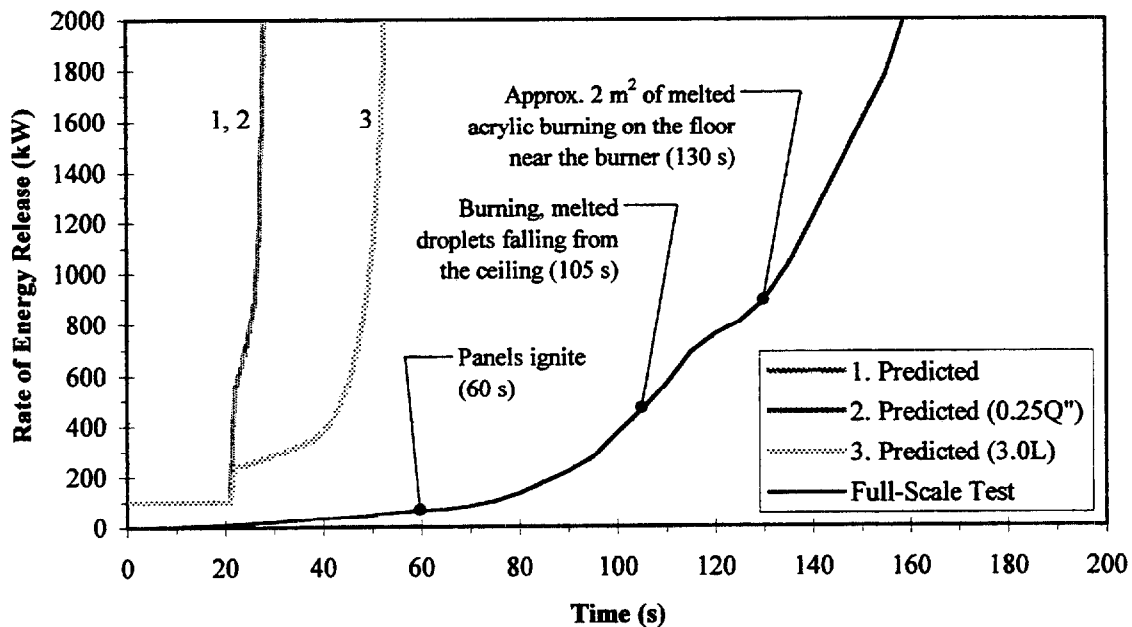


Figure 4. 6: Full-Scale Energy Release Rate for Acrylic Glazing, R 4.06.

R 4.07, Fire Retarded PVC

Thirty seconds after the ignition burner was ignited, the ceiling panels in the corner began to deform. After 85 seconds, the material in the corner was melted. This melting continued throughout the test and after 9 minutes, most of the ceiling material was melted and fallen to the floor. One minute after the ignition burner was increased to 300 kW, all of the ceiling material had fallen to the floor. The test went for the full 20 minutes without reaching the 1,000 kW indicative of flashover. In fact as Figure 4.7 indicates, the energy release rate never rose above 400 kW. This material acted much the same way as the clear acrylic glazing, R 4.06, in that it melted and fell off the walls and ceiling in soft sheets. At the conclusion of the test the ceiling panels and most of the wall panels had melted and were lying on the floor in piles.

The prediction of the fire growth for the PVC indicates very little energy release rate during the early portion of the test. However after the ignition burner is increased, the model predicts flashover after 2 minutes. The Q'' value was reduced by 50% and 70% to determine if the extensive melting and softening of the PVC sheets could be predicted. As Figure 4.7 suggests, the adjusted Q'' values better predict the fire growth, but still indicate peak energy release rates of 1100 and 900 kW, respectively.

As mentioned above, materials that tend to melt, soften and pull away from the walls and ceiling are extremely difficult to model. The methodology of reducing the energy available as the material melts is not very appropriate when entire sheets of the material melt and fall to the floor. The procedure for developing adjusted properties for these types of materials needs to be seriously addressed if any attempt at accurate modeling is going to be conducted.

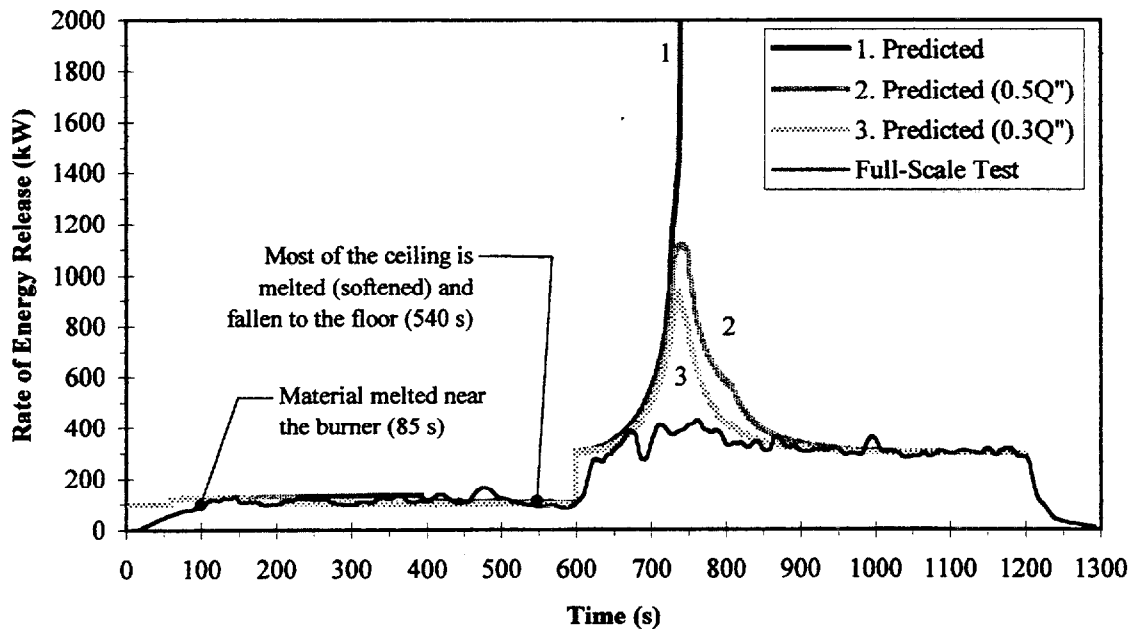


Figure 4. 7: Full-Scale Energy Release Rate for R 4.07 Fire Retarded PVC.

R 4.08, 3-Layered, Fire Retarded Polycarbonate Panel

The ceiling panels above the ignition burner began to deform 15 seconds after ignition of the burner. After 60 seconds melted material from the walls and ceiling were forming into droplets. There did not appear to be ignition or burning of any material besides in the vicinity of the ignition burner. This limited burning allowed the energy release rate to reach approximately 275 kW, but this rate quickly reduced to a level just above the baseline energy release rate from the burner. After the energy release rate increase of the ignition burner at 10 minutes, the polycarbonate panels began to soften and move away from the burner flame. Figure 4.8 reveals that very little burning occurred throughout the duration of the test except for a small burning pool of melted material near the burner. After the test all of the ceiling and a majority of the walls had melted and fallen to the floor.

Three-layered polycarbonate paneling poses a similar modeling challenge to the acrylic glazing and the PVC. The initial run of the model predicted material ignition after 120 seconds and a 1 MW energy release rate after 230 second. As before, the total energy per unit area value was reduced by 50% to simulate the melting of the panels. This adjustment provided the same prediction as with the original value. Decreasing Q'' further (20% of the original value) indicated a slight energy release rate increase followed by burnout and no significant heat release. However, after 10 minutes, the 300 kW ignition burner cause flashover after 70 seconds. Therefore, Q'' was reduced further still. At 10% of the original value, 5.8 MJ/m², the model predicted an increase to a peak energy release rate of about 800 kW after 700 seconds followed by a decrease and no significant heat release for the duration of the test.

R 4.09, Varnished Massive Timber

The lacquer finish ignited after 25 seconds and after 45 seconds the ceiling above the ignition burner had ignited. At approximately 90 seconds, flame spread down the walls clearly observed. Ten seconds later, the energy release rate was over 1 MW and ten seconds after that flames were observed out the doorway. After extinguishment, the entire ceiling and about 50% of the walls were charred. The lower half of the walls were slightly discolored but generally undamaged.

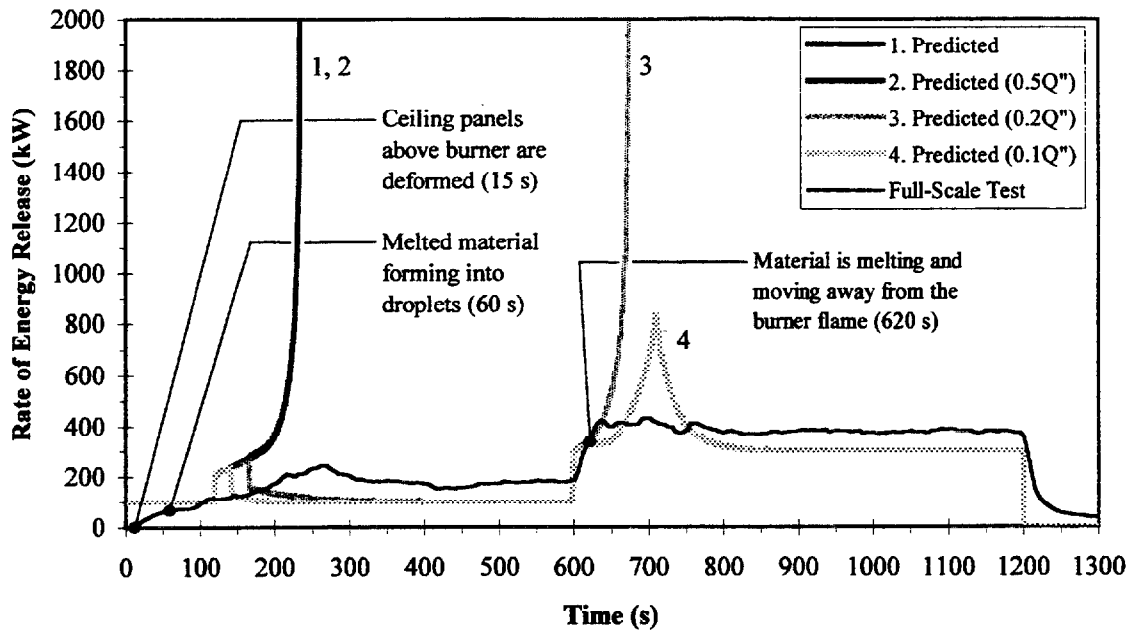


Figure 4. 8: Full-Scale Energy Release Rate for 3-Layered, Fire Retarded Polycarbonate Panel, R 4.08.

The initial run of the model predicts a minimal energy release rate (approximately 160 kW) during the first ten minutes of the test. Twelve seconds after the ignition burner heat flux is turned up, the energy release rate exceeds 1,000 kW. This poor fire growth prediction is no doubt due to the unusually high peak and peak average heat of gasification values for massive timber (as mentioned in Section 3.5). Therefore the overall average value of 6.5 kJ/g was used. This value provided a fire growth prediction that was more consistent with the full-scale test data but with an approximately 35 second difference in the times to flashover. The heat of gasification was then arbitrarily increased to 9.0 kJ/g in order to determine the appropriateness of the overall average value and the sensitivity of the model. As Figure 4.8 indicates, this increased L value provides an extremely accurate prediction of the full-scale test. A heat of gasification value of 9.0 kJ/g is completely arbitrary but indicates that although the $L_{\text{overall avg}}$ used is not too far off, a higher value may be more appropriate.

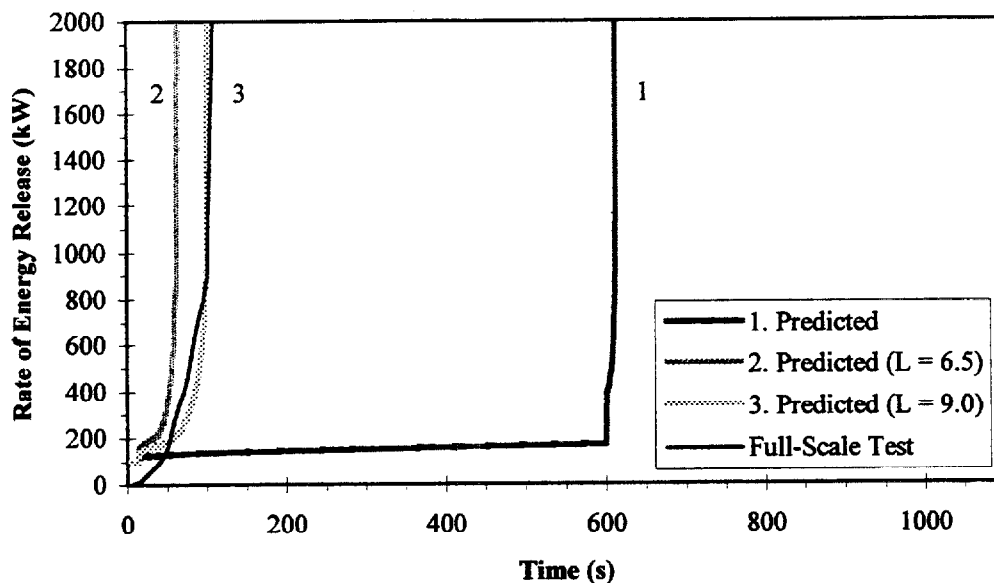


Figure 4. 9: Full-Scale Energy Release Rate for Varnished Massive Timber, R 4.09.

R 4.10, Fire Retarded Plywood

The room/corner test for fire retarded plywood showed a limited energy release rate for the first ten minutes. The ignition burner flames merely darkened and charred the material located in the corner. Ten seconds after the ignition burner was increased to 300 kW, extensive flame spread across the ceiling was observed. After 630 seconds the energy release rate reached 1 MW and 5 seconds later, flames were observed coming out the door. After 645 seconds, flames were spreading down the walls.

As Figure 4.10 indicates, the model does a good job of predicting the performance of the fire retarded plywood. However, the dependence of flashover on the increase of the energy release rate from the ignition burner does not provide a great deal of insight into the appropriateness of the material properties used. Therefore it must be assumed that the properties derived for the Cone for fire retarded plywood are reasonably legitimate and can be used to predict performance in the ISO 9705 room/corner test.

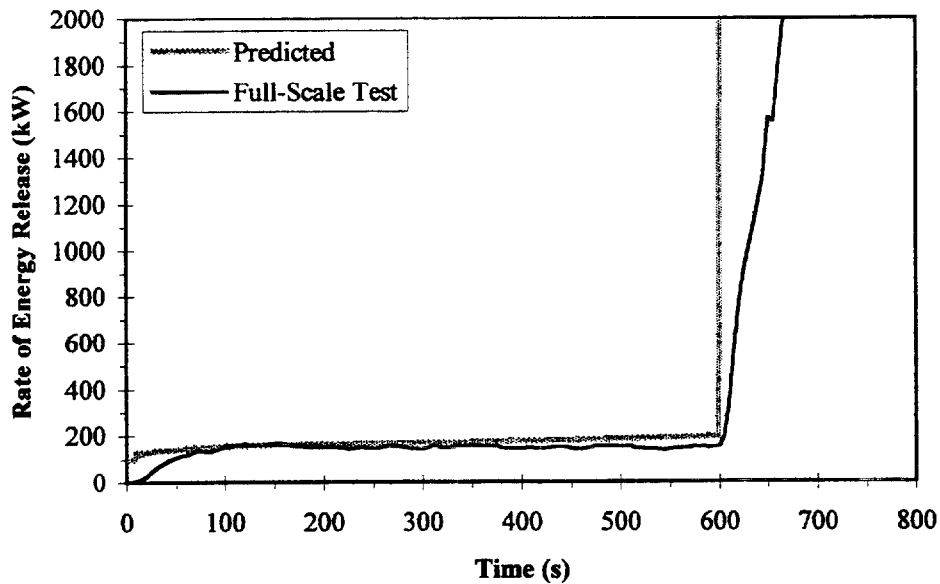


Figure 4. 10: Full-Scale Energy Release Rate for Fire Retarded Plywood, R 4.10.

R 4.11, Normal Plywood

The plywood ignited 45 seconds after ignition of the burner. Another 45 seconds later 50% of the ceiling was ignited and flames were beginning to spread down the walls. At 134 seconds flames were observed out the door and after another 4 seconds the energy release rate reached 1,000 kW. After the test, most parts of the walls and ceiling were charred.

The model does a reasonable job of predicting the flashover of the plywood but underestimates the time by about 30 seconds. To determine the appropriateness of the $L_{peak\ avg.}$ by the energy release rate method and the sensitivity of the model to this value, the $L_{peak\ avg.}$ value by the mass loss rate method (8.0 kJ/g) is used. Figure 4.11 reveals that this increased L value provides a slightly better prediction of the performance of the plywood. Although the heat of gasification derived from the mass loss data provides a better prediction than the energy release rate data, both predictions demonstrate the hazardous nature of normal plywood and the rapid flashover that results.

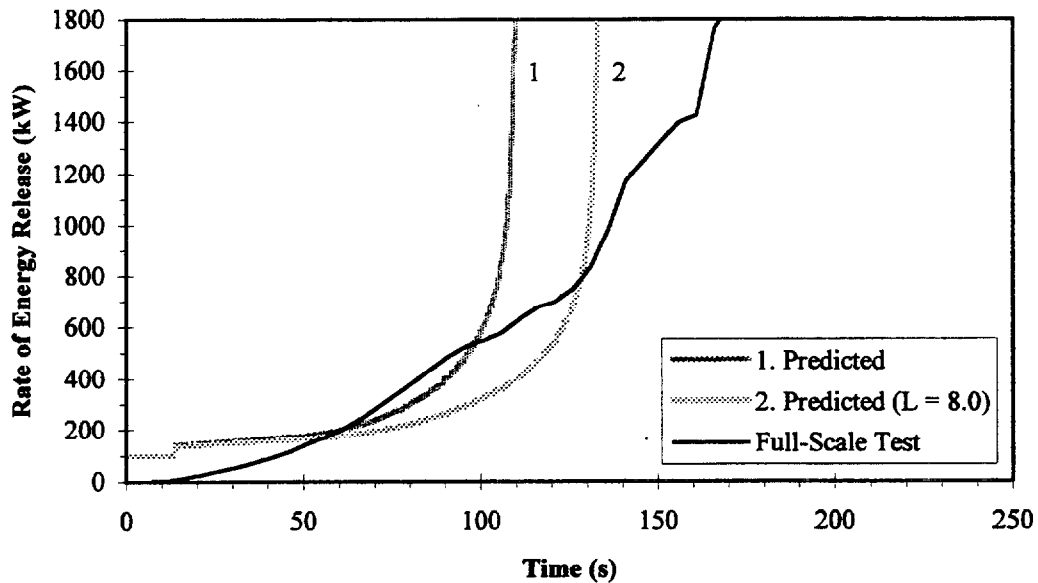


Figure 4. 11: Full-Scale Energy Release Rate for Normal Plywood, R 4.11.

R 4.20, Fire Retarded Expanded Polystyrene Board (40 mm)

The expanded polystyrene board began to melt quickly after the ignition burner was ignited. Burning, melted droplets were observed after 20 seconds and melted material was running down the walls after 40 seconds. After 80 seconds, polystyrene was dripping from the entire ceiling. About 4 seconds later the energy release rate reached 1 MW and a few flames were observed coming from the doorway. As Figure 4.12 indicates, the energy release rate from the fire then quickly reduced and remained close to the ignition burner energy release rate for the duration of the test. A slight increase occurred immediately after the increase of the ignition burner due to melting material burning away, but this increase was small and short lived. After the test almost all of the polystyrene was burned or melted from the walls and ceiling.

Despite the substantial melting that occurred, the model does an excellent job of predicting the performance of the expanded polystyrene with flashover occurring after 90 seconds. The reduced Q'' value which was used to simulate melting—30% of the original value—also provides a reasonable prediction, but with a slightly longer time to flashover. The model is able to accurately predict the flashover of the expanded polystyrene because although the material begins to melt soon after the test begins, it does not fall from the walls and ceiling in large pieces or sheets. Although melting droplets begin to fall from the entire ceiling, there is still enough material available to produce an energy release rate above 1 MW. However, once this high energy release rate is reached, most of the material has melted away and there is not enough to sustain burning.

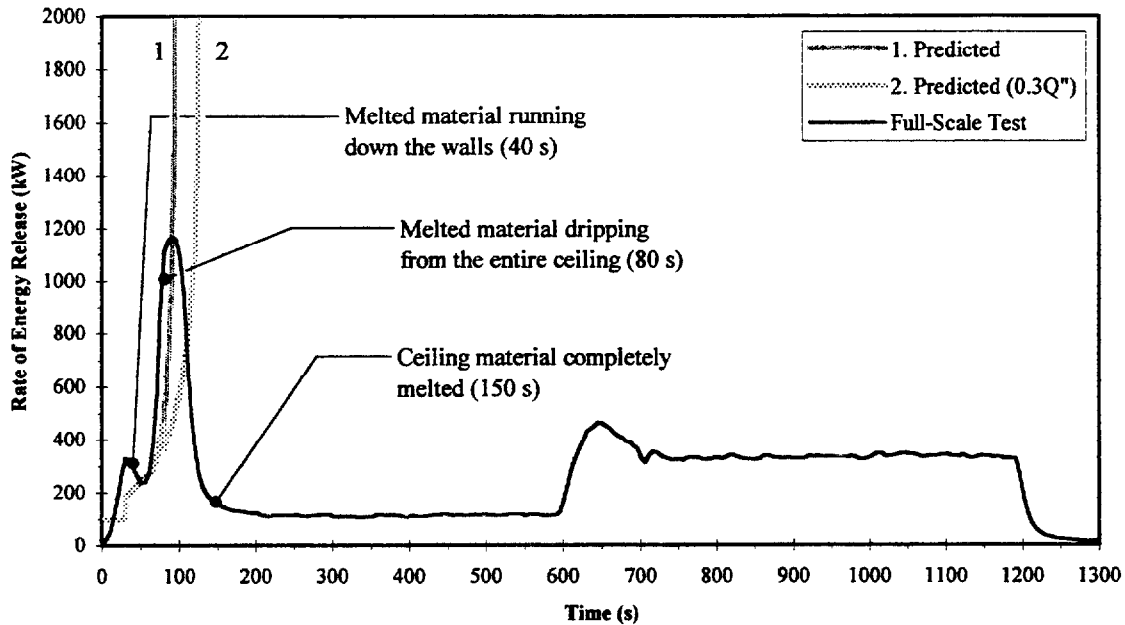


Figure 4. 12: Full-Scale Energy Release Rate for Fire Retarded Expanded Polystyrene Board (40 mm), R 4.20.

R 4.21, Fire Retarded Expanded Polystyrene Board (80 mm)

Like the 40 mm board, the 80 mm expanded polystyrene began to melt quickly in the room/corner test. After 15 seconds the material above the ceiling began to melt and melted material was running down the walls after 30 seconds. After approximately 105 seconds material was dripping from the entire ceiling, flames were coming out the doorway and the energy release rate reached 1 MW. Immediately after flashover the energy release rate rapidly reduced—approximately 50% of the walls had been consumed or melted. For the next 7 minutes burning polystyrene was minimal and could only be seen in the ignition burner corner. After the ignition burner was increased to 300 kW, the melted material immediately next to the burner ignited and caused a slight increase in the energy release rate. As Figure 4.13 indicates, the fire began to decay just like the 40 mm polystyrene board but then rapidly grew and exceeded 1,000 kW again at 798 seconds.

The initial prediction made by the model shows the same rapid fire growth as the full-scale test but happening approximately 3 minutes later. The heat of gasification used for this prediction, 12.7 kJ/g, seemed relatively high, especially when compared to the L value for the 40 mm board, 7.3 kJ/g. Therefore, in order to determine the accuracy of the heat of gasification, the lower value was used. This prediction provided good agreement with the initial energy release rate peak from the test, but did not demonstrate the decay and subsequent rise. This seems to indicate that the $L_{peak\ avg.}$ by the energy release rate method used may be too high for the material. Since there seems to be no consistency

between the L values for the 40 and 80 mm polystyrene boards, no definitive judgement can be made on which value represents the most appropriate value for this type of material.

The total energy per unit area was reduced to simulate the melting of the polystyrene, but did not provide an accurate prediction. As with the 40 mm expanded polystyrene board, the melting of the material does not seem to be as critical a factor as with the extruded polystyrene, R 4.05. This difference remains unexplained.

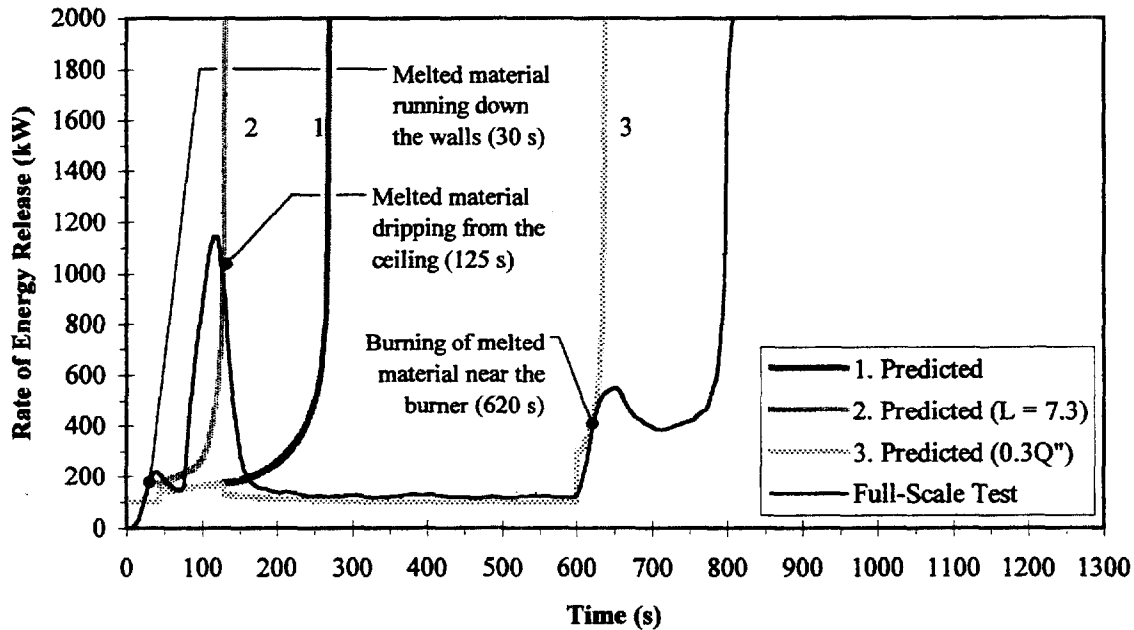


Figure 4. 13: Full-Scale Energy Release Rate for Fire Retarded Expanded Polystyrene Board (80 mm), R 4.21.

Time to Reach Flashover

As mentioned above the key factor for determining material performance in the room/corner test is the amount of time that it takes the burning material to take the room to flashover or an energy release rate of 1,000 kW. Table 4.2 shows the time to reach 1 MW for the full-scale tests and the predictions by the model. The “Basic Predictions” represent the use of the “peak average” heat of combustion and heat of gasification values for all materials. The “Adjusted Predictions” represent the time associated with a particular adjusted material property. The purpose of these adjusted predictions is to indicate the sensitivity of the model, analyze potentially erroneous material properties and to provide a possible means for handling materials that melt, drip and are generally poorly represented in the room/corner test. It should be noted that an adjusted prediction that is in excellent agreement with the full-scale test might be due to an arbitrary sensitivity adjustment to a material property and might not be necessarily legitimate.

Table 4. 2: Comparison of the Time to Reach Flashover (1,000 kW) for the Full-Scale Room/Corner Tests and the Model Predictions.

Material	Time to Flashover, $\dot{Q} = 1,000$ kW (s)			
	Full Scale	Basic Prediction	Adjusted Prediction	Adjusted Material Property
R 4.01, FR. Chipboard	∞	∞	1113	$L = 4.5$ kJ/g
R 4.02, Gypsum	∞	666	∞	$1.5 \cdot L$ or $0.5 \cdot Q''$
R 4.03, PU/Alum.	40	----	----	----
R 4.04, PU/Paper	----	9	22	$0.3 \cdot Q''$ & $2.0 \cdot L$
R 4.05, Ext. PS40	96 & 614*	64	99 616	$0.22 \cdot Q''$ $0.15 \cdot Q''$
R 4.06, Acrylic	141	27	50	$3.0 \cdot L$
R 4.07, FR. PVC	∞	726	730 ∞	$0.5 \cdot Q''$ $0.3 \cdot Q''$
R 4.08, 3-Layer PC	∞	230	669 ∞	$0.2 \cdot Q''$ $0.1 \cdot Q''$
R 4.09, Mass Timber	104	612	62 100	$L = 6.5$ kJ/g $L = 9.0$ kJ/g
R 4.10, FR. Plywood	631	601	----	----
R 4.11, Plywood	138	108	131	$L = 8.0$ kJ/g
R 4.20, Exp.PS40	84	90	118	$0.3 \cdot Q''$
R 4.21, Exp.PS80	107 & 798*	268	129 636	$L = 7.3$ kJ/g $0.3 \cdot Q''$

* Energy release rate (\dot{Q}) exceeded 1,000 kW more than one time.

4.5 Lateral Flame Spread

In order to determine the sensitivity of the lateral flame spread, the material's were modeled with the minimum temperature necessary for flame spread ($T_{s, min}$) reduced to ambient (20 °C). The results of these predictions were almost identical to those presented above—using the $T_{s, min}$ determined from test methods. In fact, the times for the room to reach 1 MW were identical or within ± 1 second. This indicates that the lateral flame spread does not play a very significant role in the predicted performance of the LSF materials in the ISO 9705 protocol. This may be true for all materials, however further testing and analysis would have to be conducted to eliminate lateral flame spread as a significant form of flame spread and fire growth.

5. UPWARD FLAME SPREAD ACCELERATION FACTOR

The spread of flame can be viewed as a critical event that is dependent on the exposure conditions and material properties. This idea of criticality is that a burning material reaches a point at which it will either grow exponentially or burn out. The potential for the flames to spread becomes a balance of the fuel being heated to ignition, the consumption rate of the fuel and the amount of fuel available [13]. The ability of a material to take a room to flashover and the time associated with the onset of that flashover can be expressed in terms of the upward acceleration of the flame spread. Cleary and Quintiere [4] have developed an empirical parameter (b) which can be used to examine the upward acceleration of a flame based on material properties.

$$b = k_f \dot{Q}'' - 1 - t_{ig}/t_b$$

where k_f is a flame length coefficient (m^2/kW), \dot{Q}'' is the energy release rate per unit area (kW/m^2), t_{ig} is the predicted time to ignition (s) and t_{bo} is the predicted burnout time (s). The flame length coefficient is based on a linear approximation of the flame length based on wall fire data and is approximately equal to $0.01 \text{ m}^2/\text{kW}$.

The energy release rate per unit area is calculated by

$$\dot{Q}'' = \frac{\Delta H_C}{L} (\dot{q}_{ig}'' - \sigma T_{ig}^4)$$

where ΔH_C and L are taken as “peak average” values, σT_{ig}^4 represents re-radiant heat flux from the surface of the material and \dot{q}_{ig}'' is the ignition burner flame heat flux. This heat flux controls ignition of the material and is taken to be constant over the height of the ignition burner flame and equal to $60 \text{ kW}/\text{m}^2$ [18].

The time to material ignition can be predicted by

$$t_{ig} = \frac{\pi}{4} k_f \rho c \left(\frac{T_{ig} - T_s}{\dot{q}_f''} \right)^2 \quad (5.1)$$

where k_f and T_{ig} come from Table 4.1, T_s is the original surface temperature of the material ($20 \text{ }^\circ\text{C}$) and \dot{q}_f'' is the heat flux from the extended wall flame. This extended flame heat flux controls upward flame spread and is taken to be approximately $30 \text{ kW}/\text{m}^2$ [18].

The burnout time for a material can be predicted by

$$t_b = \frac{Q^n}{\dot{Q}^n}$$

The b parameter for a material can indicate the tendency of the flame to accelerate towards flashover ($b > 0$) or decay until the material burns itself out ($b < 0$). Values of b that are close to zero can be considered to be “borderline” materials. This borderline region represents materials where small changes in either the material properties or the exposure conditions can effect the outcome. The time to flashover (t_{fo}) is plotted against the upward flame spread factor in Figure 5.1. The time to flashover can also be normalized by dividing it by the time to ignition which is represented by;

$$\tau_{fo} = \frac{t_{fo}}{t_{ig}}$$

This dimensionless relationship is plotted with respect to b in Figure 5.2. These values are also presented in Table 5.2.

Figures 5.1 and 5.2 represent the culmination of b values for 13 materials tested in Sweden, 10 materials from the EUREFIC program [10, 19] along with the 12 LSF materials analyzed here: the material numbers are preceded by an “S”, an “E” and an “R”, respectively. It can be seen that the materials generally follow this empirical correlation. At low, negative b values, most of the materials will not go to flashover ($t_{fo} \rightarrow \infty$). As the b number increases towards positive, the time to flashover decreases. For increasing positive b values the time to flashover appears to be asymptotically decreasing towards 0. The region of borderline materials can also be seen between b values of approximately -1 and 1 .

The only materials that do not seem follow the empirical correlation are the polyurethane foam panel with aluminum facing, R 4.04, and acrylic glazing, R 4.06. The polyurethane foam does not fall in line with the other data points only in Figure 5.2. This is due to the incredibly low ignition time of 2 seconds which is calculated from Equation 5.1 using the material properties for the paper faced foam, R 4.03. Since ignition of the foam did not occur in the room-corner test until after the aluminum facing became damaged at 14 seconds, the calculated τ_{fo} value is much lower than expected.

The acrylic glazing did not exhibit a huge deviance from the correlation but a shorter time to flashover was expected for such a high b number. This difference is most likely due to the glazing being such a thin material and local melting that tends to occur in the region of the burner. This melting most likely extended the times to ignition and flashover beyond the predicted value.

Surprisingly, even materials that tended to melt, soften, deform and fall off of the walls are well predicted by the b factor correlation. Therefore, it can be implied that this empirical result gives an extremely good categorization of the flashover potential in the ISO 9705 room/corner test.

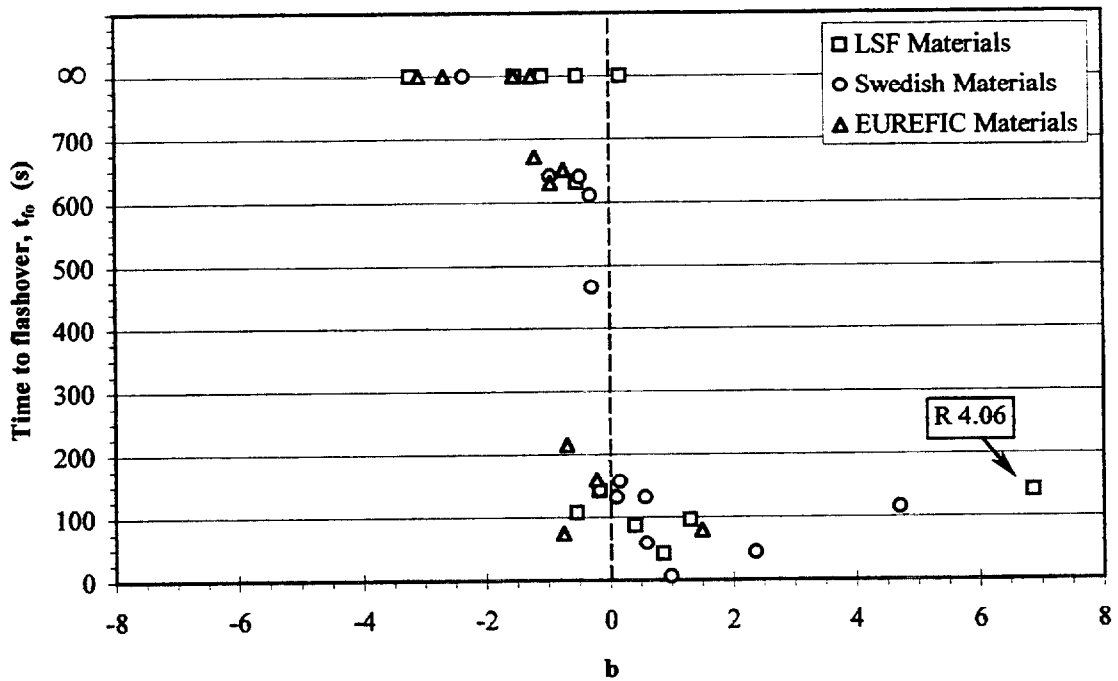


Figure 5. 1: Time to Flashover as a Function of the Flame Spread Acceleration Factor.

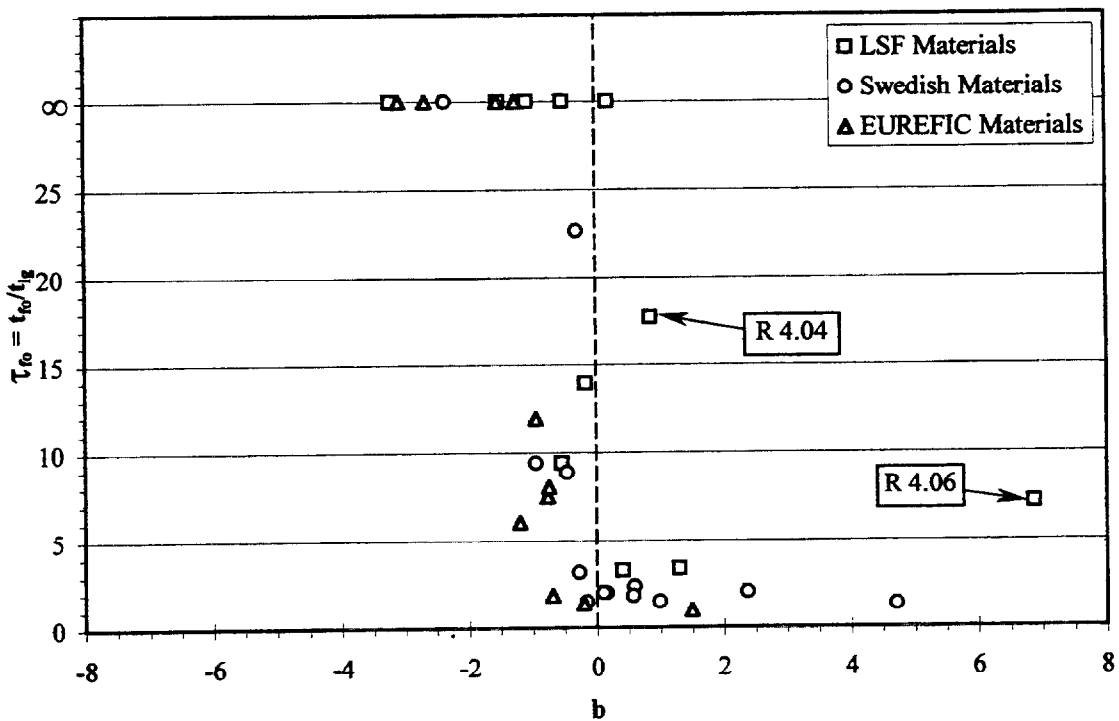


Figure 5. 2: Dimensionless Time as a Function of the Flame Spread Acceleration Factor.

Cleary and Quintiere [4] indicate that the ratio of the energy release rate of the material, \dot{Q} , to the energy release rate of the burner, \dot{Q}_o , is equal to

$$\frac{\dot{Q}}{\dot{Q}_o} = \frac{[(1+a)^2 \cdot e^{a(\tau-1)} - 1]}{a} \quad \text{for } 1 \leq \tau \leq \tau_b + 1$$

$$\frac{\dot{Q}}{\dot{Q}_o} = \left\{ \frac{[(1+a)^2 \cdot (e^{a\tau_b-1})]}{a} \right\} \cdot e^{b(\tau-1-\tau_b)} \quad \text{for } \tau \geq \tau_b + 1$$
(5.2)

where τ and τ_b are the dimensionless time and burnout time, respectively:

$$\tau = \frac{t}{t_{ig}} \quad \tau_b = \frac{t_b}{t_{ig}}$$

a is calculated by

$$a = k_f \dot{Q}^n - 1$$

with k_f equal to 0.01 m²/kW, and

$$b = a - \frac{1}{\tau_b}$$

Kim [10] also shows that \dot{Q}/\dot{Q}_o is a function of the material fire properties:

$$\frac{\dot{Q}}{\dot{Q}_o} \approx f\{a, a(\tau-1), a\tau_b, b(\tau-1-\tau_b)\}$$

where the empirical b parameter is based on the final parameter.

For a typical flashover energy release rate of 1,000 kW

$$\frac{\dot{Q}}{\dot{Q}_o} = \text{constant}$$

Therefore, for small values of τ_b :

$$b(\tau_{fo} - 1 - \tau_b) \approx \text{constant} \quad \text{for } \tau_{fo} \geq (\tau_b + 1)$$

Based on this empirical correlation, when $\tau_{fo} - 1 - \tau_b$ is plotted with respect to b , the data should provide a parabolic relationship with the y-axis, $x = 0$, being the vertical asymptote. As Figure 5.3 indicates, the data does indeed indicate a parabolic relationship with those values below approximately -1.25 indicating infinite values. However, the figure indicates a vertical asymptote of approximately -0.75 as opposed to 0.0.

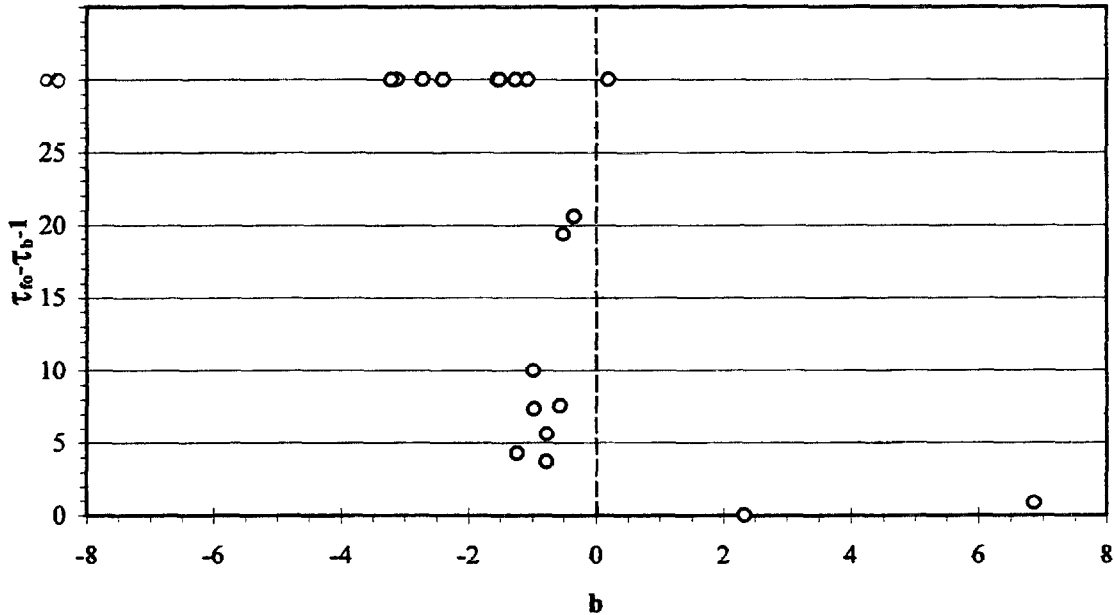


Figure 5. 3: $\tau_{fo} - 1 - \tau_b$ versus b .

On the other hand, for large τ_b values, $1/\tau_b$, is approximately equally to zero, resulting in

$$a(\tau_{fo} - 1) \approx \text{constant} \quad \text{for } \tau_{fo} \leq (\tau_b + 1)$$

Figure 5.4 also indicates an asymptotic relationship which is consistent with the correlation. The vertical asymptote appears to be equal to -0.5 as opposed to the y-axis.

The previous analysis provides further indication that the empirical correlation which has been presented provides an accurate method for categorizing materials in terms of their potential to burnout or take a room to flashover. However, the current data indicates that a and b values closer to approximately -0.5 to -0.7 are more consistent with "borderline" materials which are more sensitive to the ignition burner output and material properties.

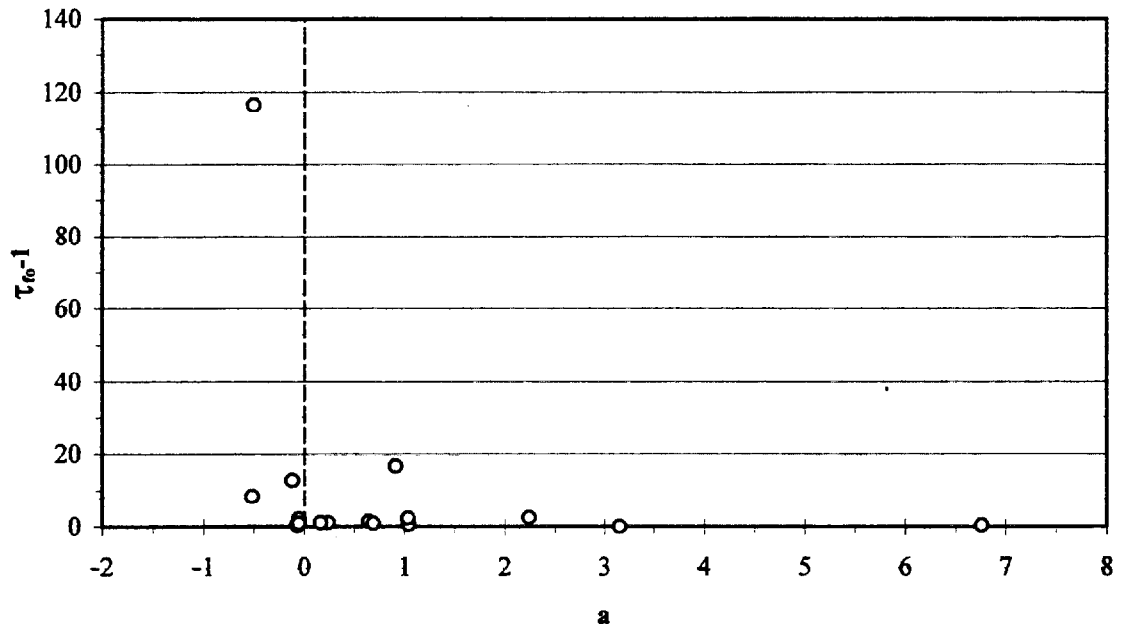


Figure 5. 4: $\tau_{f_0} - 1$ versus a .

Table 5. 1: Flame Spread Acceleration Factor for Swedish, EUREFIC and LSF Materials.

Material	t_{fo} (s)	t_{ig} (s)	t_b (s)	τ_{fo}	τ_b	b
S1, Ins. Fiberboard	59	25	413	2.36	16.52	0.59
S2, Med. Den. Fiberboard	131	72	590	1.82	8.20	0.57
S3, Particle Board	157	79	964	1.99	12.20	0.16
S4, Gypsum	∞	89	45	∞	0.50	-2.35
S5, PVC/Gyp. Board	611	27	27	22.63	1.02	-0.30
S6, Paper/Gyp. Board	640	68	70	9.41	1.03	-0.95
S7, Tex/Gyp. Board	639	72	20	8.88	0.28	-0.46
S8, Tex/Mineral Wool	43	21	21	2.05	1.01	2.37
S9, Mel/Part. Board	465	147	631	3.16	4.29	-0.28
S10, Exp. PS	115	85	41	1.35	0.49	4.71
S11, PU Foam	6	4	68	1.50	17.09	0.99
S12, Wood Panel	131	66	1026	1.98	15.55	0.11
S13, Pap/Part. Board	143	95	1076	1.51	11.33	-0.16
E1, Painted Gyp. Board	∞	176	86	∞	0.49	-2.67
E2, Birch Plywood	160	116	804	1.38	6.93	-0.21
E3, Tex/Gyp. Board	670	111	80	6.04	0.72	-1.20
E4, Mel/Non-Comb Board	∞	102	130	∞	1.28	-1.25
E5, PF Steel/Min. Wool	∞	162	260	∞	1.61	-1.53
E6, FR Part. Board	630	53	47	11.89	0.90	-0.95
E7, Comb. Min. Wool	75	10	28	7.50	2.77	-0.76
E8, FR Part. Board	∞	669	294	∞	0.44	-3.08
E9, PF Steel/PU	215	115	179	1.87	1.56	-0.69
E10, PVC/Gyp. Board	650	81	114	8.02	1.41	-0.74
E11, Ext. PS	80	80	48	1.00	0.60	1.49
R 4.01, FR. Chipboard	∞	234	948	∞	4.05	-0.84
R 4.02, Gypsum	∞	33	43	∞	1.28	-1.40
R 4.03, PU/Alum.	41	2		17.72		1.04
R 4.04, PU/Paper	----	----	161	----	69.51	----
R 4.05, Ext. PS40	96	28	119	3.38	4.19	2.27
R 4.06, Acrylic	141	19	104	7.12	5.24	7.83
R 4.07, FR. PVC	∞	47	343	∞	7.30	-0.61
R 4.08, 3-Layer PC	∞	81	244	∞	3.00	1.88
R 4.09, Mass Timber	107	11	1394	9.41	122.69	-0.46
R 4.10, FR. Plywood	631	5	1029	117.44	191.58	-0.32
R 4.11, Plywood	142	10	729	13.92	71.47	-0.04
R 4.20, Exp. PS40	87	26	166	3.26	6.23	1.07
R 4.21, Exp. PS80	∞	30	290	∞	9.65	0.06

6. CONCLUSIONS

A simulation model provides fair predictive results of the ISO 9705 Room-Corner test provided that the material test data are modified with a reduced energy release rate per unit area to account for the removal of the material from the wall-ceiling orientation by melting, dripping and other effects.

A methodology has been established that provides accurate representation of time-resolved material data from the Cone Calorimeter including heat of combustion, heat of gasification and total energy per unit area. A refined ignition model was developed to account more exactly for radiation effects and long time ignition behavior. This leads to a more appropriate way to extrapolate ignition data to determine the critical heat flux for ignition.

A correlation based on linearized upward flame spread continues to give good predictive results for the time to flashover.

This is an interim result and we expect to perform the same process for data provided by the Building research Institute of Japan in the near future.

ACKNOWLEDGEMENTS

We are very grateful for the cooperative support of the L S Fire Laboratories of Italy and in particular Mr. Silvio Messa for providing the test data for this study. This is a significant contribution in-kind to this project, which clearly enhances its value many fold. We are indebted to the financial support of NIST/BFRL and the guidance and interest of our technical monitor, Dr. Thomas Ohlemiller.

REFERENCES

1. ASTM E1354-90, "Standard Test Method for Heat and Visible Smoke Release Rates for Materials and Products Using an Oxygen Consumption Calorimeter", *Annual Book of ASTM Standards*, American Society for Testing and Materials, Philadelphia, 1990, pp. 803 to 817
2. Atreya, A., "Pyrolysis, Ignition and Fire Spread on Horizontal surfaces of Wood", Ph.D. Thesis, Harvard University, Cambridge, MA, 1983.
3. Back, G., Beyler, C., DiNenno, P. and tatem, P., "Wall Incident Heat Flux Distributions Resulting From an Adjacent Fire", *Fire Safety Science—Proceedings of the Fourth International Symposium*, ed. T. Kashiwagi, IAFSS, 1994.
4. Cleary, T. G. & Quintiere, J. G., "A Framework for Utilizing Fire Property Tests", *Fire Safety Science*, Proceedings of the 3rd International Symposium, ed. G. Cox & B. Langford, Elsevier Applied Science, London, 1991, pp. 647 to 656.
5. Drysdale, Dougal, *An Introduction to Fire Dynamics*, John Wiley & Sons, Chichester, 1994.
6. Haynes, G. A., "Analysis of a Model to Predict Flame Spread Over a PMMA Wall in a compartment", M.S. Thesis, Department of Fire Protection Engineering, University of Maryland, College Park, Maryland, 1996.
7. Hopkins, Jr. D. & Quintiere J. G., "Material Fire Properties for Thermoplastics", *Fire Safety Journal*, 26 (3), 1996, pp. 241-268.
8. Incropera, Frank P., & DeWitt, David P., *Fundamentals of Heat and Mass Transfer*, Third Edition, John Wiley & Sons, New York, 1990.
9. Janssens.
10. Kim, Woon Hyung & Quintiere, J. G., "Applications of a Model to Compare Flame Spread and Heat Release Properties of Interior Finish Materials in a Compartment", *International Symposium on Fire Science and Technology*, Seoul, November 12 – 14, 1997.
11. Kokkala, M. A., "Characteristics of a Flame in an Open Corner of Walls", *Interflam '93*, Inter Science Communications Limited, London England, 1993, pp. 13 to 24.
12. Kokkala, M. Goransson, U. & Soderbom, J., "EUREFIC – Large Scale Fire Experiments in a Room with Combustible Linings", SP Report 1990:41, Swedish National Testing and Research Institute, Boras, 1990.
13. Mowrer, F. R. & Williamson, R. B., "Flame Spread Evaluation for Thin Interior Finish Materials", *Fire Safety Science*, Proceedings of the 3rd International Symposium, ed. G. Cox & B. Langford, Elsevier Applied Science, London, 1991, pp. 689 to 698
14. Ohlemiller, T., Cleary, T. & Shields, J., "Effect of Ignition Conditions on Upward Flame Spread on a Composite Material in a Corner Configuration", (private communications, to be published).
15. Quintiere, J. G., "Estimating Fire Growth on Compartment Interior Finish Materials", Department of Fire Protection Engineering, University of Maryland, College Park, MD, 1995.
16. Quintiere, J. G., "Fire Tests and Hazard Evaluation", 7th International Research and Training Seminar on Regional Development Planning for Disaster Prevention—

- Improved Firesafety Systems in Developing Countries, October 17, 1994, Tokyo, Japan.
17. Quintiere, J. G., "Modeling Room Corner Tests", Heat Release and Fire Hazard, Proceedings of the First Japan Symposium, Volume 1, Tsukuba, Japan, May, 1993.
 18. Quintiere, J. G., "A Simulation Model for Fire Growth on Materials Subject to a Room/corner Test", *Fire Safety Journal*, Volume 18, 1992.
 19. Quintiere, J. G., Haynes, G. & Rhodes, B. T., "Applications of a Model to Predict Flame Spread Over Interior Finish Materials in a Compartment", *Journal of Fire Protection Engineering*, Volume 7, Number 1, 1995, pp. 1 to 13.
 20. Quintiere, J. G., Hopkins, M. & Hopkins, D. Jr., "Fire Hazard Prediction for Textile Wall Materials", Final, ATMI, January, 1995.
 21. Quintiere, J. G., Hopkins, M. & Hopkins, D. Jr., "Room-Corner Fire Prediction for Textile Wall Materials", International Conference on Fire Research and Engineering, BFRl and SFPE, Orlando Marriot International, FL, Sept. 10 -15, 1995.
 22. Quintiere, J. G. & Iqbal, N., "An Approximate Integral Model for the Burning Rate of a Thermoplastic-like Material", *Fire and Materials*, Vol. 18, 1994, pp. 89 to 98.
 23. Quintiere, J. G. and Lee, C. H., Ignitor and Thickness Effects on Upward Flame Spread", *Fire Technology*, Volume 34, Number 1, March 1998, pp. 39-59.
 24. Quintiere, J. G. & Rhodes, B. T., "Fire Growth Models for Materials", *Fire Safety Journal*, 26 (3), 1996, pp. 221-240.
 25. Rhodes, B. T., "Burning Rate and Flame Heat Flux for PMMA in the Cone Calorimeter", M. S. Thesis, Department of Fire Protection Engineering, University of Maryland, College Park, Maryland, May, 1994.
 26. Su, Chen-Hsiang, "Downward and Lateral Flame Spread in Roland Apparatus Phase 5", M. S. Degree Scholarly Paper, Department of Fire Protection Engineering, University of Maryland, college Park, Maryland.
 27. Tewarson, Archibald, "Generation of Heat and Chemical Compounds in Fires", *SFPE Handbook of Fire Protection Engineering*, National Fire Protection Association, Quincy, MA, 1988, pp. 1-179 to 1-199.
 28. Thureson, Per, "Fire Tests of Linings According to Room/Corner Test, ISO 9705", Swedish National Testing and research Institute, Fire Technology, Report 95R22049, January, 1996.

NIST-114
(REV. 11-94)
ADMAN 4.09

U.S. DEPARTMENT OF COMMERCE
NATIONAL INSTITUTE OF STANDARDS AND TECHNOLOGY

(ERB USE ONLY)

ERB CONTROL NUMBER	DIVISION
PUBLICATION REPORT NUMBER	CATEGORY CODE
NIST-GCR-98-753	
PUBLICATION DATE	NUMBER PRINTED PAGES
July 1998	

MANUSCRIPT REVIEW AND APPROVAL

INSTRUCTIONS: ATTACH ORIGINAL OF THIS FORM TO ONE (1) COPY OF MANUSCRIPT AND SEND TO THE SECRETARY, APPROPRIATE EDITORIAL REVIEW BOARD.

TITLE AND SUBTITLE (CITE IN FULL)

Determination of Properties and the Prediction of the Energy Release Rate of Materials in the ISO 9705 Room-Corner Test

CONTRACT OR GRANT NUMBER

60NANB2D1266

TYPE OF REPORT AND/OR PERIOD COVERED

Interim Report June 1998

AUTHOR(S) (LAST NAME, FIRST INITIAL, SECOND INITIAL)

Dillon, S.E., Kim, W.H., Quintiere, J.G.

PERFORMING ORGANIZATION (CHECK (X) ONE BLOCK)

- NIST/GAITHERSBURG
- NIST/BOULDER
- JILA/BOULDER

LABORATORY AND DIVISION NAMES (FIRST NIST AUTHOR ONLY)

SPONSORING ORGANIZATION NAME AND COMPLETE ADDRESS (STREET, CITY, STATE, ZIP)

U.S. Department of Commerce
National Institute of Standards and Technology
Gaithersburg, MD 20899

PROPOSED FOR NIST PUBLICATION

- | | | |
|---|--|--|
| <input type="checkbox"/> JOURNAL OF RESEARCH (NIST JRES) | <input type="checkbox"/> MONOGRAPH (NIST MN) | <input type="checkbox"/> LETTER CIRCULAR |
| <input type="checkbox"/> J. PHYS. & CHEM. REF. DATA (JPCRD) | <input type="checkbox"/> NATL. STD. REF. DATA SERIES (NIST NSRDS) | <input type="checkbox"/> BUILDING SCIENCE SERIES |
| <input type="checkbox"/> HANDBOOK (NIST HB) | <input type="checkbox"/> FEDERAL INF. PROCESS. STDS. (NIST FIPS) | <input type="checkbox"/> PRODUCT STANDARDS |
| <input type="checkbox"/> SPECIAL PUBLICATION (NIST SP) | <input type="checkbox"/> LIST OF PUBLICATIONS (NIST LP) | <input type="checkbox"/> OTHER _____ |
| <input type="checkbox"/> TECHNICAL NOTE (NIST TN) | <input type="checkbox"/> NIST INTERAGENCY/INTERNAL REPORT (NISTIR) | |

PROPOSED FOR NON-NIST PUBLICATION (CITE FULLY)

- U.S.
- FOREIGN

PUBLISHING MEDIUM

- PAPER
- DISKETTE (SPECIFY) _____
- OTHER (SPECIFY) _____
- CD-ROM

SUPPLEMENTARY NOTES

ABSTRACT (A 2000-CHARACTER OR LESS FACTUAL SUMMARY OF MOST SIGNIFICANT INFORMATION. IF DOCUMENT INCLUDES A SIGNIFICANT BIBLIOGRAPHY OR LITERATURE SURVEY, CITE IT HERE. SPELL OUT ACRONYMS ON FIRST REFERENCE.) (CONTINUE ON SEPARATE PAGE, IF NECESSARY.)

A simulation model is implemented in order to predict the performance of materials in the ISO 9705 Room-Corner Test. These materials were tested by the L S Fire Laboratories of Italy, and the data they provided is analyzed in this report. A method was established to define material properties including the heat of combustion, heat of gasification, thermal inertia, ignition temperature and the total energy per unit area. These methods were developed from refinements in the theoretical model of ignition and in resolving time dependent effects in the Cone Calorimeter. The materials examined consist of some of the worst behaving since they melt, drip, expand and de-laminate from the wall and ceiling configuration of the room-corner test. Corrections have been included in the simulation modeling to account for these effects. the correction involves reducing the total energy per unit area content of the material to accordingly reduce its contribution as a wall-ceiling oriented element. An empirical correlation based on a linearized upward flame spread model is shown to provide very good correlation to the flashover time in the full-scale ISO test.

KEY WORDS (MAXIMUM OF 9; 28 CHARACTERS AND SPACES EACH; SEPARATE WITH SEMICOLONS; ALPHABETIC ORDER; CAPITALIZE ONLY PROPER NAMES)

Ceilings; Cone Calorimeters; Fire Models; Flame Resistant Materials; Flame Spread; Flashover; Ignition; Walls

AVAILABILITY

- UNLIMITED
- FOR OFFICIAL DISTRIBUTION - DO NOT RELEASE TO NTIS
- ORDER FROM SUPERINTENDENT OF DOCUMENTS, U.S. GPO, WASHINGTON, DC 20402
- ORDER FROM NTIS, SPRINGFIELD, VA 22161

NOTE TO AUTHOR(S): IF YOU DO NOT WISH THIS MANUSCRIPT ANNOUNCED BEFORE PUBLICATION, PLEASE CHECK HERE.

ELECTRONIC INFORMS